POLYTECHNIC SCHOOL OF ENGINEERING OF GIJÓN

MASTER DEGREE IN TELECOMMUNICATION ENGINEERING (MINGTELE)

AREA OF SIGNAL THEORY AND COMMUNICATIONS

MASTER THESIS NUMBER 201803

FILTENNA ANALYSIS AND DESIGN FOR IMPROVING FREQUENCY SELECTIVITY OF ARRAY ELEMENTS

FERNÁNDEZ GONZÁLEZ, Juan Carlos
THALES SUPERVISOR: OUDE VELTHUIS, Robert
ACADEMIC SUPERVISOR: ÁLVAREZ LÓPEZ, Yuri

DATE: JULY 2018

ACKNOWLEDGEMENTS

The work presented in this thesis was carried out at Thales Nederland, B.V. in Hengelo, the Netherlands, and is the last part of my Master's Degree in Telecommunication Engineering at the Polytechnic School of Engineering of Gijón, Univeristy of Oviedo, Spain. I would like to thank both Thales and the Univeristy for the opportunity they have given me to develop my thesis in a leading company and a friendly yet challenging environment.

I would also like to give special thanks to Gertjan, Robert, David and Stephan for sharing their advice and technical expertise, from which I have learned a lot.

Finally, I would like to thank my colleagues for making of this period at Thales a fun and stimulating experience and, of course, my family for their continuous and devoted support, without which none of this would have been possible.

ABSTRACT

Modern radar systems are used for a variety of applications, ranging from traffic radars and medical scanners to air traffic control and military radar systems. As a response to the growing demand for innovation in these fields, Thales Nederland focuses on the improvement and development of military radar systems. The present work was proposed in this context as a way to explore new possibilities to improve such systems.

Microstrip antennas are a key part of radar systems, since they are the interface between the transmitter/receiver and the environment. Thus, improving antenna parameters and performance can have a significant impact on the overall radar system. With this in mind, two main objectives were proposed: incorporating a filtering functionality to an antenna operating at 3 GHz, and increasing its operating band roll-off. Given that the operating frequency is 3 GHz, the frequency components to reject with the filtenna design were classified in two bands: one around the 2nd harmonic, located at 6 GHz (4-7 GHz band), and another one around the 3rd harmonic, located at 9 GHz (7-11 GHz band).

To achieve that, several options were considered, including existing filtering structures and CMA (Characteristic Mode Analysis) techniques. EBG (Electromagnetic Band Gap) structures were preferred due to their novelty and the potential that they have shown in different studies. Their theoretical model was analyzed, paying special attention to their Bloch impedance and band gap features. Some structures were considered and the mEBG (mushroom EBG) was chosen due to its design flexibility and band gap properties.

Next, different mEBG unit cells were modeled, both using MatLab and ANSYS HFSS. Their physical parameters were varied and their impact on band gap frequencies and width was defined. A study was carried out to investigate how the mEBG could be integrated with a microstrip line and a patch antenna to achieve a filtering behavior. Different arrangements were analyzed, achieving an optimal stop band behavior in the 7-11 GHz band for a row of mEBG underneath the microstrip line and parallel to it. The mEBG was then adapted to an odd multiple of a quarter wavelength to achieve good impedance matching at the operating frequency and placed at the same level as the ground plane for the same purpose. Its band gap was also enhanced by varying via diameter, substrate permittivity and mEBG height. The designed mEBG filter, combined with CMA techniques to reduce 2nd harmonic levels (4-7 GHz) yielded satisfactory results for the final filtenna design.

Finally, it was concluded that, although the roll-off factor of the antenna was not directly affected by the mEBG structre, a filtering functionality was successfully achieved, with a low-profile design and good rejection levels. The mEBG potential as a filtering structure was validated, theoretically allowing to replace the CMA techniques for 2nd harmonic rejection in future filtenna designs.

RESUMEN

Los sistemas radar actuales tienen múltiples aplicaciones, desde radares de tráfico y escáneres médicos hasta control de tráfico aéreo y radares militares. Dada la creciente demanda de innovación en este ámbito, Thales Nederland se dedica a mejorar y desarrollar sistemas militares de radar. El presente trabajo se plantea en este contexto con la finalidad de explorar nuevas técnicas para mejorar dichos sistemas.

Las antenas microstrip son una parte clave de los sistemas radar, ya que actúan como interfaz entre el transmisor/receptor y el entorno. Por tanto, mejorar los parámetros y el rendimiento de las antenas puede tener un impacto significativo sobre el sistema final. Teniendo esto en cuenta, se han fijado dos objetivos principales: dotar de capacidad de filtrado a una antena funcionando a 3 GHz, e incrementar el roll-off de la banda de operación. Dado que la frecuencia de operación es de 3 GHz, se definieron dos bandas de frecuencia que la filtena debería rechazar: una en torno al segundo armónico, situado en 6 GHz (banda de 4-7 GHz), y otra en torno al tercer armónico, situado en 9 GHz (banda de 7-11 GHz).

Para ello se han planteado varias opciones, como estructuras de filtrado existentes y técnicas CMA (Characteristic Mode Analysis). Se ha decidido emplear las estructuras EBG (Electromagnetic Band Gap) por su carácter innovador y el potencial que han mostrado en diferentes estudios. Se ha estudiado su modelo analítico, prestando especial atención a los parámetros impedancia de Bloch y banda prohibida. Tras considerar varias estructuras, se optó por el mEBG (mushroom EBG) por su flexibilidad y propiedades de banda prohibida.

A continuación, se modeló la celda unidad de la estructura, empleando tanto MatLab como ANSYS HFSS. Se variaron sus parámetros físicos para determinar su impacto en la banda prohibida. Después se realizó un estudio para investigar la posible integración del mEBG con una línea microstrip y una antena de parche para conseguir funcionalidad de filtrado. Se analizaron distintas configuraciones, obteniendo una respuesta óptima (banda de rechazo de 7-11 GHz) para una fila de mEBG situada bajo la línea microstrip y paralela a ella. La estructura se ajustó a un múltiplo impar de un cuarto de longitud de onda para conseguir buena adaptación de impedancia a la frecuencia de operación. También se posicionó en el plano de masa por el mismo motivo. Luego se variaron los parámetros diámetro de vía, permitividad del sustrato y altura del mEBG para aumentar su banda prohibida. El filtro mEBG diseñado, en combinación con técnicas CMA para reducir los niveles del segundo armónico (4-7 GHz), generó resultados satisfactorios en el diseño final de la filtena.

Por último, se concluyó que, aunque el factor de roll-off de la antena no se vio directamente afectado por la estructura mEBG, sí se obtuvo con éxito la funcionalidad de filtrado, por medio de un diseño compacto y con niveles de rechazo significativos. Se validó el potencial del mEBG como filtro, en teoría posibilitando reemplazar las técnicas CMA para el rechazo de los armónicos de segundo orden en futuros diseños de filtena.

CONTENTS

LIST OF TABLES

LIST OF FIGURES

LIST OF ACRONYMS

AECTP	Allied Environmental Conditions Testing Publication
AMC	Artificial Magnetic Conductor
CMA	Characteristic Mode Analysis
CRLH	Composite Right Left Handed
DNG	Double Negative
EBG	Electromagnetic Band Gap
EMC	Electromagnetic Compatibility
FDTD	Finite Difference Time Domain
FEM	Finite Element Method
Filtenna	Filtering Antenna
FSS	Frequency Selective Surface
HIS	High Impedance Surface
LH	Left Handed
LHM	Left Handed Material
mEBG	Mushroom EBG Structure
MIL	Military
MoM	Method of Moments
NRI	Negative Refractive Index
PBG	Photonic Band Gap
PEC	Perfect Electric Conductor

PMC	Perfect Magnetic Conductor
RF	Radiofrequency
SC	Smith Chart
SW	Surface Wave
TE	Transverse Electric
TEM	Transverse Electromagnetic
TM	Transverse Magnetic

1.- INTRODUCTION

The work behind this master thesis is part of an existing line of work at Thales Nederland B.V., located in Hengelo, Netherlands. Thales Hengelo is specialized in the development, assembly and test of military radar systems. Such systems often need to abide by strict standards. Meeting and even exceeding such standards is critical for product quality and its commercialization. A good design is the first step towards obtaining the desired product. As an integrating subsystem of radar systems, the design of low-profile, efficient antennas has a considerable impact on the overall system performance and should be as optimal as possible. Thus, this work is defined in terms of what improvements can be made to antenna designs for radar systems and why such improvements are desirable. In the following sections, a general view of the state of the art is provided, the main objectives of this work are established, and some ideas are proposed towards achieving them.

1.1.- Microstrip patch antennas and filters in radar systems: an overview

Microstrip patch antennas are a key part of modern radar systems. When integrated in arrays, it is possible to improve radiation parameters and to apply useful techniques like beamforming or electronic beamscanning. Such antennas are part of a larger system that forms the transmitter-receiver chain of the radar, containing elements such as oscillators, mixers, amplifiers, filters, circulators, and others. In this thesis, especial emphasis is put on the antenna and filtering stages. Conventional microstrip patch antennas resonate not only at the desired design frequency band, but also at a certain range of frequencies immediately around it, and at higher harmonic frequencies. Typically, harmonic modes are rejected by means of low-pass or band-pass filters placed before the antenna. The other frequencies, close to the working frequency, are not easy to reject due to limitations in the roll-off factor of filters and the antenna itself. A new line of work is proposed consisting of the integration of radiating and filtering elements in one compact filtenna (filtering antenna) design, in order to improve antenna selectivity and spurious rejection, as is presented in the following sections.

1.2.- Objective and motivation

The work carried out and presented in this thesis involves the design of a new filtenna component with the following key objectives:

- Reduction of second harmonic: minimum aimed rejection of 20 dB in the frequency band around the second harmonic.
- Reduction of third harmonic: minimum aimed rejection of 20 dB in the frequency band around the second harmonic.
- Reduction of other spurious components. In this work, the word "spurious" refers to any unwanted frequency component.
- Roll-off factor improvement.

And the main factors motivating such goals can be explained as follows:

- System robustness: in military applications, the robustness of the system is of particular importance, since it has defense and security implications. Antennas are the interface between the system and the outside world, capturing all sorts of signals from the environment. These signals can be unwanted, either caused by natural radiation, accidental interferences or, in the worst case, intentionally generated jamming or misleading signals. Reducing harmonic levels, as well as increasing operating frequency band roll-off factor of the antennas can avoid capturing some of these signals, minimizing the risk of getting false information (like false alarms or undetected targets) and overload system failure.
- System simplification: an efficient filtering antenna makes eliminating or simplifying filtering stages in the radar chain possible, reducing the cost of the complete system. Most importantly, having fewer elements in the system chain lowers noise levels (the noise figures of removed filters are no longer affecting the Friis system noise calculation). This means that the final signal to noise ratio can be potentially increased, thus achieving a longer radar range, as can be derived from the radar equation [1].
- Electromagnetic Compatibility Standards (EMC): harmonic level reduction and frequency selectivity improvement can ensure system compliance with EMC emission standards (transmission), which are particularly strict for military systems. Additionally, mobile radar systems are often deployed for international missions. This means that, from the susceptibility (reception) point of view, they must be able to deal with different spectrum regulations, although some specifications such as MIL or AECTP are internationally used. An efficient filtering antenna can help reject a wider number of unwanted signals (improved susceptibility), improving system performance in an international context.

- Spectrum usage optimization: although not the case for radar systems, if applied to communication systems, a faster roll-off means that channels can be placed closer together in the frequency spectrum because frequencies immediately outside the desired bandwidth will be more strongly rejected. This results in more efficient spectrum usage, subsequently leaving room for other applications and cutting costs.

Several techniques have been explored to achieve the above mentioned goals, and some designs have been created that show promising results in this direction.

1.3.- Proposed ideas

From a transmission point of view, conventional microstrip filters are often placed before the antenna, that is, in between the power amplifier and the antenna. Similarly, from a reception point of view, they are placed between the antenna and the receiver, that is, after the antenna. Such filters are used to reduce harmonic levels (usually generated by the amplifying stages, in transmission, and by interferences, in reception) and other unwanted components.

Design techniques for such filters are well developed and applied to real systems. Another way of eliminating unwanted modes in microstrip patch antennas is by means of Characteristic Mode Analysis (CMA). This method consists of inspecting the fields and currents of the different modes on the patch so that they can be eliminated by opening slots or placing vias at certain places. The CMA technique is limited by the fundamental patch mode, that gives the desired radiation pattern at the fundamental frequency (set at 3 GHz for our designs), because vias or slots cannot be placed where they would downgrade the desired radiation pattern.

Both traditional filters and CMA designs have been widely studied and applied in real systems. In order to obtain a component that acts both as a filter and an antenna, new technologies need to be explored. In this thesis, special attention has been drawn to the use of metamaterials, and EBG structures in particular. The main feature that makes EBG structures interesting is the band gap that appears in a certain range of frequencies that keeps any modes from propagating in that frequency band, resembling a filtering behavior. Additionally, different studies [2-16] have shown that adding EBG structures to different antenna designs (dipoles, horn antennas, patches...) can significantly improve radiation parameters, namely bandwidth, cross-polarization, secondary lobe level and backward radiation. Because of these interesting features and some promising studies, EBG structures are chosen in this thesis to develop the desired filtenna.

Metamaterials are typically periodic structures composed of unit-cells that are much smaller than the operating wavelength, and that show electromagnetic behaviors not found in nature. In most metamaterials, both the electric permittivity and magnetic permeability take

negative values, resulting in a negative refraction index. This means that an incident wave gets refracted on a direction in the half-plane that contains the direction of incidence and is limited by the straight line normal to the surface between the air and the metamaterial. For each structure, this behavior only occurs at certain frequencies and for certain modes, and can be used for different purposes, such as leaky-wave radiation or surface-wave suppression [19].

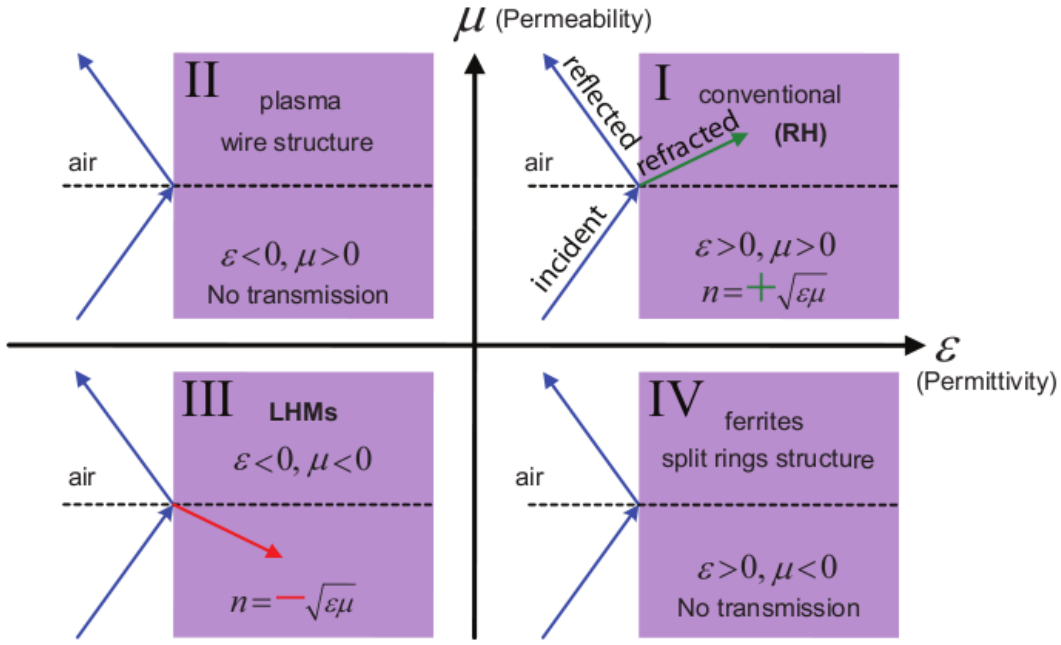

Figure 1.1.- $\epsilon - \mu$ diagram. In a double negative material (third quadrant) electric field, magnetic field and the wavevector form a left-handed triad, Snell's Law, Doppler Effect and Vavilov-Cerenkov radiation are reversed and frequency dispersion effects occur.

The third quadrant of Figure 1.1 [19] sums up the properties of metamaterials, also referred to as left-handed materials (LHM). In them, backward waves appear because group and phase velocity take opposed signs (positive and negative, respectively), meaning that power flows away from the source, whereas the phase front travels towards the source. Additionally, the propagation constant β in a metamaterial evolves non-linearly with frequency, as do ϵ and μ. This effect is referred to as frequency dispersion, and the relation between the propagation constant and frequency is plotted in dispersion diagrams (Figure 1.2 [19]).

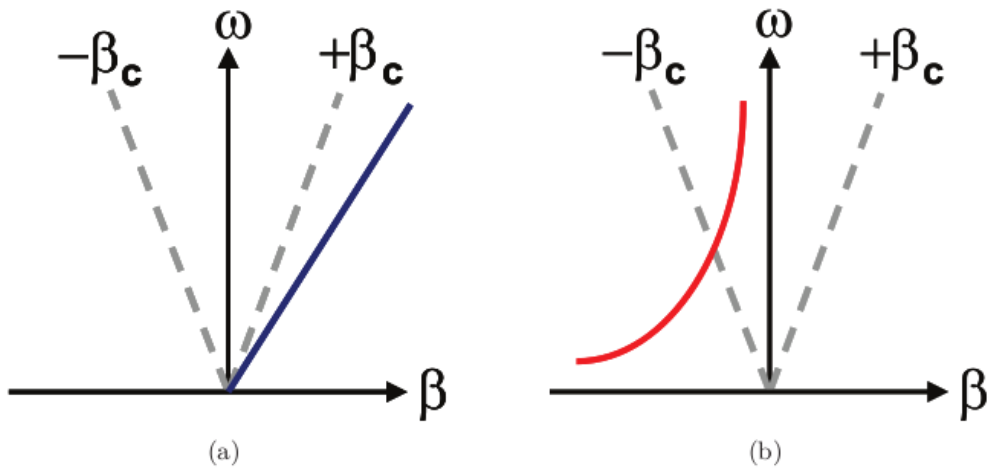

Figure 1.2.- Dispersion diagram of (a) right-handed unit cell versus (b) left-handed unit cell. β_c is referred to as the light line, representing the propagation constant at the speed of light.

Metamaterial unit cells can be modeled using two transmission line models: one for the frequency band where behavior is right-handed (Figure 1.3.a) and another one for the frequency band where behavior is left-handed (Figure 1.3.b). As it can be seen in Figure 1.3 [19], the models are inverted, which explains the non-linear evolution of β in the left-handed case.

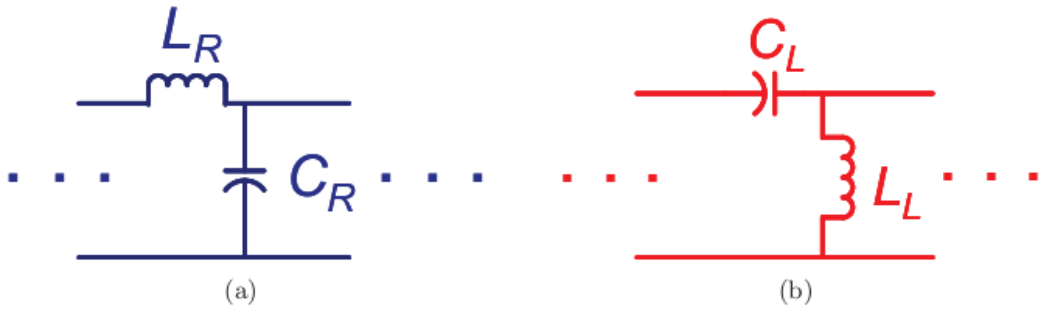

Figure 1.3.- Transmission line model of unit cells: (a) right-handed, (b) left-handed.

Thus, the values of β are given by equations (1.1) and (1.2):

$$\beta_{RH} = \omega \cdot \sqrt{C_R L_R} \tag{1.1}$$

$$\beta_{LH} = -\frac{1}{\omega\sqrt{C_L L_L}} \tag{1.2}$$

In reality, pure LH structures cannot be obtained, due to the existence of parasitic reactances. Therefore, a new composite right/left-handed (CRLH) model is built. The new circuit model is shown in Figure 1.4.a [19]. Its corresponding dispersion diagram is depicted in Figure 1.4.b [19] and the new equation for the propagation constant is shown in equation

(1.3). The dispersion diagram in Figure 1.4.b corresponds to an electromagnetic mode in an unbalanced metamaterial (purely EBG), meaning that there is a frequency band gap in the transition from left-handed behavior to right-handed behavior. In this gap, the mode does not propagate, and the material behaves as a band-stop filter. When such band gap does not exist, and the transition takes place without interruption, the structure is said to be balanced.

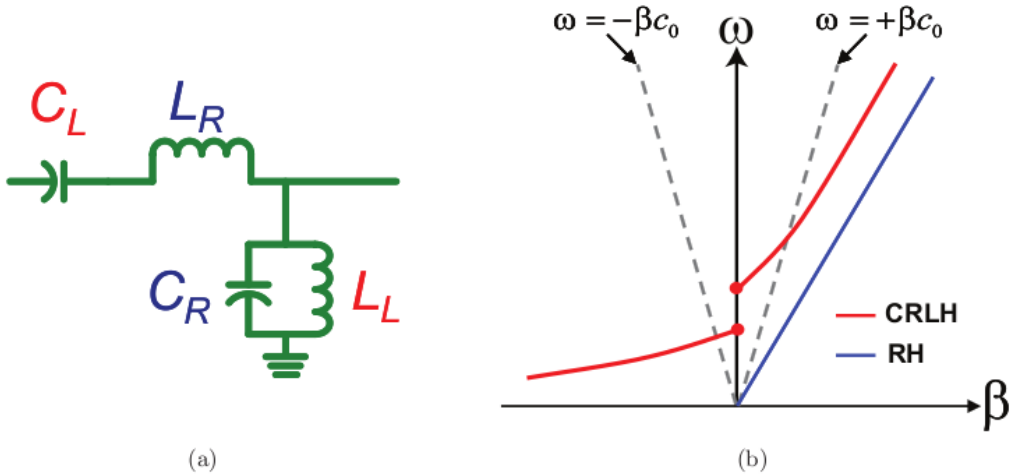

Figure 1.4.- CRLH model: (a) unit-cell equivalent circuit and (b) dispersion diagram.

$$\beta_{CRLH} = s(\omega)\sqrt{\omega^2 L_R C_R + \frac{1}{\omega^2 L_L C_L} - \left(\frac{L_R}{L_L} + \frac{C_R}{C_L}\right)} \tag{1.3}$$

where

$$s(\omega) = \begin{cases} -1 & if \quad \omega < \omega_{\Gamma 1} = min\left(\frac{1}{\sqrt{L_R C_L}}, \frac{1}{\sqrt{L_L C_R}}\right) \\ +1 & if \quad \omega < \omega_{\Gamma 2} = max\left(\frac{1}{\sqrt{L_R C_L}}, \frac{1}{\sqrt{L_L C_R}}\right) \end{cases} \tag{1.4}$$

In order to characterize the unit-cell, its Bloch impedance needs to be obtained. It is simply the ratio between voltage and current at the input terminal of a periodic unit-cell (Figure 1.5) [19]. It shows a flat response in the pass-band when the structure is balanced, and varies with frequency when the structure is unbalanced. Therefore, a balanced structure is desired for broadband applications, while an unbalanced structure is more suitable for resonant/narrow band applications.

A given metamaterial structure can be fully characterized by means of its dispersion diagram and its Bloch impedance. Specific types of metamaterials, such as EBGs, can be modeled more precisely with the above mentioned model as a starting point.

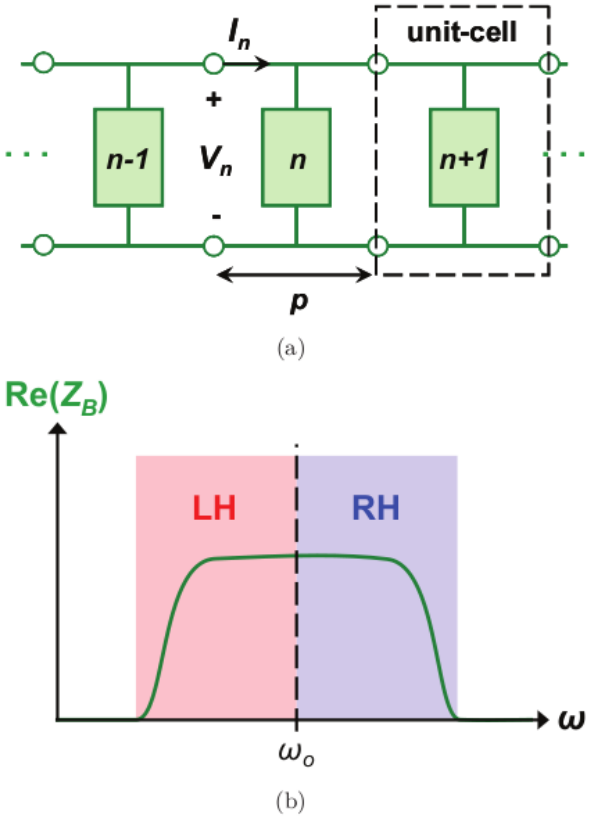

Figure 1.5.- (a) Unit cell distribution and (b) Bloch impedance diagram.

As a type of metamaterials, EBG structures can generally be defined as "*artificial periodic (or sometimes non-periodic) objects that prevent/assist the propagation of electromagnetic waves in a specified band of frequency for all incident angles and all polarization states*" [3]. EBG structures can be constructed in all 3 dimensions, but 2D structures have the advantages of low-profile, light weight and low fabrication cost, and they are also easier to model than 3D structures, so the EBG models and designs presented in this thesis will be two-dimensional (Figure 1.8 [3]).

Such structures show interesting electromagnetic properties with respect to incident electromagnetic waves:

- When the incident wave is a surface wave ($k_x^2 + k_y^2 \leq k_0$, with k_z purely imaginary), a frequency band gap appears in which surface wave propagation is prohibited for all incident angles and polarization states. The band gap is usually plotted in dispersion diagrams. [3]
- When the incident wave is a plane wave ($k_x^2 + k_y^2 \leq k_0$, k_z has a real value), the reflection phase of the EBG structure varies with frequency. At the frequency where the reflection phase is zero, the structure behaves as a PMC (Perfect Magnetic Conductor), which does not exist in nature. [3]

Where k_0 is the wavenumber of the incident wave in vacuum, and k_x, k_y and k_z are the *x*, *y* and *z* components of the wavenumber of the incident wave in the medium of propagation, given that the *x* and *y* components form a plane parallel to the EBG surface, and the *z* component is perpendicular to it. The above mentioned properties can be understood by examining the Effective Surface Impedance Model of EBG structures. As explained in [5], each EBG cell can be seen as a symmetric two port network, with its corresponding ABCD parameters. By performing a simple mathematical analysis, it can be derived that the effective surface impedance of an infinite periodic structure composed of cascaded EBG cells is equivalent to the characteristic impedance (usually referred to as Bloch impedance) of just one unit cell. Thus, given a certain EBG geometry, a lumped element equivalent model can be used to find its Bloch impedance and, ultimately, its surface impedance. A general lumped element model is shown in Figure 1.6 [5], and its surface impedance is given in (1.5) [5].

$$Z_s = \frac{j\omega L_1(1-\omega^2 L_2 C)}{1-\omega^2(L_1+L_2)C} \tag{1.5}$$

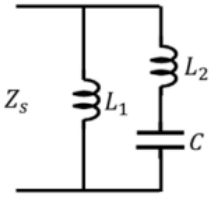

(a)

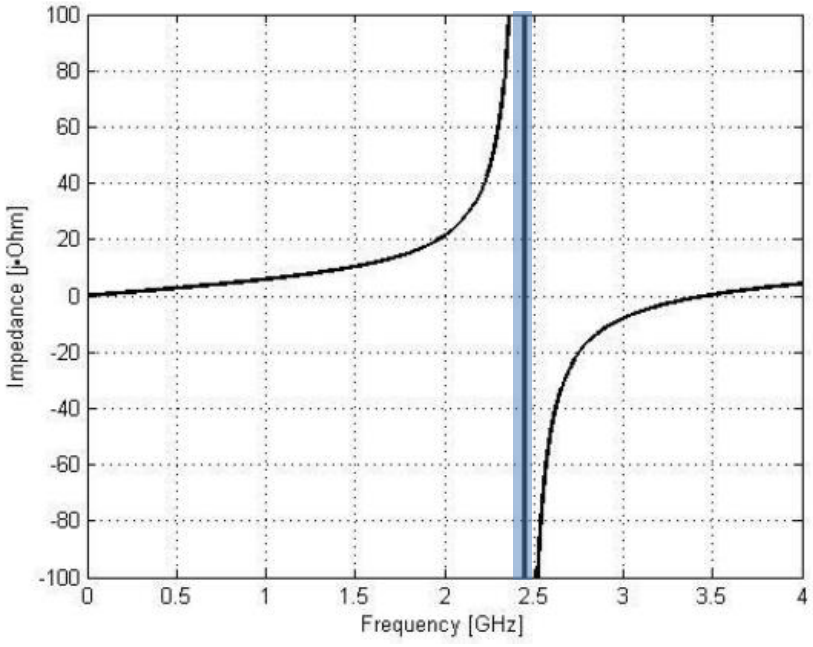

(b)

Figure 1.6.- Surface impedance lumped element model of EBG structure (a) and its frequency variation (b). Band gap in blue.

The surface impedance can be used to explain the band gap feature of EBG structures. At low frequencies, it shows an inductive behavior supporting propagation of TM waves, as can be seen in the dispersion diagram (Figure 1.7 [5]). Close to resonance (just before 2.5 GHz in Figure 1.7), TM waves propagate more and more slowly as they move away from the light line, up to a point where they do not propagate anymore. This limit is the beginning of the band gap. Around resonance, the surface impedance is very high as seen in Figure 1.6.b, yielding low group velocities for TM and TE waves as their dispersion curves bend away from the light line. Finally, at a certain point where the behavior of the unit cell switches to capacitive and is far away enough from resonance, propagation of TE waves is allowed. This point is the upper limit of the band gap.

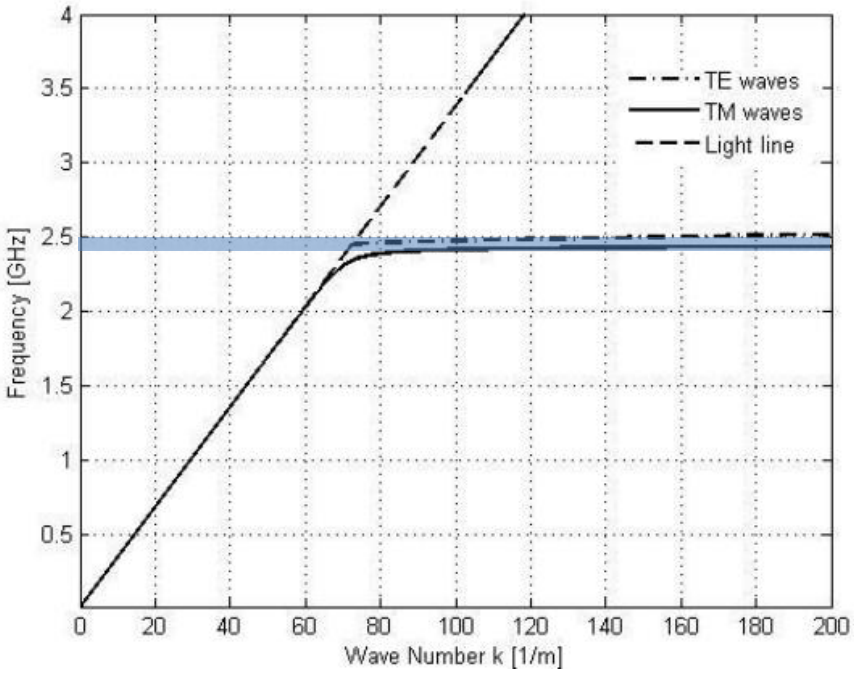

Figure 1.7.- Dispersion diagram from effective surface impedance. Band gap in blue.

From the analysis above, it can be concluded that EBG structures are fully characterized by their Bloch impedance and dispersion diagram. The presented model is a general one, as complex EBG structures may show variations as inductances and capacitances appear in different places. Before jumping to the analysis and design stages, research was carried out regarding some well-known EBG structures. Figure 1.11 shows an EBG classification in terms of band gap, geometry and position within the microwave circuit, either at the feeding or radiating stage. Since there is not a unified model from which particular two-dimensional EBG models can be derived, it becomes necessary to choose a few EBG structures with known models in order to analytically understand how they behave. In this master thesis, several EBG designs have been considered (Figure 1.8):

- Jerusalem cross
- Mushroom EBG structure (mEBG)
- Hilbert curve EBG
- Interdigitated structure
- Others

Of all of them, the mEBG is preferred because its model has been widely studied and validated, and some designs already exist [3][14-16][20-23] that show promising results, mostly for surface wave suppression, but also some initial studies on possible filtering behavior.

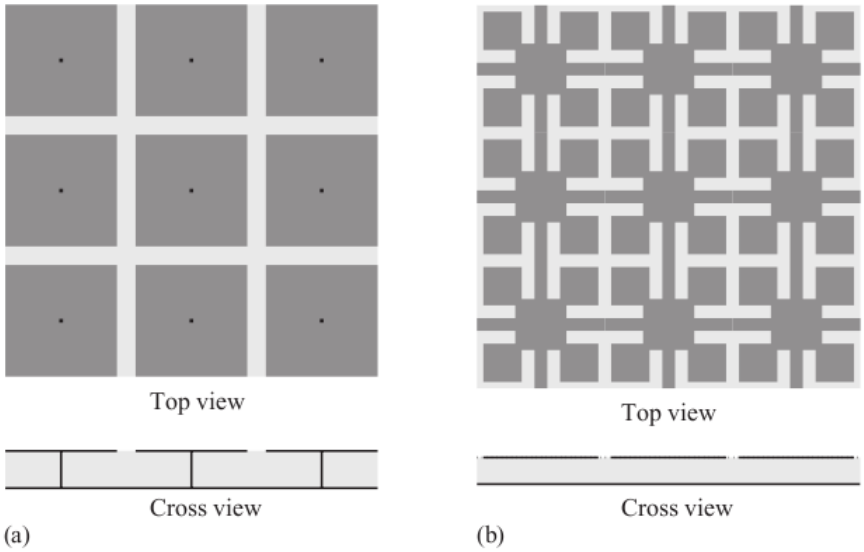

Figure 1.8.- (a) Mushroom surface EBG, (b) Jerusalem cross EBG.

Regarding the application of the mEBG to our filtenna design, it has been noted that EBG structures are more and more common in antenna designs because their band gap behavior helps to increase antenna gain, reduce back lobe radiation, and reduce mutual coupling in array elements through surface wave suppression. Using higher permittivity substrates to achieve smaller patch antennas is also facilitated by the use of EBG structures, because they help compensate the downsides of using high permittivity substrates, namely: increased back lobe radiation, higher surface wave excitation, and a reduction of directivity. In [6], several EBG structures are integrated with a patch antenna and their effect is analyzed. Special attention is paid to two main designs using the mEBG structure:

- Patch surrounded by mEBG (Figure 1.9). This arrangement improves radiation efficiency, directivity and back lobe radiation thanks to the suppression of surface waves, and has also decoupling purposes when integrated in antenna arrays.

- Mushroom EBG underneath the patch (Figure 1.10). This arrangement improves bandwidth, gain and cross polarization, but it significantly affects the near field of the antenna.

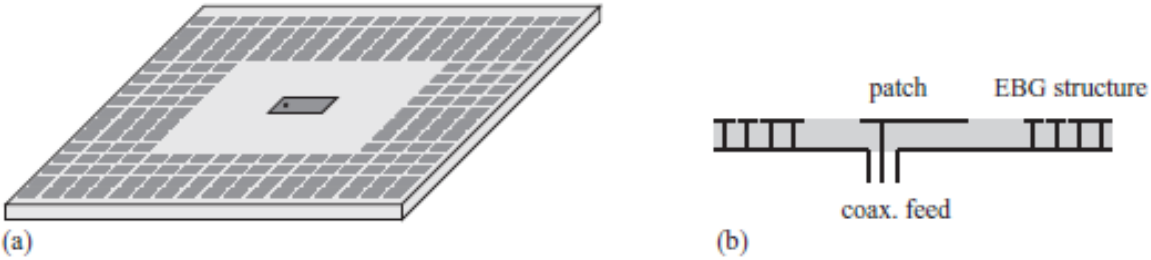

Figure 1.9.- Layout of microstrip patch antenna surrounded by mushroom EBG structures.

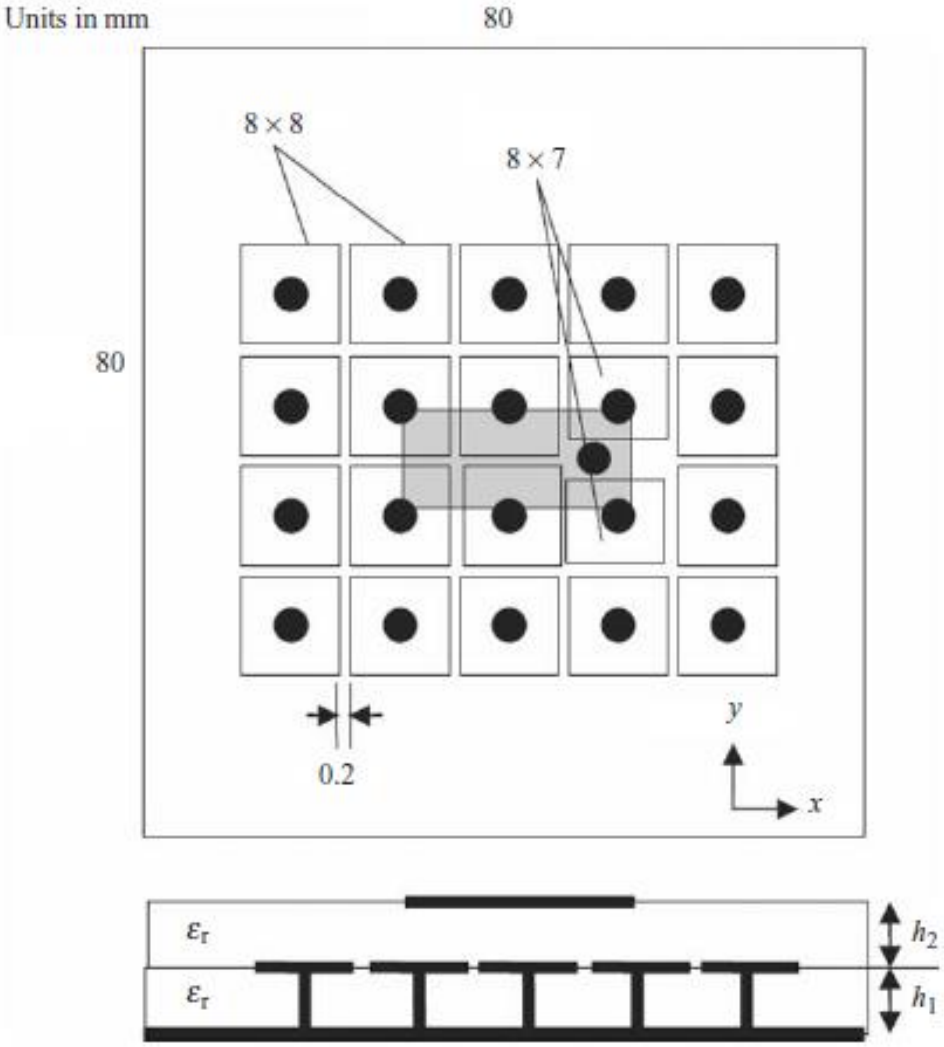

Figure 1.10.- Layout of the microstrip patch antenna on top of a grid of mushroom EBG structures.

From a design point of view, it is possible to obtain the main parameters and behavior of the mEBG through analytical methods, although their precision and application is limited. They offer a good initial insight of the structure's behavior but need to be complemented with other methods for better results. Numerical techniques based on Maxwell's equations, such as the method of moments (MoM), the finite element method (FEM), and the finite difference time domain (FDTD) method are powerful tools that enable a deeper and more complete analysis of EBG structures, and are implemented in various software suites like CST Microwave Studio or ANSYS HFSS. HFSS is the software available for the development of this work, which uses the FEM method to generate results.

With all this in mind, the proposed idea is to create a filtenna design using mEBG structures that offers better rejection to harmonics and a faster roll-off factor (achieved by placing the band gap accordingly) compared to conventional designs, also analyzed in this work, ideally eliminating the need for a filtering stage. The organization of chapters 2 to 5 of this thesis is arranged to match the design procedure, and their content can be summarized as follows:

- Chapter 2: the different elements that will be part of the filtenna design are modeled from a theoretical point of view. Such elements are the microstrip line, microstrip patch antenna, microstrip filters and the mEBG.
- Chapter 3: patch size definition and reference designs obtained from traditional microstrip antenna model. Patch antenna feeding techniques.
- Chapter 4: definition of mEBG unit-cell geometry and size. Initial decisions from known analytical models. Experimental (simulated) study of the mEBG: dispersion diagrams and band gap, integration with microstrip line and patch elements and mEBG filter design.
- Chapter 5: integration of all elements into a filtenna design.

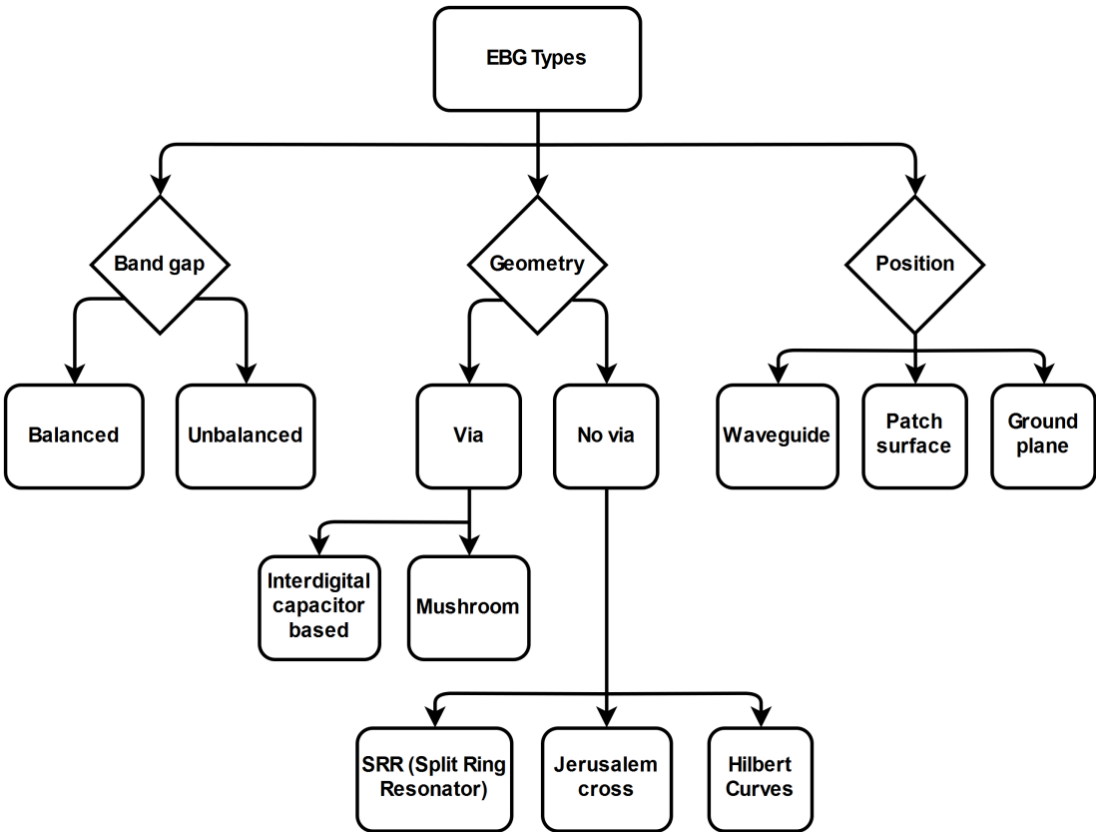

Figure 1.11.- EBG types.

2.- METHODOLOGY AND THEORETICAL BACKGROUND

Before getting into the design of the filtenna, the behavior and design procedures of certain microwave components need to be understood, since they are the starting point that will lead to the final design. Such components are the microstrip line, microstrip patch antenna and microstrip filters, and their models are briefly covered in section 2.1. Their combination with the EBG models explained in section 2.2 will facilitate the design of the final filtering antenna using EBG and traditional microstrip technology. Designs will be validated using HFSS full-wave simulation software, as detailed in appendix A.

2.1.- Analytical models of microstrip elements: an overview

2.1.1.- Microstrip line

The microstrip line is the most basic component of microstrip technology circuits. It is a planar transmission line built using a conducting line above a ground plane, separated from it by means of a dielectric substrate (Figure 2.1 [17]). The substrate often has a permittivity different from that of the air that usually surrounds the microstrip line, so TEM modes cannot propagate along the line [17]. The propagating wave is therefore a hybrid TM-TE wave, but for simplicity it can be assumed that propagating modes are quasi-TEM because the substrate is very thin compared to wavelength ($h \ll \lambda$) [17]. From this starting point, formulas can be derived to determine line impedance and effective dielectric constant, using line width and substrate permittivity and height as input parameters (2.1)(2.2).

$$\epsilon_{eff} = \frac{\epsilon_r + 1}{2} + \frac{\epsilon_r - 1}{2} \cdot \frac{1}{\sqrt{1 + \frac{12d}{W}}} \tag{2.1}$$

$$Z_0 = \begin{cases} \dfrac{60}{\sqrt{\epsilon_{eff}}} \cdot ln\left(\dfrac{8d}{W} + \dfrac{W}{4d}\right), & for\ \dfrac{W}{d} \leq 1 \\ \dfrac{120\pi}{\sqrt{\epsilon_{eff}} \cdot \left[\dfrac{W}{d} + 1.393 + 0.667 \cdot ln\left(\dfrac{W}{d} + 1.444\right)\right]}, & for\ \dfrac{W}{d} \geq 1 \end{cases} \tag{2.2}$$

These formulas allow to rapidly obtain the physical parameters of a standard 50 Ω impedance line. It is interesting to note that the design process does not take the operating frequency, f_0, into account. This will only be necessary when determining the length of the microstrip line, since depending on frequency, different lengths will produce different phase delays.

When the line is propagating fields, these do not completely stay between the line and the ground plane, but they partly radiate outside of the line. This can generate unwanted effects as it can distort the radiation pattern of the fed patch antenna and produce coupling effects on adjacent components. Luckily, some feeding techniques have been developed that mitigate this effects or take advantage of them, as discussed in chapter 3.

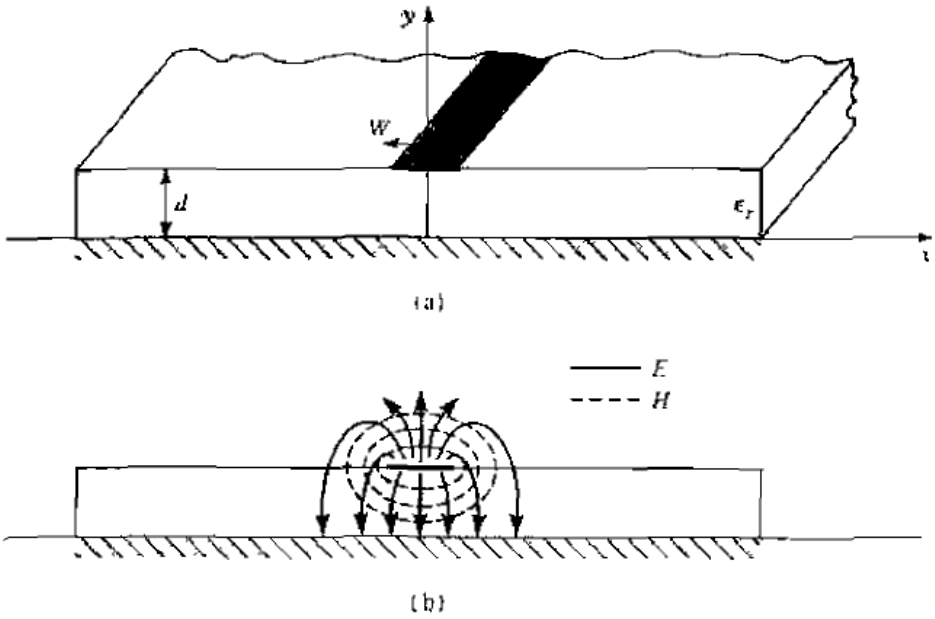

Figure 2.1.- Microstrip line and field representation.

2.1.2.- Microstrip patch antenna

A microstrip patch antenna consists of a radiating patch placed on top of a dielectric slab and a ground plane underneath. The patch can be excited by means of different feeding techniques (see section 3.1). When excited, radiation occurs thanks to fringing electric fields that form at two opposed edges of the patch (assuming a square or rectangular patch, see Figure 2.2). By choosing the excitation mode beneath the patch, both broadside (maximum normal to the patch) or endfire (maximum in the same plane as patch) can be achieved, although broadside configuration is most commonly used. The length L of a rectangular patch is usually $\lambda_0/3 \leq L \leq \lambda_0/2$. The electric permittivity of the dielectric substrate underneath the patch can take many different values depending on its material, but it is usually in the range $2.2 \leq \epsilon_r \leq 12$ [18]. Thicker and lower permittivity substrates yield better antenna

performance as they provide higher bandwidth and efficiency, and fields are more loosely bound for radiation into space, with the downside of larger patch size.

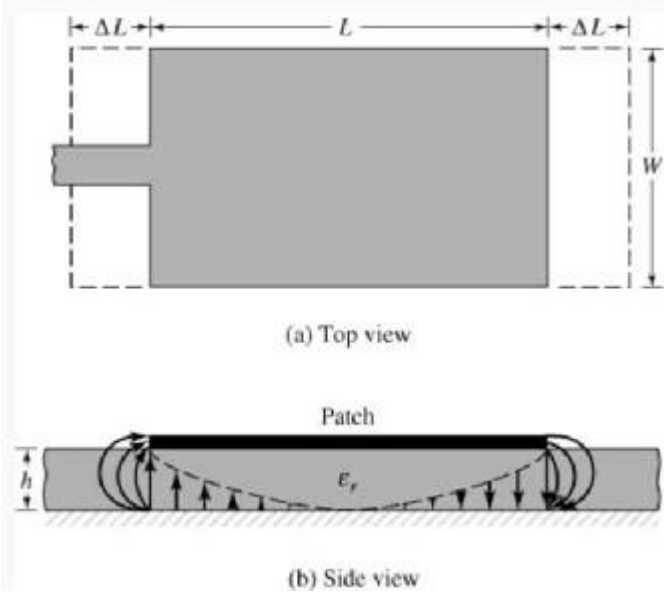

Figure 2.2.- Microstrip patch antenna and field representation.

The starting point when designing a patch antenna is then the desired operating frequency (f_0), dielectric height (h) and permittivity (ϵ_r). From f_0, free space wavelength can be derived:

$$\lambda_0 = \frac{c}{f_0} \tag{2.3}$$

Which can then be used to determine substrate thickness, as it should be in the range $0.003\lambda_0 \leq h \leq 0.05\lambda_0$ [18]. Patch width and length can then be calculated using the formulas in [18].

Different models can be used to anlayze the behavior of the designed patch. Analytical models like the transmission-line or cavity models are widely used and give a good insight of the concepts behind the patch antenna electromagnetic behavior, and are extensively explained in [18]. In this thesis, however, full-wave methods were used based on ANSYS HFSS software (release 2017b) to study such behavior.

2.1.3.- Main microstrip filters

In order to achieve a filtering antenna, it is necessary to be familiar with the traditional filter configurations, since it might be possible to adapt or combine them in the new filtenna design. Such structures include defected filtering stubs, coupled line filters, ground structures (filtering slots), shorted/open quarter wavelength resonators and other techniques (like varying the length of the overlap between proximity coupled patch and feedline for second harmonic

reduction). These structures can be integrated in the antenna (meander line antenna, for example) and/or combined with EBG structures for enhanced parameters. The studied filter theory and some designs are not further explained here since it is outside the scope of this thesis, but they can be found in the literature [17].

2.2.- Mushroom EBG analytical model

The mEBG has attracted some interest in the scientific community for its simplicity, its interesting properties and its potential applications. Therefore, analytical models have been developed that can predict its behavior. A mEBG can be seen as a patch with a via connecting it to the ground plane. The first step to obtain the mEBG model is to understand how a mushroom-like HIS (High Impedance Surface) works. Then, the mEBG model can be derived by taking into account the effect of the vias (Figure 2.3 [25]).

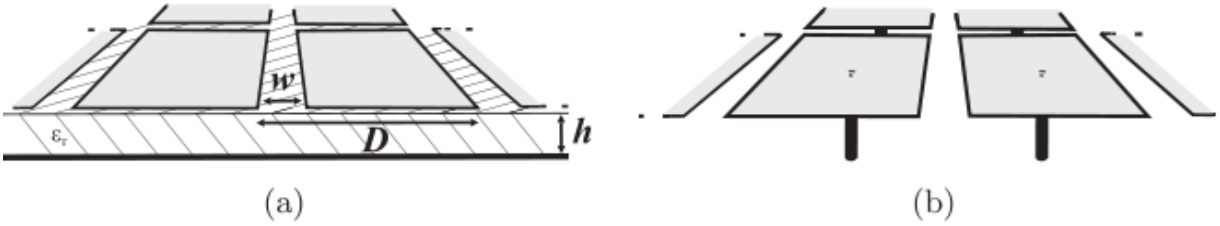

Figure 2.3.- HIS without vias (a), HIS with vias (b).

The HIS in Figure 2.3.a is modeled by an input surface impedance Z_{inp} connecting the cell-averaged tangential fields at the grid plane [25]. It is important to note that the model is only valid for structures with periodicity a lot smaller than wavelength ($D \ll \lambda$), since both HIS and the mEBG are considered metamaterials. The input impedance Z_{inp} can be seen as the parallel combination of the impedance of the grounded dielectric slab, Z_s', plus the capacitive impedance of the patch grid, Z_g' (2.4):

$$Z_{imp}^{-1} = {Z_g'}^{-1} + {Z_S'}^{-1} \tag{2.4}$$

Zg' is calculated in [26] using a combination of known analytical models for strip grids (Figure 2.4.a [26]) and the approximate Babinet principle [26] for planar grids placed at a dielectric interface.

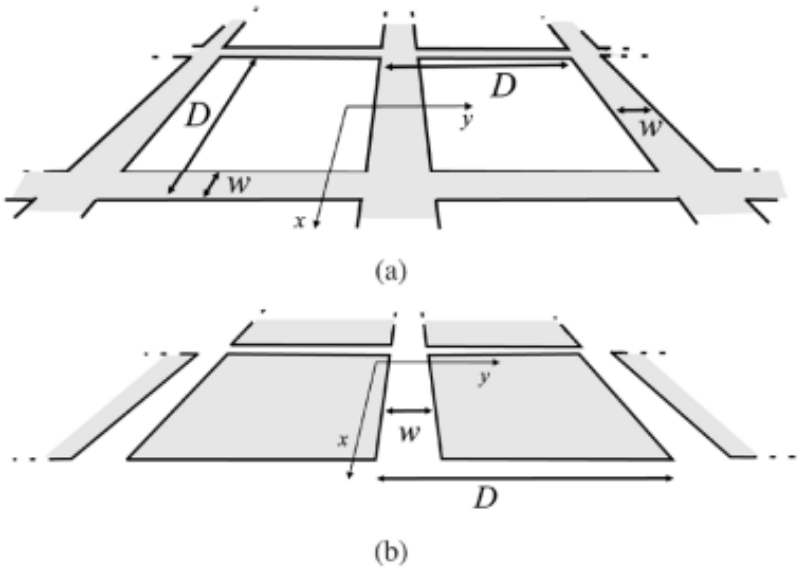

Figure 2.4.- Array of conducting strips (a), array of conducting patches (b). Metal in grey.

The derivation of the equations that lead to the final Z_g' expression can be found in [26]. The main ideas in the process are described in the following steps:

1. Find the metallic strip grid impedance, Z_g. The metallic strip grid in Figure 2.4.a is a nearly isotropic structure and its electromagnetic behavior weakly depends on the choice of the plane of incidence. Therefore, Z_g can be obtained by relating the averaged (over period *D*) tangential component of the electric field in the grid plane, E_{tot}, to the averaged surface current density *J* induced by the incident plane wave and flowing along the strips.
2. Repeat the process in 1. to obtain Z_g for both TE and TM incident wave polarizations. The resulting expressions are equations (2.5), (2.6).

$$Z_g^{TM} = \frac{j\eta_{eff}}{2}\alpha\left(1 - \frac{k_0^2}{k_{eff}^2}\frac{\sin^2\theta}{2}\right) \tag{2.5}$$

$$Z_g^{TE} = \frac{j\eta_{eff}}{2}\alpha \tag{2.6}$$

where $\eta_{eff} = \sqrt{\frac{\mu_0}{\epsilon_0\epsilon_{eff}}}$ is the wave impedance of the uniform host medium with relative effective permittivity $\epsilon_{eff} = \frac{\epsilon_r+1}{2}$ on top of which the grid is located, $k_{eff} = k_0\sqrt{\epsilon_{eff}}$ is the wave number of the incident wave vector in the effective host medium, θ is the angle of incidence, and α is called the grid parameter, calculated as:

$$\alpha = \frac{k_{eff} D}{\pi \ln \frac{1}{\sin(\pi \frac{w}{2D})}} \tag{2.7}$$

where *w* is the strip width and *D* is the period of the structure.

3. Apply the approximate Babinet principle in terms of grid impedances (2.8) to transform the metallic strip grid impedance into a patch grid impedance:

$$Z_g^{TE} Z_{g'}^{TM} = \frac{\eta_{eff}^2}{4} \tag{2.8}$$

Applying the Babinet principle, we get $Z_{g'}^{TM}$ and $Z_{g'}^{TE}$ in equations (2.9),(2.10):

$$Z_{g'}^{TM} = \frac{-j\eta_{eff}}{2\alpha} \tag{2.9}$$

$$Z_{g'}^{TE} = \frac{-j\eta_{eff}}{2\alpha \left(1 - \frac{k_0^2}{k_{eff}^2} \frac{\sin^2 \theta}{2}\right)} \tag{2.10}$$

Where $Z_{g'}^{TM}$ is the grid impedance of the complementary structure for TM-polarized incident fields, and $Z_{g'}^{TE}$ is the same as $Z_{g'}^{TM}$, but for TE-polarized incident fields.

Next, Z_s' for a grounded dielectric slab with vias is calculated:

1. Find Z_s for a grounded dielectric slab without vias through the impedance transformation equations for transmission lines [27], yielding eq. (2.11):

$$Z_S^{TM} = j\omega\mu \frac{\tan(\beta_{TM} d)}{\beta_{TM}} \left(I_{t,TM} - \frac{k_t k_t}{k^2}\right) \tag{2.11}$$

$$Z_S^{TE} = j\omega\mu \frac{\tan(\beta_{TE} d)}{\beta_{TE}} \left(I_{t,TE} - \frac{k_t k_t}{k^2}\right) \tag{2.12}$$

Where $\mu = \mu_0 \mu_r$ is the absolute permeability of the substrate, $k = k_0 \sqrt{\epsilon_r}$ is the wave number in the substrate material, k_t is the tangential wave number component, as imposed by the incident wave, and $\beta = \sqrt{k^2 - k_t^2}$.

2. Include the effect of the vias. To achieve that, the dielectric slab is seen as a uniaxial wire medium containing infinetly long, thin wires. This is possible assuming that both the ground plane and the patch grid plane can be treated as image planes. Since the period of the HIS is a lot smaller than wavelength lambda, the length of the wires is also small compared to lambda, so the propagation of surface waves can be assumed to be perpendicular to the wires. Considering the mentioned simplifications, an expression for Z'^{TM}_S is obtained (2.13):

$$Z'^{TM}_{S} = j\omega\mu \frac{\tan(\gamma_{TM} h)}{\gamma_{TM}} \left(\frac{k^2 - \beta^2 - k_p^2}{k^2 - k_p^2} \right) \tag{2.13}$$

Where $\omega = 2\pi f$, h is substrate thickness, and:

$$\gamma_{TM} = \sqrt{\omega^2 \epsilon_0 \epsilon_t \mu_0 - \frac{\epsilon_t}{\epsilon_n} \beta^2} \tag{2.14}$$

$$k_p = \frac{1}{a \sqrt{\frac{1}{2\pi} \ln \frac{a^2}{4 r_0 (a - r_0)}}} \tag{2.15}$$

Where $a = D$, r_0 is the via radius, and epsn is the relative permittivity for the fields normal to the slab,

$$\epsilon_n = \epsilon_t \left(1 - \frac{k_p^2}{k_0^2 \epsilon_t} \right) \tag{2.16}$$

3. Note that the given expression is particularized for TM-polarized incident waves. For TE-polarized incident waves, eq. (2.13) is still valid because, for thin vertical vias, the relative permittivity for the fields along the transversal plane and the relative permittivity of the host medium are the same, meaning that transversal electric field components do not interact with the vias.

Having defined Z'_g and Z'_s, Z_{inp} can be found using (2.4). From Z_{inp}, dispersion, reflection and band gap characteristics of the mEBG can be analytically estimated. For that purpose, the MatLab code in **[**28**]** was developed and used to obtain initial mEBG building parameters.

The analytical model of the mEBG is useful to find the impact variating input parameters causes on the dispersion diagram and band gap. Once a suitable configuration is achieved, the model is simulated in HFSS and adjusted for finer results, since it is expected that there will be some kind of mismatch between analytical and simulated results. The results of such simulations are presented in chapter 4.

3.- DESIGN CONSIDERATIONS

3.1.- Building parameters and excitation

In radiofrequency engineering, it is important to compare new designs to existing solutions with similar functionalities, in order to have some kind of measure of what the new design offers and how it affects different parameters. New designs are often based on previous ones and comparing them can help understand how different parameters are interconnected and determine how good or bad the new design is. In this work, the final developed filtenna will be compared to a reference microstrip antenna, whose characteristics are not only useful for comparison purposes, but also as a starting point of the final design.

Due to size constraints and electromagnetic behavior, substrate layers in microstrip designs usually have a thickness ranging from 0.5 mm to 2 mm. As for the dielectric permittivity, designs will be based on a $\epsilon_r = 3.55$ substrate (RO4003), since it is widely used in practice, although some simulations are also run using different substrates to analyze performance and parameter variations. The main variables defining patch size and other building parameters are specified in Figure 3.1 (top view, top; side z-x cut view, bottom):

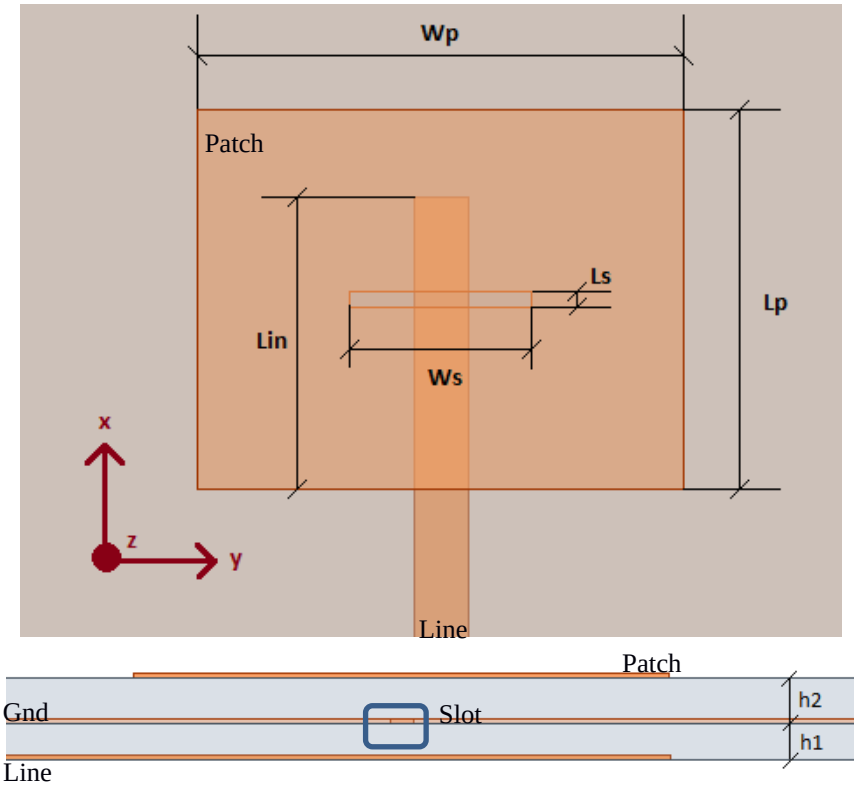

Figure 3.1.- Patch dimensions.

Where W_p and W_s are patch and slot widths, respectively, L_p and L_s patch and slot lengths, and L_{in} is the distance that the feed advances under the patch. Dielectric layer heights will be denoted with *h1* and *h2*, from bottom to top. In the case of the coaxial feed, the inner and outer radii are denoted R_i and R_e, respectively, and the position of the coaxial feed in the x direction will also be denoted with L_{in}. The width of the microstrip line in each case is calculated according to (2.1)(2.2) to achieve an impedance of 50 Ω, depending on the height of substrate material underneath the microstrip line and its permittivity. Using the above mentioned parameters all patch designs in this work are fully characterized.

An initial study of different feeding techniques was carried out in HFSS in order to decide which technique is potentially more desirable for designing the filtenna, as well as to have reference solutions. The considered feeding techniques are: microstrip feed, coaxial feed, proximity coupled feed and aperture feed (Figure 3.2). The main characteristics of each feeding technique are summarized in Figure 3.2, and the results obtained for the proposed reference designs are summarized in Table 3.2. A description of the HFSS driven mode simulation set up can be found in appendix A.1.

Patch antennas are most commonly fed using proximity coupled lines or similar feeding structures. Coaxial feeding is also a feasible option. Microstrip feeding is also analyzed as a reference point, but is not so much used in practice. The feeding technique of the microstrip patch affects aspects of the radiation pattern such as polarization, back lobe radiation, radiation efficiency and mutual coupling. Figure 3.2 shows the considered feeding configurations for our filtenna, and Table 3.1 [40] summarizes the main advantages and disadvantages of each type of feed.

With this in mind, an initial study of feeding techniques has been carried out for our desired frequency, with initial substrate permittivity and thickness parameters, obtaining the results shown in Figure 3.3 and summarized in Table 3.2 (see appendix A.1 for details about tolerance, convergence and resolution of results). For the proximity coupled technique, a 2nd order harmonic suppression method has been used, consisting on adjusting the feeding line overlap length underneath the patch as explained in [14].

Note that the S11 values in Figure 3.3 and Table 3.2* show a matching level of up to 50 dB at the operating frequency. These values should be taken carefully, since in real antennas such values of S11 are not usually achieved. Therefore, although they indicate good matching, it is important to take into account that such high values will most likely not be reached in practice.

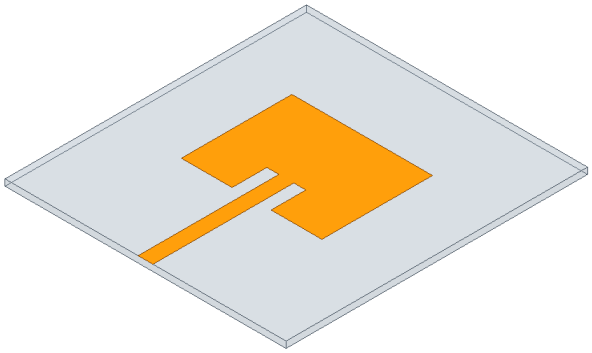

(a) h1 = 1.5 mm, Wp = 33.13 mm, Lp = 26.07 mm, Ls = 8.20 mm, Ws = 2.85 mm.

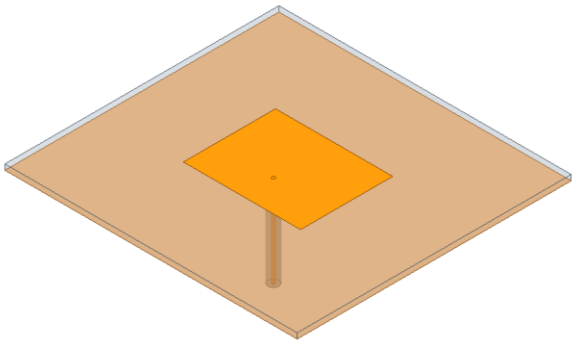

(b) h1 = 1.5 mm, Wp = 32.05 mm, Lp = 25.22 mm, Ri = 0.46, Re = 1.48 mm, Lin = 8.61 mm.

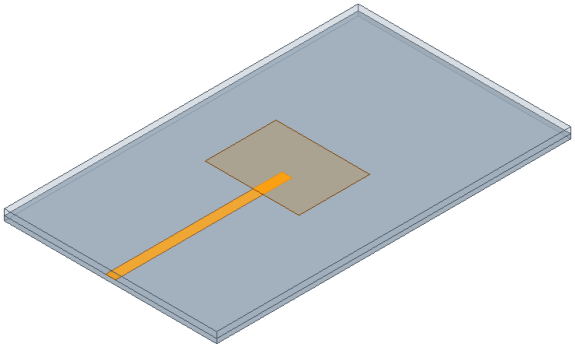

(c) h1 = 1.5 mm, h2 = 2 mm, Wp = 31.14 mm, Lp = 23.51 mm, Lin = 11.60 mm.

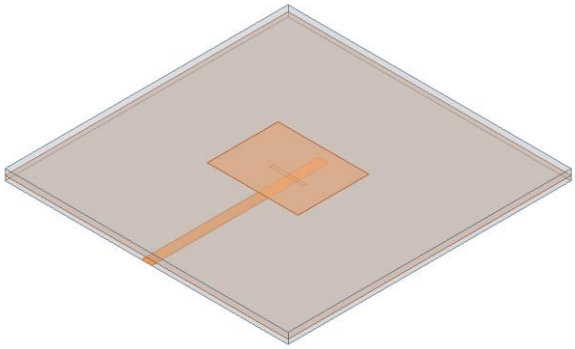

(d) h1 = 1.5 mm, h2 = 2 mm, Wp = 30.04 mm, Lp = 23.43 mm, Lin = 23.5 mm, Ls = 1 mm, Ws = 11.20 mm.

Figure 3.2.- (a) Microstrip feed, (b) coaxial feed, (c) proximity coupled feed, (d) aperture feed. Ground plane in bottom layer.

Due to the characteristics of our design, the chosen feeding techniques are proximity coupled line and aperture feed. This is because they are more adaptable to different antenna designs and more prone to integration with EBG structures. Additionally, for the proximity coupled case, varying the overlap length of the coupled line helps reduce harmonic radiation, namely, the frequencies around the 2^{nd} harmonic, as shown in [14]. Coupled techniques also show low spurious radiation and higher bandwidth than the contacting feeding techniques. The difference in bandwidth with respect to the figures in Table 3.1 is due to the fact that the reference patches have not been optimized in terms of bandwidth, since the main objectives of the thesis is the filtering spurious frequencies and frequency selectivity improvement. However, a final design should also be optimized in terms of bandwidth by means of bandwidth enhancement techniques, such as increasing dielectric slab thickness or using coupled patches.

	Microstrip	Coaxial	Proximity coupled	Aperture
Spurious feed radiation	Feeding line radiation affects antenna radiation pattern.	Probe can radiate in undesired directions.	Minimum.	Low.
PCB manufacturing complexity	Easy (one layer Cu etching and 1 substrate).	Drilling required.	Alignment required + more boards needed → cu/etching steps.	Alignment required + more boards needed → cu/etching steps.
Impedance matching	Inset feed.	Matching is achieved by correctly positioning probe.	Feedline positioning and dimensions, width-to-length patch ratio.	Slot positioning and dimensions.
Bandwidth	BW 1-2%	BW 1-2%	BW 2-4%	BW 2-3%
Others	Spurious feed line radiation, coupling effects.	Parasitic inductance, critical for thick substrates Inherent asymmetries lead to high order modes which produce cross-polarization.	Need for an additional substrate layer Extra degree of freedom of design Gap produces capacitance that can cancel out feed inductance.	Need for an additional substrate layer Feed shielded from antenna by PEC Independent optimization of feed mechanism element.

Table 3.1.- Comparison of feeding techniques.

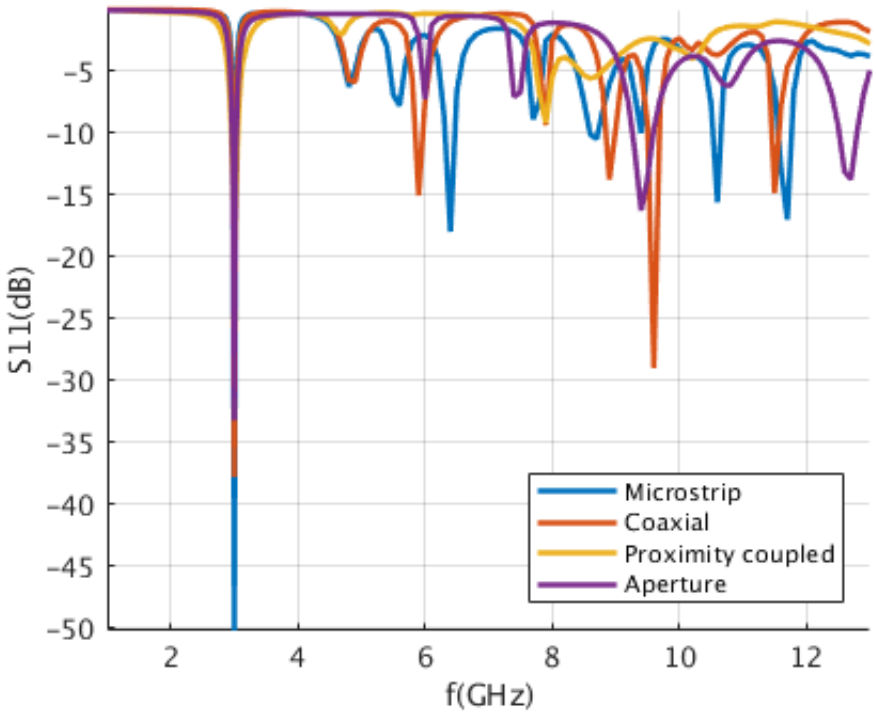

Figure 3.3.- Design feeding techniques comparison.

	Microstrip	Coaxial	Proximity coupled	Aperture
f0	3 GHz	3 GHz	3 GHz	3 GHz
f0 matching (S11)*	-50.20 dB	-37.77 dB	-25.42 dB	-33.19 dB
Bandwidth (-10dB)	1.60%	1.67%	3.50%	2.33%
2nd harmonic frec.	6.4 GHz	5.9 GHz	-	6 GHz
2nd harmonic S11	-17.96 dB	-15.01 dB	-	-7.25 dB
3rd harmonic frec.	8.7 GHz	8.9 GHz	7.9 GHz	9.4 GHz
3rd harmonic S11	-10.45 dB	-13.73 dB	-9.17 dB	-16.23 dB
Other spurious frec.	10.6 GHz, 11.7 GHz	9.6 GHz, 11.5 GHz	-	12.7 GHz
Other spurious S11	-15.58 dB, -16.97 dB	-28.98 dB, -14.85 dB	-	-13.71 dB

Table 3.2.- Parameters of analyzed patches by feeding technique.

The following chapter focuses on improving antenna characteristics by introducing EBG structures in the design. For comparison purposes, the final design will be shown taking both the proximity coupled fed and the aperture fed patches as a references.

3.2.- Reference patch

The proximity coupled feed is the technique used for the reference patch because of its inherent 2nd harmonic filtering feature described in the previous section. The reference design is shown in Figure 3.2.c and its frequency response is seen in yellow in Figure 3.3. It can be seen from Figure 3.3 that the main source of spurious radiation for this design, but also for the other designs, is located in the frequency band of 7 GHz to 11 GHz. Spurious components in this band are spread around the 3rd harmonic due to the excitation of different modes. Therefore, chapter 4 focuses on the design of a filtering structure, based on the mEBG, that allows to achieve a filtenna that has a passband around 3 GHz and successfully filters out the frequencies in the band from 7 GHz to 11 GHz, with a minimum rejection level of 20 dB, as specified in the objectives (section 1.2).

4.- MUSHROOM EBG CONFIGURATIONS AND RESULTS

The objective of this chapter, as announced in section 3.1, is to design an EBG filtering structure that has its stopband in the range of frequencies from 7 GHz to 11 GHz. For that purpose, the mEBG has been chosen among the different available EBG structures, as was indicated at the end of section 2.2, because:

- An analytical model (section 2.2) exists for the mEBG that allows to understand its features and behavior, and is useful to create initial designs.
- The mEBG has been analyzed by researchers around the world and publications are available that validate the EBG nature of this structure [3-5] and its potential filtering applications [14-15], that do not exist for other EBG structures.
- The mEBG shows a wider band gap than other EBG structures [2] thanks to its ground vias. This feature can be useful for the design of a wideband band stop filter.

The organization of this chapter is as follows: in section 4.1, the mEBG structure described in section 2.2 is modeled using both MatLab and HFSS software, in order to characterize its behavior and find the building parameters that are suitable for our filtenna design. In this section, the mEBG is also simulated in combination with microstrip line and patch antenna elements, having the mushroom patch on the same level as microstrip line and antenna patch. In sections 4.2 and 4.3, the mEBG obtained in section 4.1 is tuned so that its band gap is maintained when an additional conducting layer (microstrip line or patch antenna) is placed above it. Therefore, the analysis in sections 4.2 and 4.3 is the same as that in section 4.1, but the way that the mEBG is integrated with the microstrip line and the patch antenna is different, since it is located underneath them and not on the same level. An overview of the configurations analyzed in each section is given in Figure 4.1.

Results obtained in this chapter allow to check the suitability or not of different mEBG configurations for its use in the final design, that is shown in chapter 5.

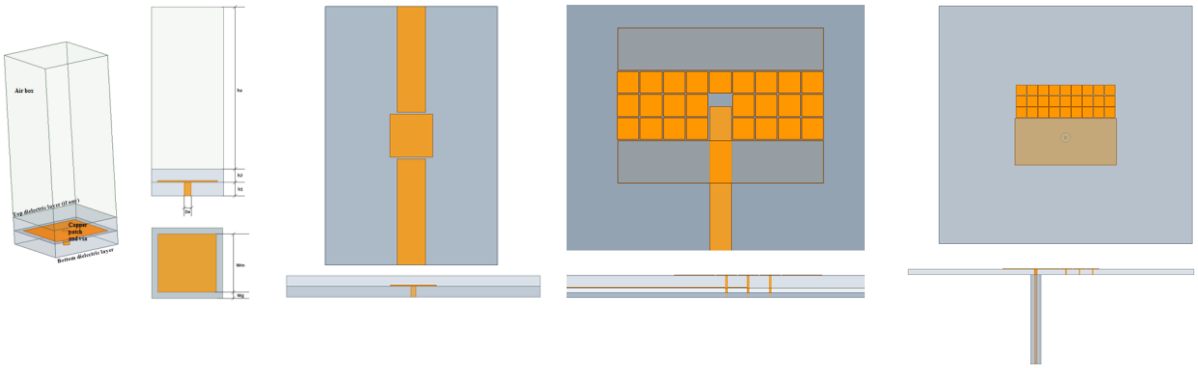

(a)

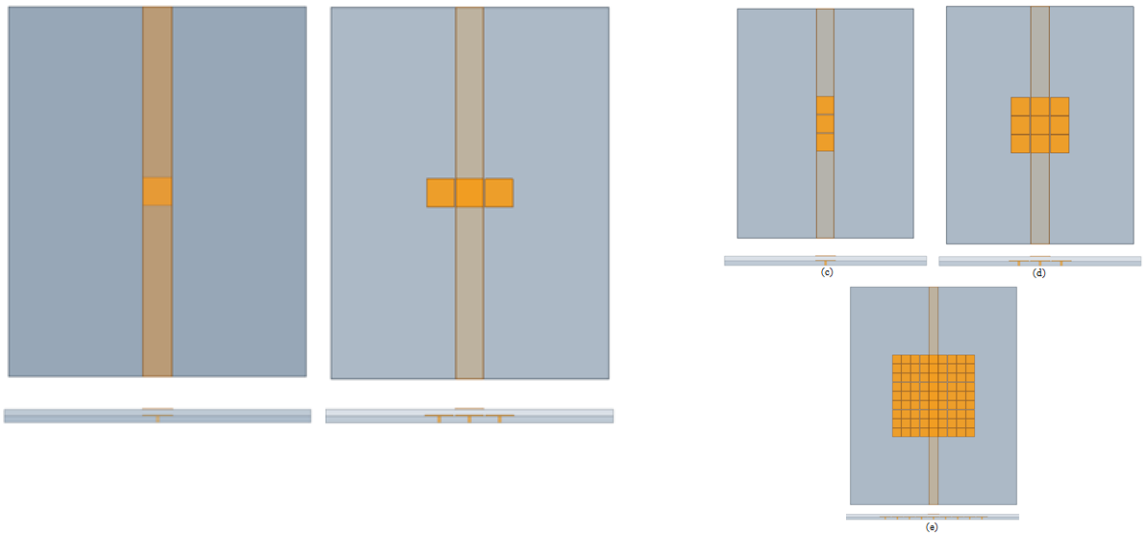

(b)

(c)

Figure 4.1.- Overview of configurations studied in (a) section 4.1, (b) section 4.2, and (c) section 4.3.

4.1.- Standalone mushroom EBG

In sections 4.1.1 and 4.1.2, the mEBG will be characterized with generic building parameters, as described in figure 4.2, using both the MatLab model and HFSS eigensolver (see appendix A.2 setup details). Different configurations are explored, and one of them showing the desired band-gap is proposed. The mEBG is then integrated with a 50 Ω microstrip line, as explained in section 4.1.3. Finally, in section 4.1.44.1.4.-, integration with both a coaxial and a proximity coupled fed patch antenna are analyzed.

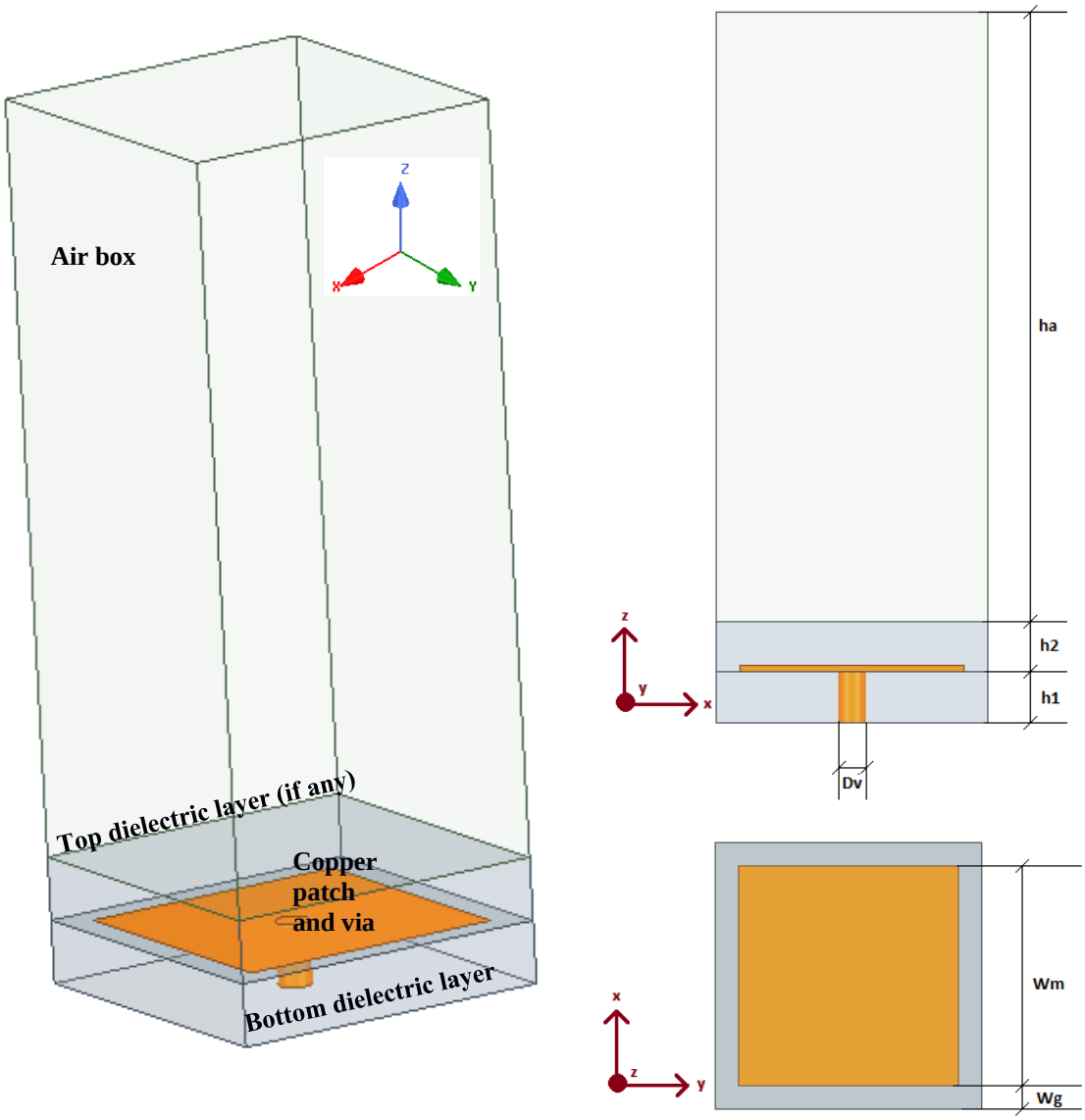

Figure 4.2.- Generic building parameters (mm) of mushroom EBG unit cell.

4.1.1.- Determining band gap and modes with MatLab model

An analytical model based on the theory in section 2.2 was developed in [28] with its corresponding MatLab code (not disclosed due to Thales confidentiality policy). Luckily, it has been possible to use it in this work, which has enabled a theoretical first estimation of mEBG building parameters. Using such code, the dispersion diagram shown in Figure 4.3 was obtained with the initial parameters in Table 4.1. The yielded analytical bandgap goes approximately from 7.8 to 10.8 GHz and is highlighted in grey.

The fact that propagation of electromagnetic modes is forbidden in this band gap means that the mEBG can potentially be used to build a band stop filter and integrated in microwave subsystems, in the case of this work, a microstrip line (sections 4.1.3 and 4.2) and a microstrip patch antenna (sections 4.1.4 and 4.3).

Name	h1 (mm) - er1	Wm (mm)	Wg (mm)	Periodicity (mm)	Dv (mm)	h2 (mm) - er2
MushInit	0.75 – 3.55	5	0.2	5.2	0.4	Air

Table 4.1.- Initial mEBG building parameters.

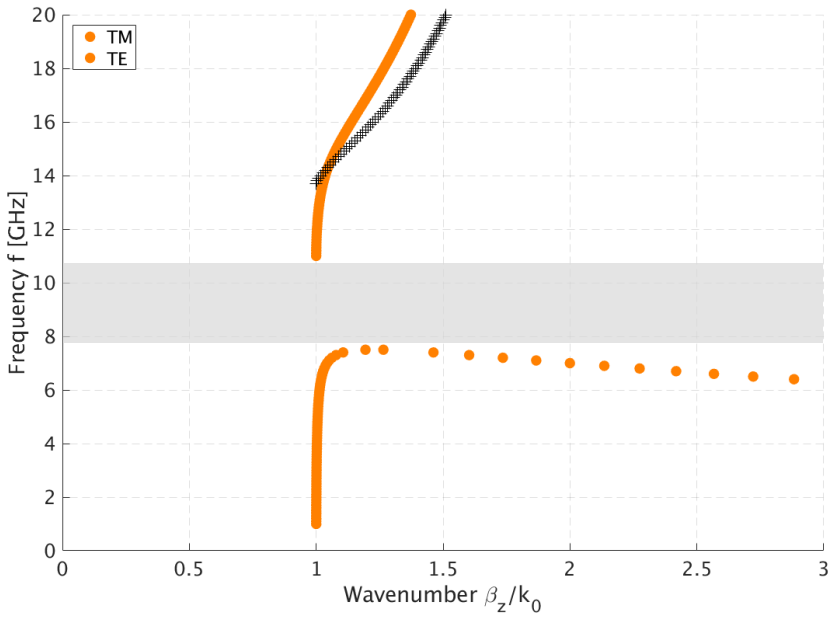

Figure 4.3.- Initial mEBG dispersion diagram.

4.1.2.- Determining band gap and modes with HFSS eigensolver

With the previous initial design as a reference, different mushroom configurations have been analyzed to see how changes in mushroom dimensions and dielectric slabs affect its electromagnetic properties, particularly band gap width and border frequencies. The characteristics of each mushroom configuration are summarized in Table 4.2, and results are displayed in Figure 4.4.

Please note that dispersion diagrams generated with the MatLab code have the propagation constant β (rad/m) normalized to k_0 (rad/m) (vacuum propagation constant), whereas HFSS diagrams show the propagation constant β (deg/m) multiplied by distance d (m) to amount for a phase difference of up to 180 degrees. This is due to the way that the HFSS eigensolver is set up (see appendix A.2). However, this difference in the *x*-axis does not affect the frequency position of the band gap, so a comparison between HFSS and MatLab results in terms of band gap is still valid. In both HFSS and MatLab, β and β_z, respectively, translate to β_x from the point of view of the coordinate system used for our designs, so the surface wave direction of propagation is the *x* direction.

Name	h1 (mm) - er1	Wm (mm)	Wg (mm)	Periodicity (mm)	Dv (mm)	h2 (mm) - er2
MushInit	0.75 – 3.55	5	0.2	5.2	0.4	Air
Mush2	1.5 – 3.55	5	0.2	5.2	0.4	Air
Mush3	0.75 – 10.2	5	0.2	5.2	0.4	Air
Mush4	0.75 – 3.55	3	0.2	3.2	0.4	Air
Mush5	0.75 – 3.55	5	1	6	0.4	Air
Mush6	0.75 – 3.55	5	0.2	5.2	0.2	Air
Mush7	0.75 – 3.55	5	0.2	5.2	0.4	0.75 – 3.55

Table 4.2.- Analyzed mushroom configurations. Dimensions in mm.

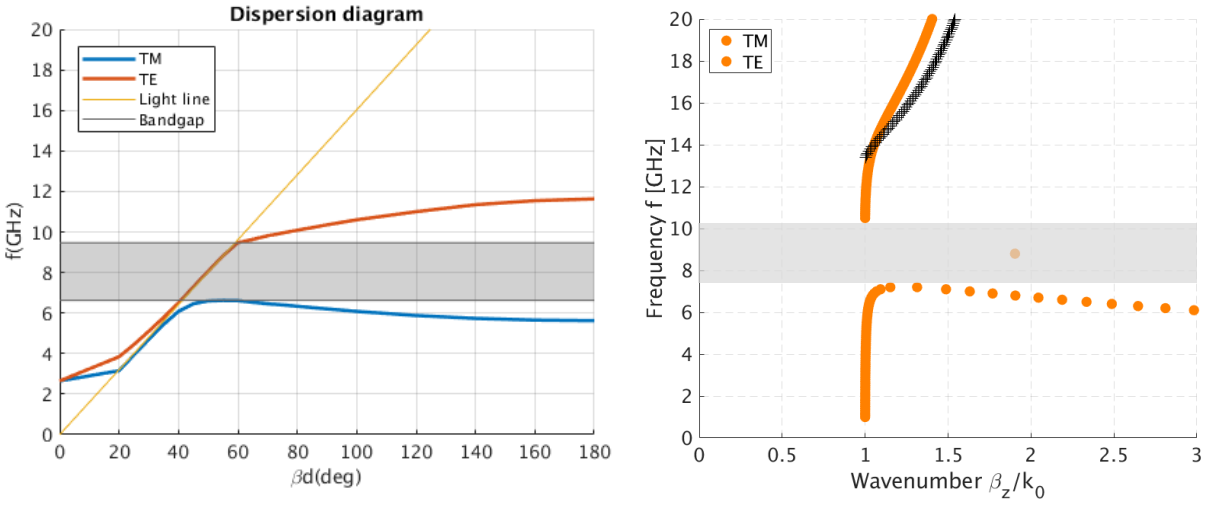

(a) MushInit

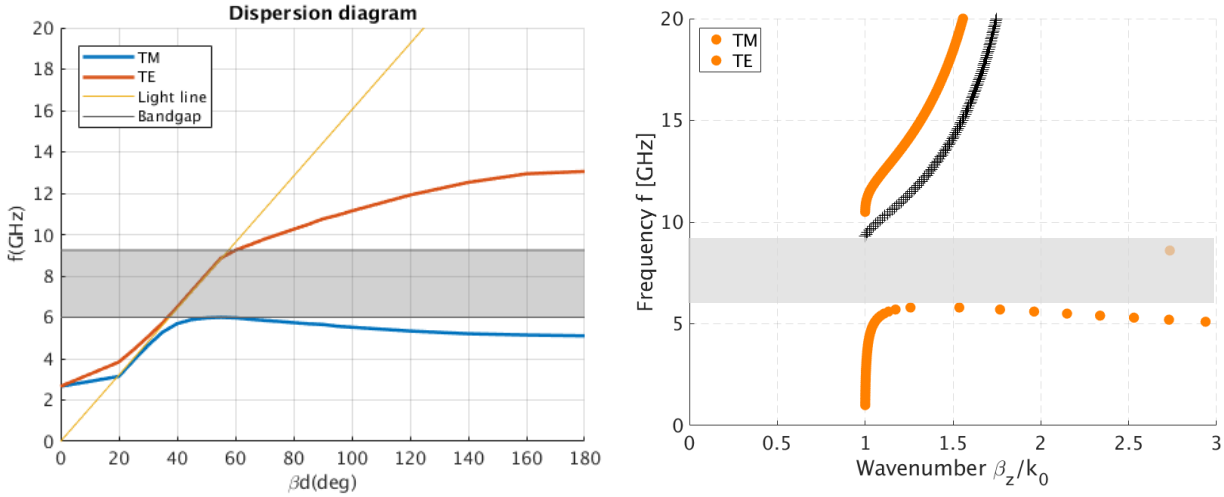

(b) Mush2

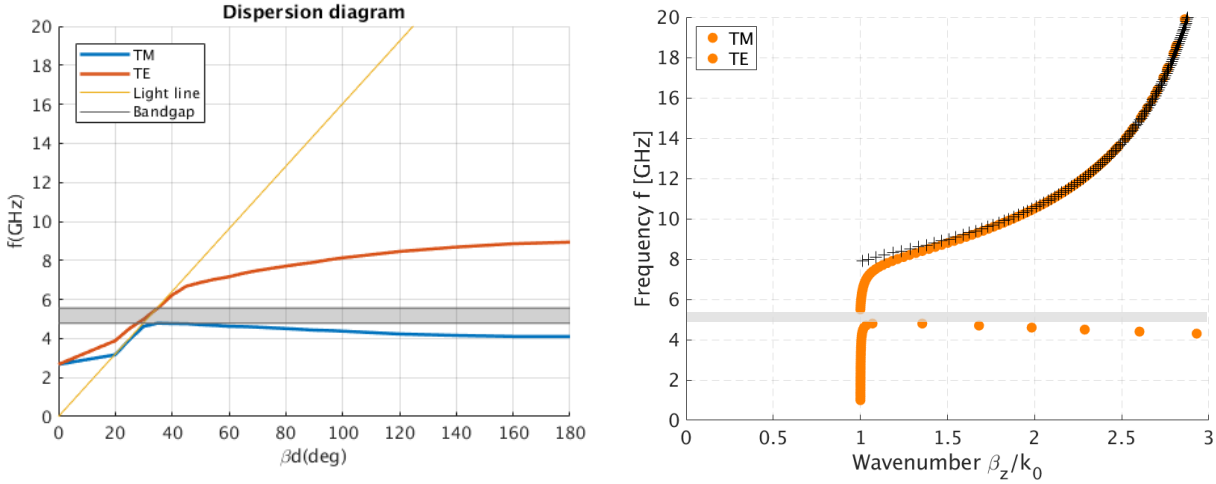

(c) Mush3

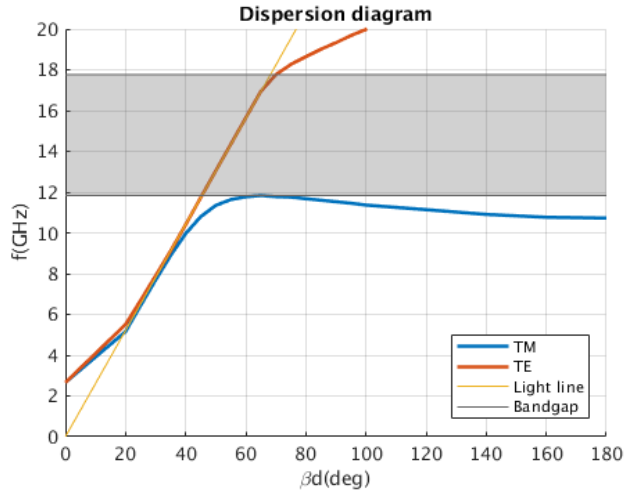

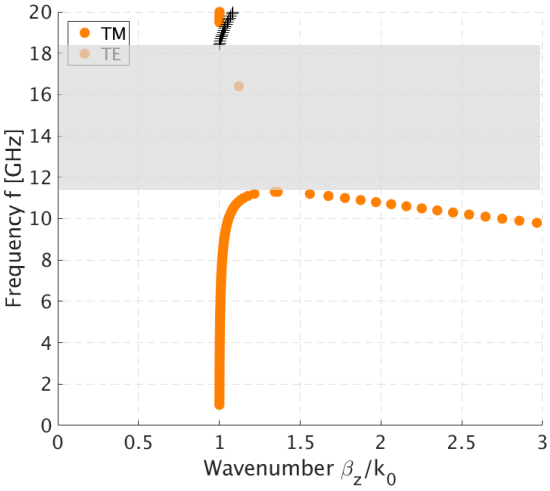

(d) Mush4

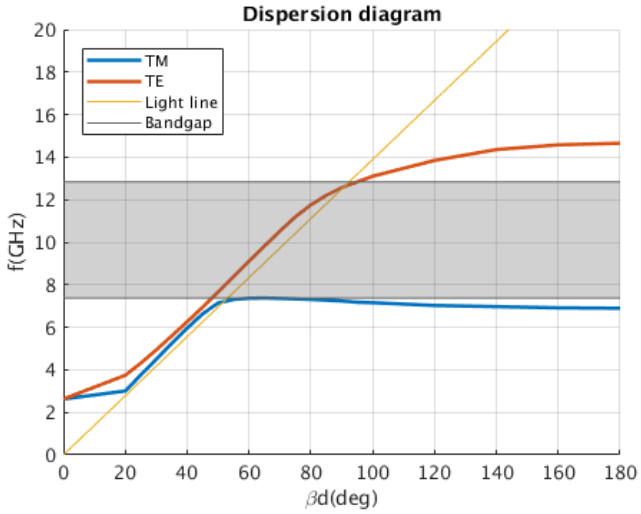

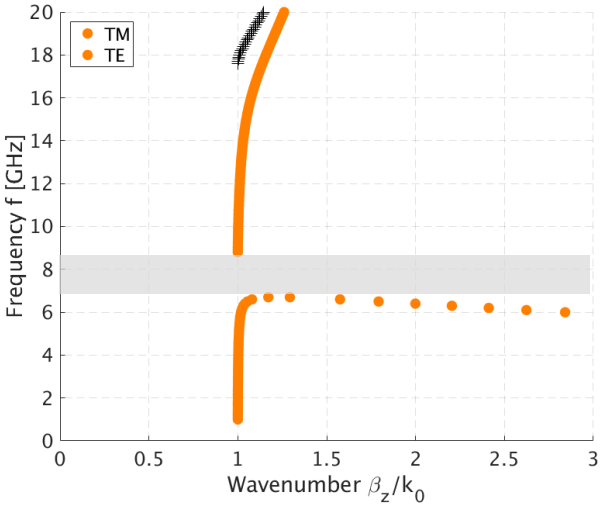

(e) Mush5

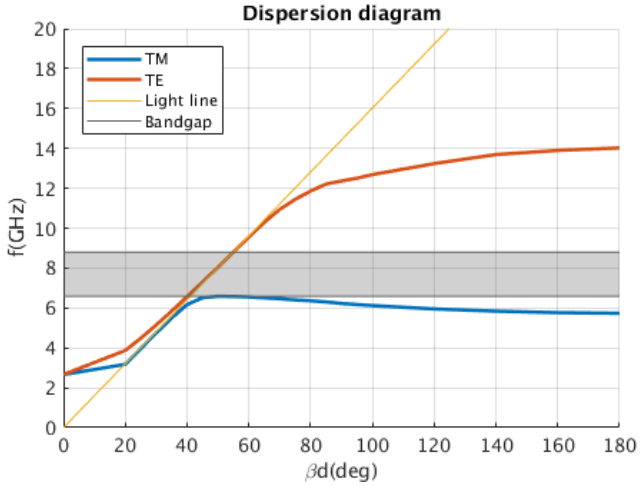

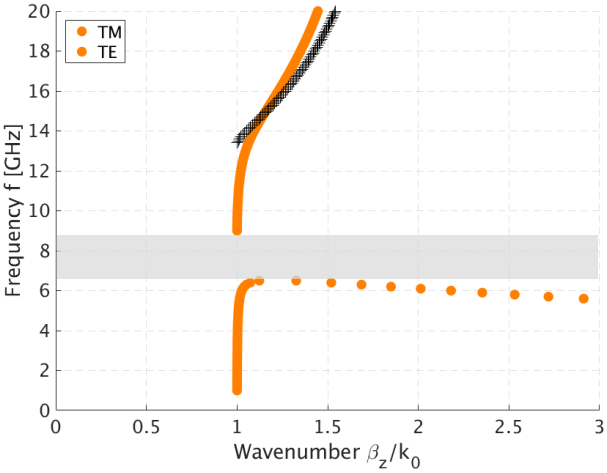

(f) Mush6

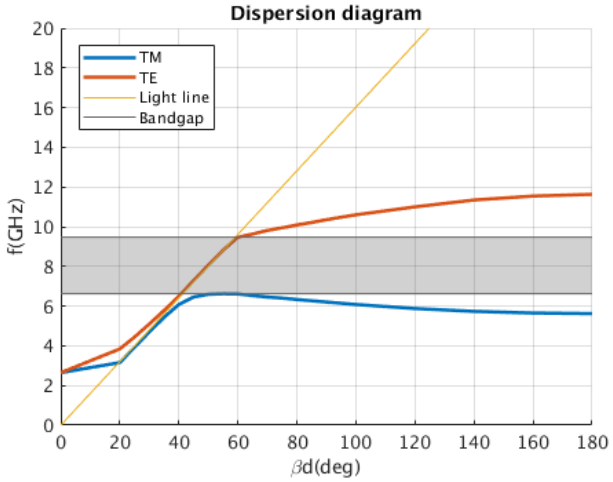

Not in model.

(g) Mush7

Figure 4.4.- Dispersion properties of mushroom configurations. HFSS solution (left) vs. MatLab model (right).

Taking configuration MushInit as a reference, Table 4.3 is created, and some conclusions can be obtained as to how physical configuration affects the band gap:

- Increasing mushroom height reduces band gap frequency.
- Increasing permittivity of mushroom slab leads to narrower, lower frequency band gap.
- Decreasing mushroom patch area leads to broader, higher frequency band gap.
- Increasing gap width leads to narrower, lower frequency band gap.
- Decreasing via diameter leads to lower frequency band gap.
- Adding a dielectric slab on top of mushroom structure does not seem to affect the frequency band gap when the dielectric material is the same as that of the substrate layer and for similar dimensions of both layers.

Name	**Parameter change**	**MatLab model bandgap**	**HFSS bandgap**
MushInit	-	7.2 – 10.5 GHz	6.62 – 9.47 GHz
Mush2	Increased mushroom slab height (h1)	5.8 – 9.3 GHz	6.00 – 9.24 GHz
Mush3	Increased mushroom slab permittivity (er)	4.8 – 5.5 GHz	4.78 – 5.56 GHz
Mush4	Reduced mushroom patch size (Wm)	11.3 – 18.4 GHz	11.83 – 17.76 GHz
Mush5	Increased gap width (Wg) / increased periodicity	6.7 – 8.8 GHz	7.37 – 12.84 GHz
Mush6	Reduced via diameter (Dv)	6.5 – 9.0 GHz	6.58 – 8.80 GHz
Mush7	Dielectric top slab (h2)	-	6.62 – 9.47 GHz

Table 4.3.- Parametric bandgap comparison for both MatLab and HFSS solvers.

With this in mind, it is possible to design a structure that creates a band gap with the desired width and frequency limits. The first specific design was made for the 3rd harmonics in the proximity coupled fed patch, because thanks to the technique in [14] (variation of inset length of the feed line with respect to the patch), the 2nd harmonics are initially suppressed (Figure 3.3).

The following subsections focuses on the use of the mushroom structure in different positions in the design, with the objective of determining an optimal position that allows to effectively suppress the unwanted frequency components.

4.1.3.- Application to microstrip line

Mushroom configuration Mush7 was placed along a 50 Ω microstrip line, as shown in Figure 4.5, and a driven mode analysis was performed to find how its predicted bandgap affect wave transmission in the microstrip line. Mushroom configuration Mush7 was chosen because it shows the same band gap as MushInit, but has an additional layer of dielectric material on top, that will be necessary for the latter integration of the design with the patch antenna. The obtained band gap can be seen in Figure 4.6. For our purpose, this is not the desired band stop behavior, but more of a band pass from 6 GHz to 11 GHz. The reason for this behavior is that the configuration in Figure 4.5 is that of a coupled line band pass filter, so using the mushroom as part of the feed line is discarded.

Note, as was the case for reference patches (section 3.1), that an S21 value of -70 dB is the result of the application of electromagnetic equations by the HFSS software and most likely does not match real results, that will have a smaller magnitude.

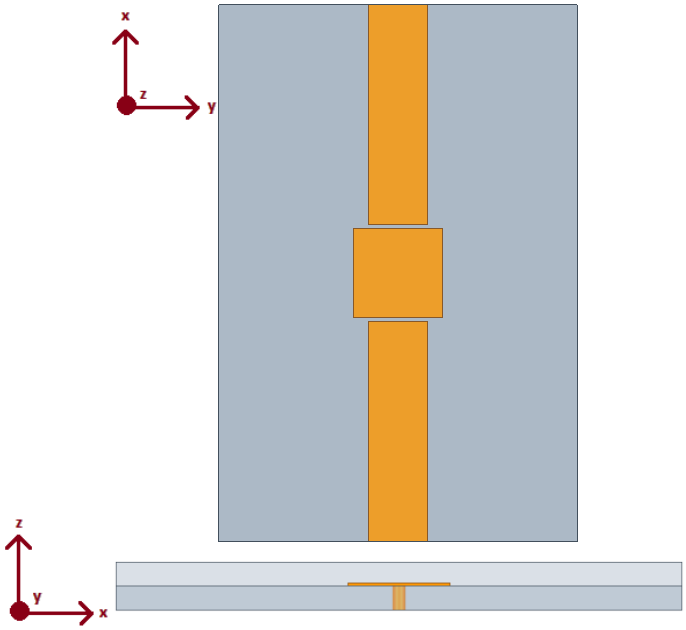

Figure 4.5.- Mushroom EBG along the microstrip line.

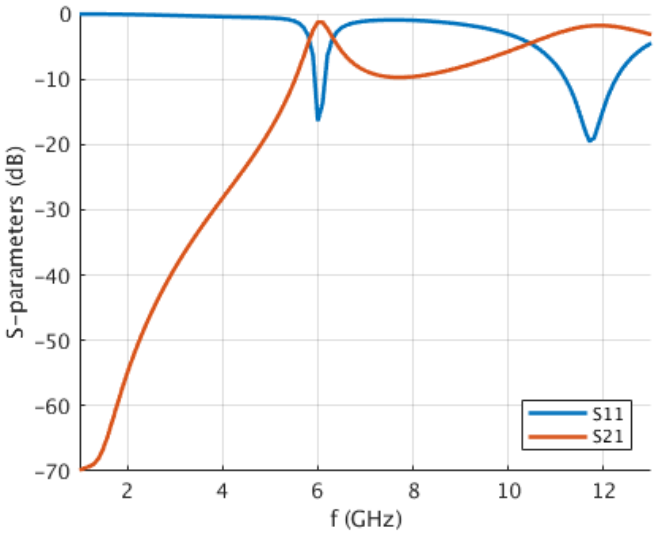

Figure 4.6.- S-parameters of mushroom in feed line.

4.1.4.- Application to microstrip patch antenna

For this analysis, mushroom configuration Mush2 is selected because its height of 1.5 mm matches the height of the substrate layers supporting the patch antenna and also shows a band gap similar to that of MushInit. The mushroom was integrated in two patch designs, differing only in the feeding technique (one proximity coupled, the other one coaxial fed). Such configurations are depicted in Figure 4.7, and results are shown in Figure 4.8.

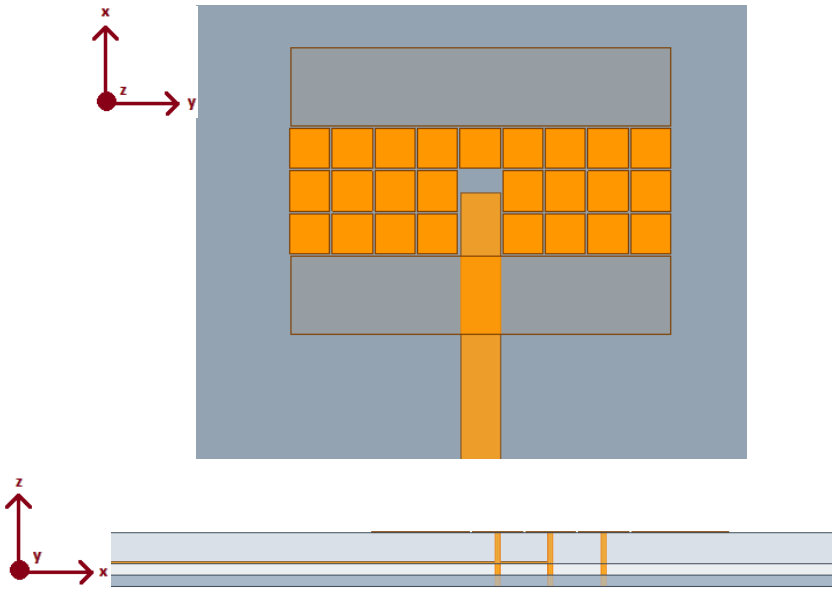

(a)

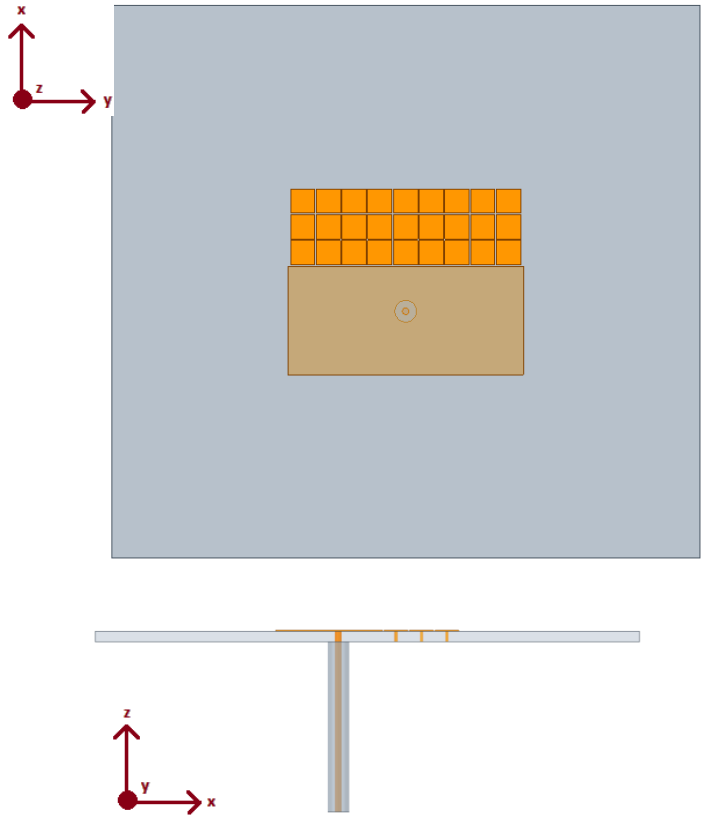

(b)

Figure 4.7.- Patch designs integrating mushroom EBG.

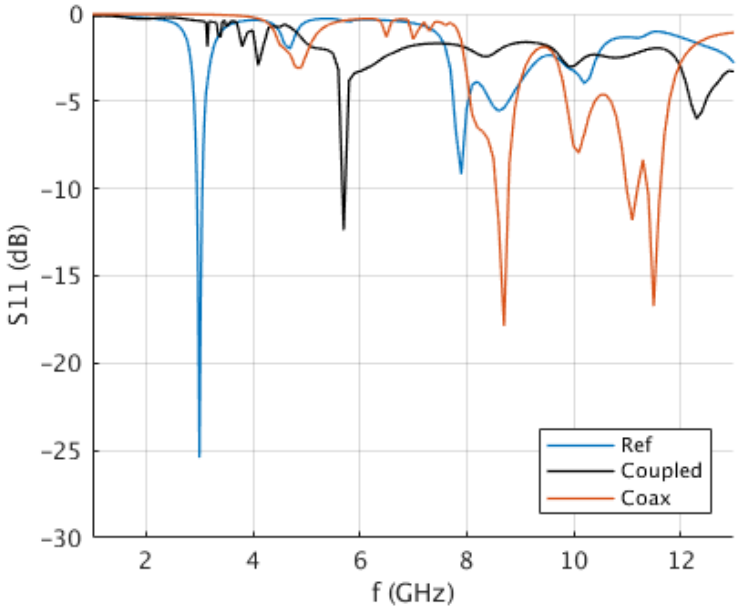

Figure 4.8.- S-parameters of proximity coupled design and coaxial fed design.

4.2.- Microstrip line – Mushroom EBG

In this section the mushroom structure is placed underneath a microstrip line in order to observe how the band gap affects the propagation of waves along the line and confirm or deny the possibility of using the mushroom EBG as a filtering element. This study is necessary before integrating the mushroom structure underneath a patch antenna because a microstrip patch antenna is nothing but a larger piece of microstrip line with specific dimensions to achieve resonance at desired frequencies.

4.2.1.- Determining band gap and modes with HFSS

The parametric study carried out in section 4.1.2 is useful to determine the behavior of the isolated mushroom grid, but cannot be used to describe the behavior of mushroom EBG structures when they are integrated with other RF components, such as a microstrip line or a patch antenna, because they interact with each other, altering the impedance and dispersion properties of the new structure. Therefore, a new dispersion analysis need to be carried out for each new configuration before deciding whether the integration shows desired properties or not. Such studies are presented in the subsequent sections.

4.2.1.1.- Row of mushrooms

Due to the interaction between the microstrip line and the mushroom (their combination shows an impedance different from that of the isolated mushroom structure), Mush7 can no longer be used to achieve the desired band gap, and its size needs to be adjusted. The easiest way to find out what parameters to adjust is to run a driven mode simulation using Mush7 and observing the results. For that purpose, a microstrip line was placed on top of substrate 2 of Mush7 to check its behavior (as in Figure 4.15.a). The total height of both substrates equals $h1 + h2 = 1.5\,mm$, so for RO4003 material the width of the microstrip line is 3.3 mm to achieve a 50 Ω impedance. Results for this configuration are shown in Figure 4.9.

The S21 minimum when using a single mEBG, as seen in Figure 4.9, indicates the center frequency of the band gap, located at 5.5 GHz approximately, instead of the desired and predicted 8.5 GHz. As a result, this frequency shift needs to be corrected. This can be done relatively easily by reducing mEBG patch area, resulting in a higher resonance frequency (smaller capacitance) and thus higher frequency band-gap. For this purpose, simulations for different configurations have been run, yielding the new mEBG parameters shown in Table 4.4, that will be used for the designs from now on.

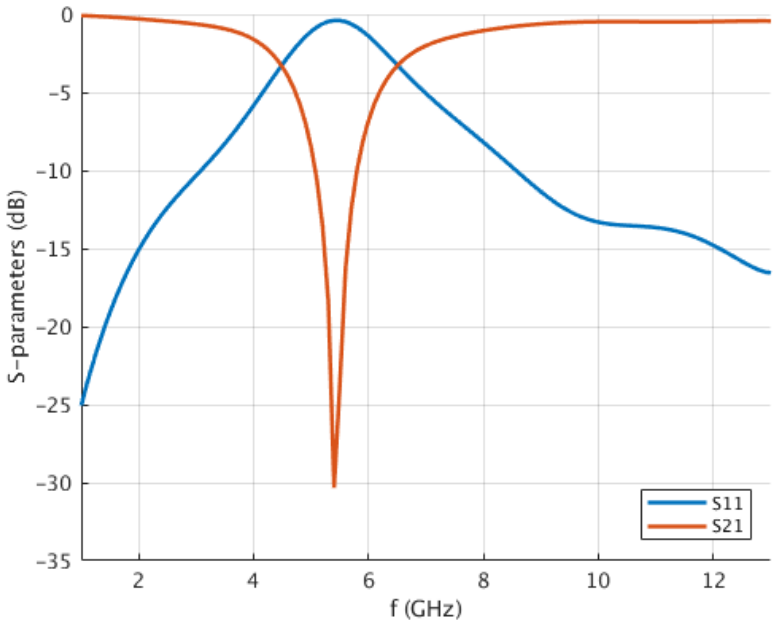

Figure 4.9.- Mush7 results for single mEBG cell.

Name	h1 (mm) - er1	Wm (mm)	Wg (mm)	Periodicity (mm)	Dv (mm)	h2 (mm) - er2
MushTuned	0.75 – 3.55	3.3	0.2	3.5	0.4	0.75 – 3.55

Table 4.4.- Adjusted mEBG parameters.

To confirm that MushTuned shows the desired band gap properties, an eigenmode solver simulation is run with the configuration shown in Figure 4.10, which yields the desired results, as seen in Figure 4.11. The periodic boundary conditions are set in the *x* direction (see appendix A.2), simulating a long row of mEBG with a microstrip line on top.

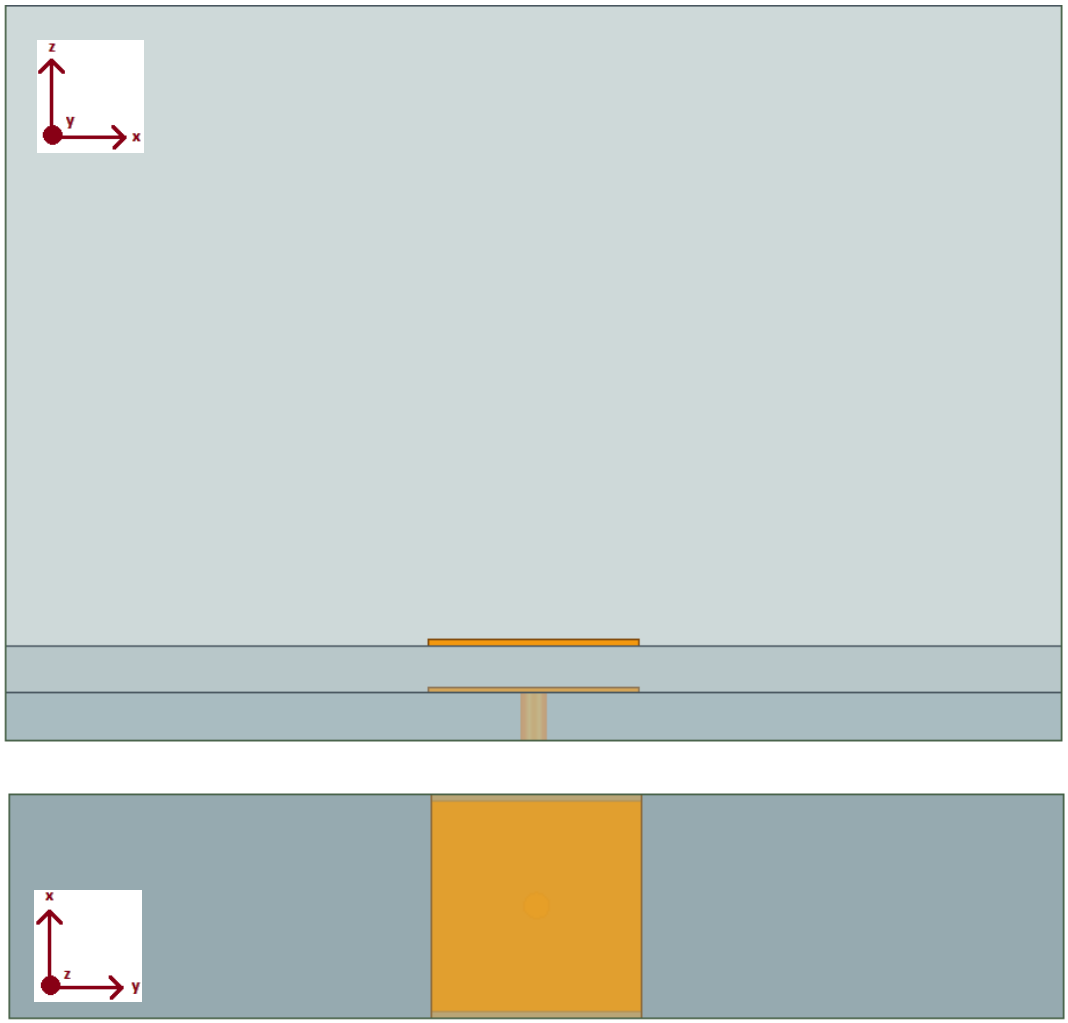

Figure 4.10.- Microstrip line on top of tuned mEBG.

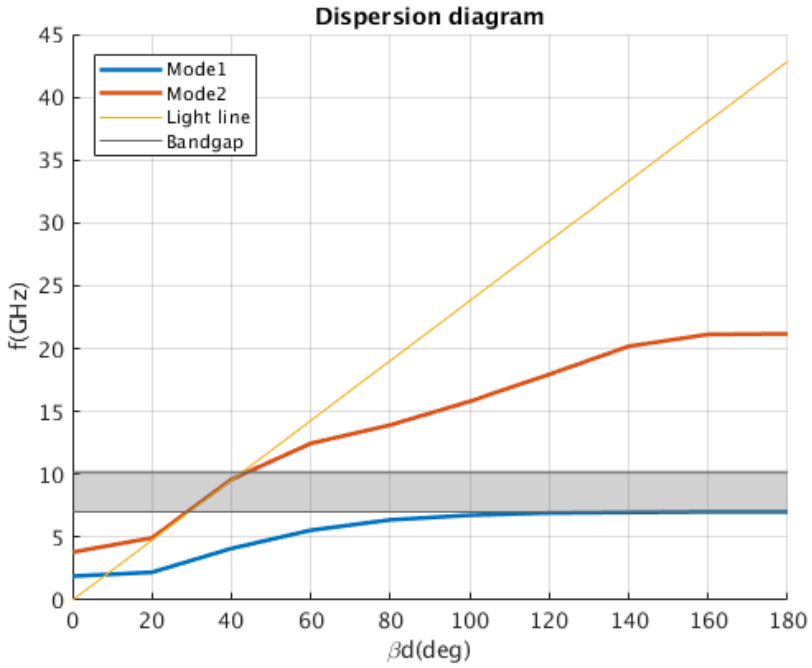

Figure 4.11.- Dispersion diagram of tuned mEBG structure with microstrip line above.

4.2.1.2.- Grid of mEBG

A dispersion analysis of the MushTuned structure is performed using HFSS Eigenmode solver. The set up is shown in Figure 4.12, and results are displayed in Figure 4.13.

From Figure 4.13 it can be observed that mode 3 matches the field propagation in the driven mode solution in Figure 4.23, while the normal microstrip mode still exists (mode 1). At 7.4 GHz, however, mode 1 cannot propagate, so the propagation is produced my mode 3, ruining the band stop behavior at this and other frequencies inside the band gap.

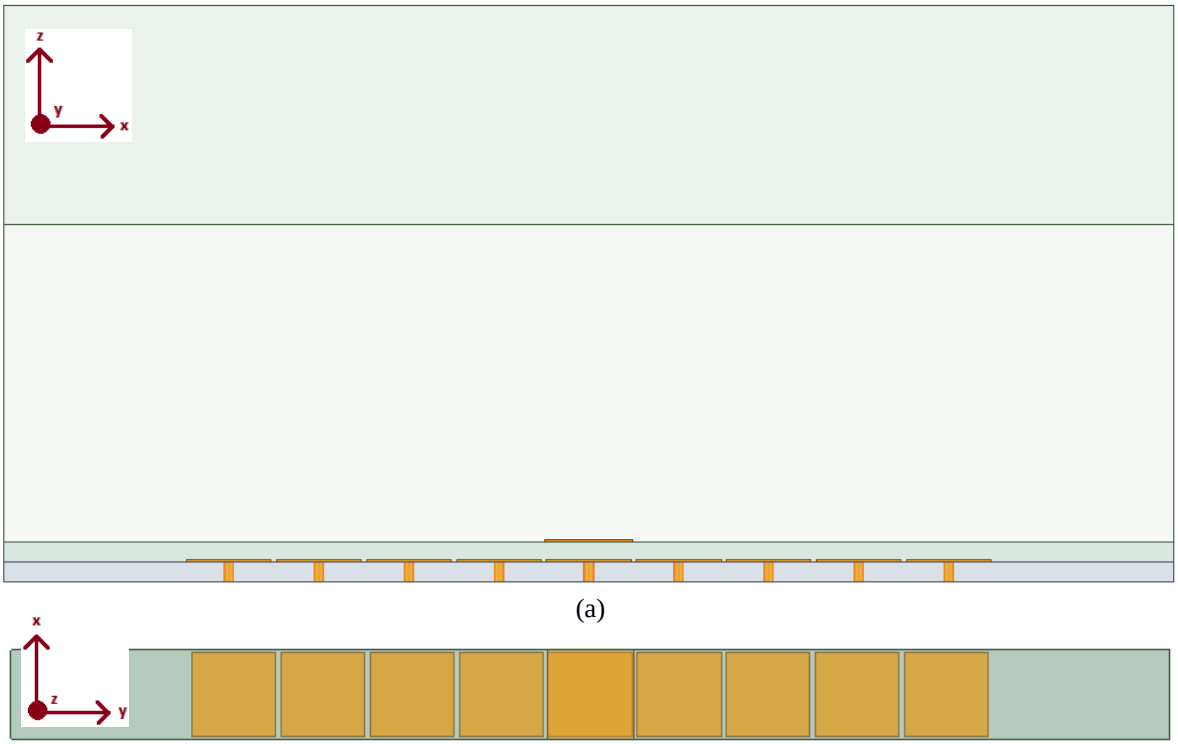

(a)

(b)

Figure 4.12.-mEBG grid configuration for eigenmode solver.

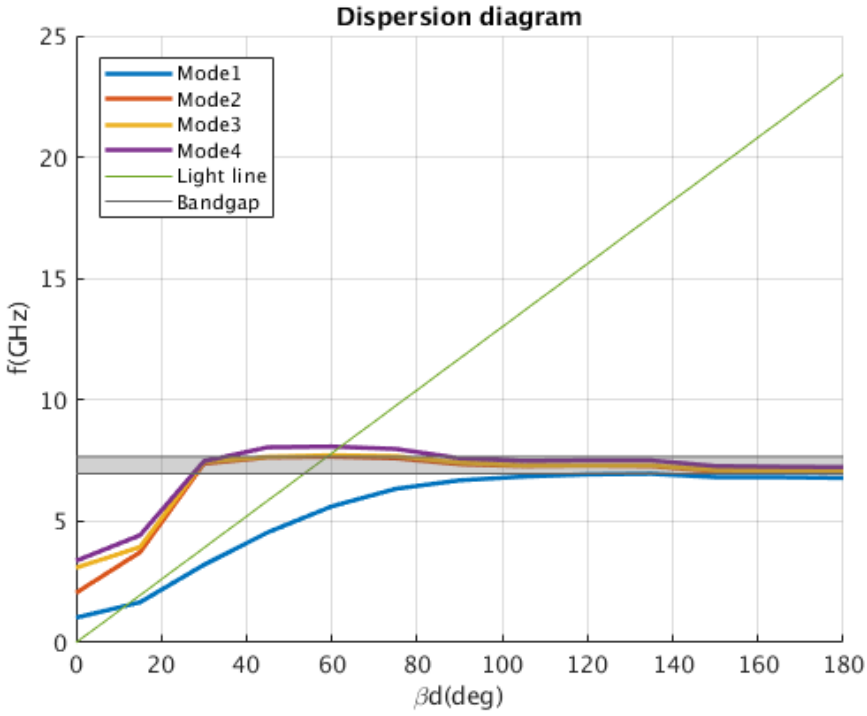

Figure 4.13.-Dispersion diagram of mushroom grid.

4.2.2.- Application as a filter

The MushTuned structure is placed underneath the microstrip line in the configurations shown in Figure 4.14. Thanks to the tuning stage, a stop band appears approximately from 6.5 GHz to 10.5 GHz. This band stop feature can be useful to suppress 3rd order harmonics that exist in these frequencies.

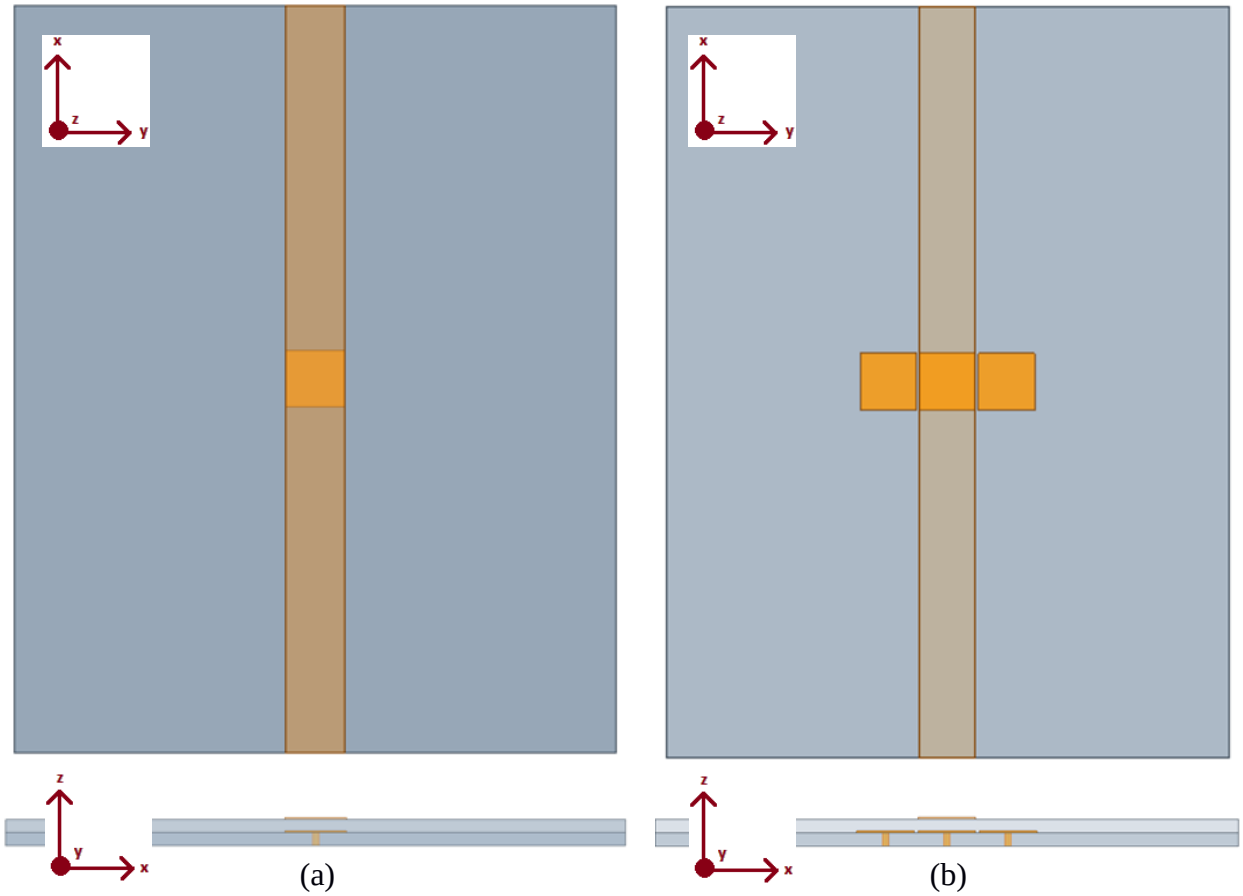

(a) (b)

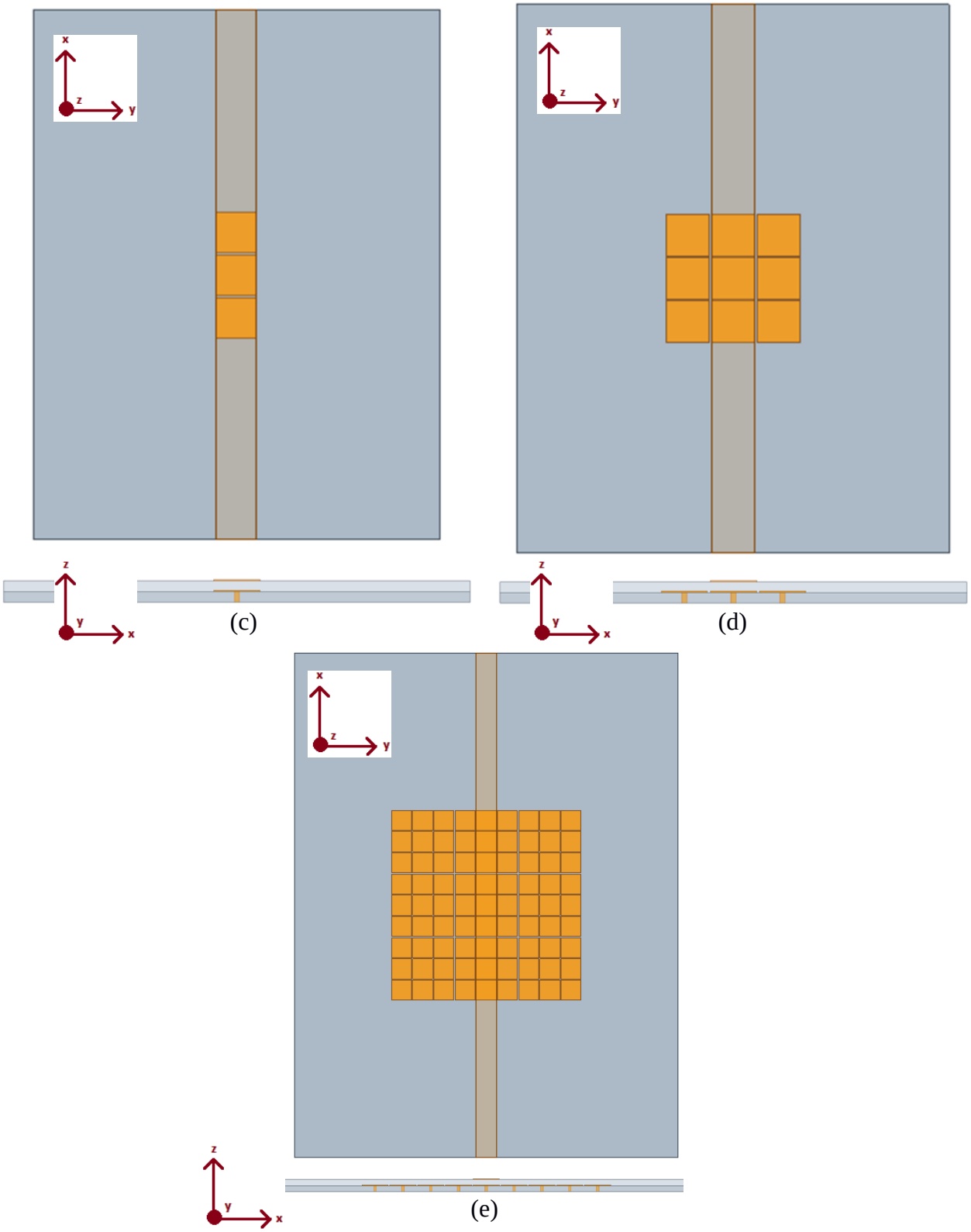

Figure 4.14.- Different configurations of MushTuned under microstrip line.

Figure 4.15 shows the S-parameters for each configuration in Figure 4.14. It can be observed that one mEBG shows a well-defined narrow stop band. When several mEBG are concatenated (Figure 4.14.b and Figure 4.14.c), the band stop width increases. However, the response is quite different for an arrangement perpendicular and parallel to the microstrip line. A wider, more selective stop band is found when the arrangement is parallel. When the mushrooms are placed perpendicularly, the band gap is severely reduced because, for this arrangement, there are other eigenmodes that are allowed to propagate, narrowing the band gap. This is in line with results in section 4.2.1.2. Last, the S-parameters for 3x3 and 9x9 mEBG grids are also plotted.

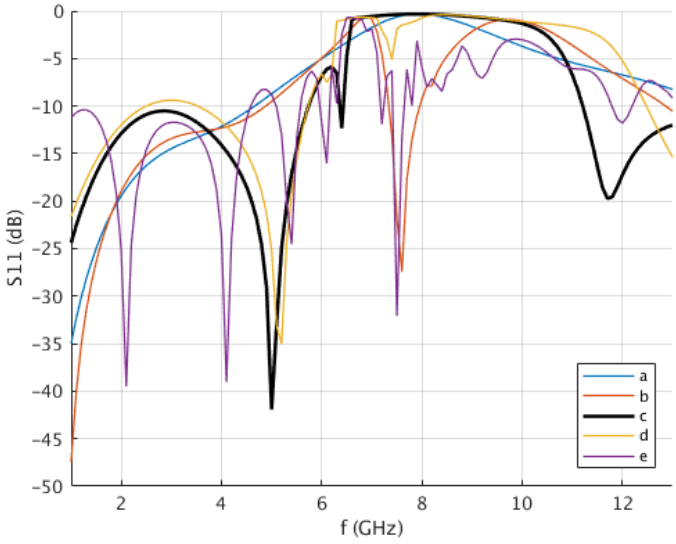

(a)

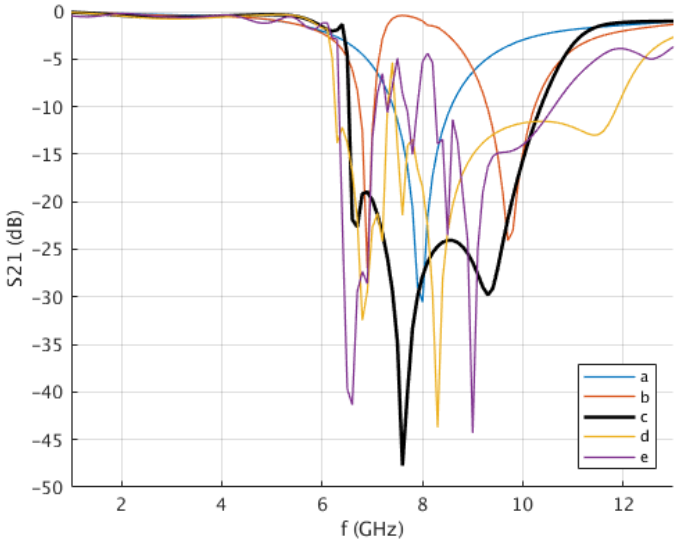

(b)

Figure 4.15.- S-parameters of mEBG underneath feed line.

From the results in Figure 4.15 it can be concluded that the configuration that best fits the filtering purposes is the mEBG grid parallel to the microstrip line, in the direction of wave propagation, as seen in Figure 4.14.c. However, these results and those in section 4.2.1.24.2.1.2.- pose a new question, because they are not completely coherent with the theory. Theoretically, an ideal band gap would be achieved with an infinite grid of mEBG unit cells expanding in both the x and y direction. Instead, optimal results are obtained for a mEBG row, that is, a structure that is infinite in the x direction and consists of only one period of mEBG in the y direction. This phenomenon, predicted by the eigenmode solver simulation in section 4.2.1.2, can be explained in terms of the fringing fields of the microstrip line and their effect on the mEBG. The starting point for this analysis is the field inspection of each structure at three relevant frequencies, one outside the band gap and two inside it. One of the frequencies inside the band gap shows an undesired behavior for the cases where there are mEBG at the sides of the microstrip line (Figure 4.14.b, Figure 4.14.d and Figure 4.14.e). The selected frequencies are:

- f = 3 GHz. It is outside the band gap for all cases, so the mEBG does not affect propagation, that occurs normally.
- f = 6.9 GHz. It is inside the band gap. All configurations work well at this frequency.
- f = 7.4 GHz. It is inside the band gap, but configurations with mushrooms perpendicular to the microstrip line show non-band gap behavior.

Please note that showing results for 6.9 GHz and 7.4 GHz together does not mean that the fields are exactly the same for both frequencies, but the differences are not significant and the interpretation of both is the same. The associated fields for each configuration are:

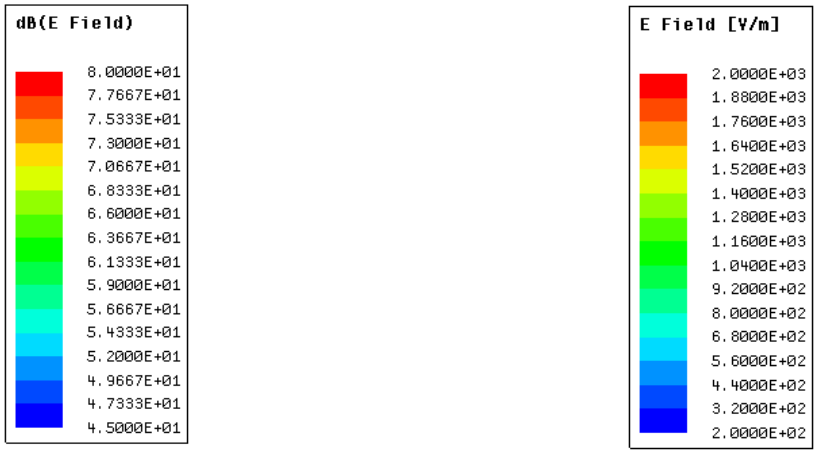

(a) Magnitude plots. (b) Vector plots.

Figure 4.16.-Scales for (a) magnitude and (b) vector plots..

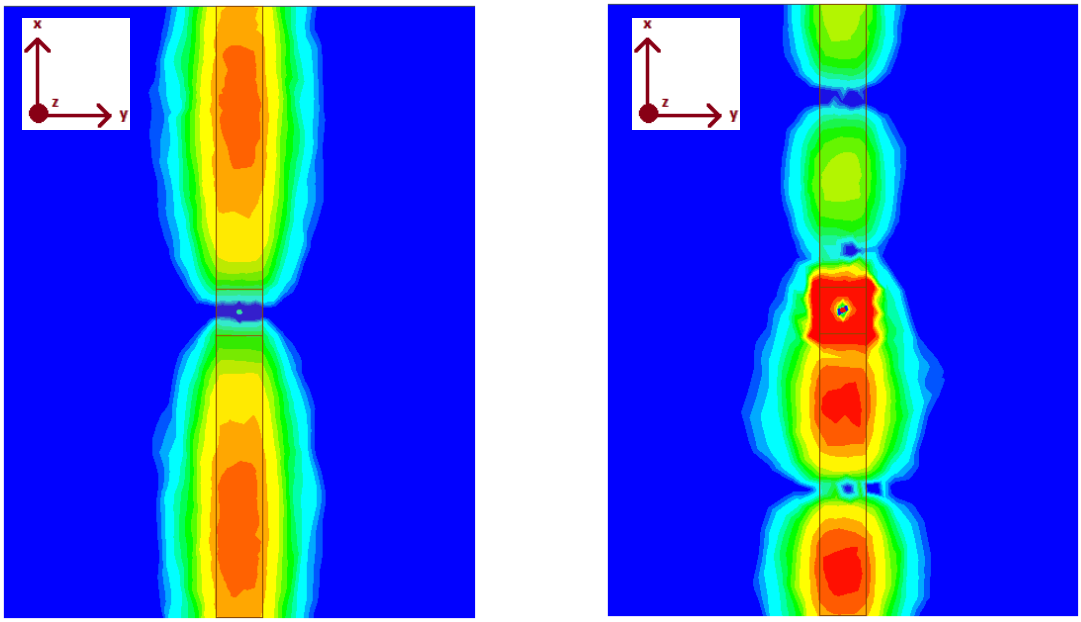

(a) 3 GHz (b) 6.9 GHz and 7.4 GHz

Figure 4.17.- Magnitude of the electric field E on the plane between dielectrics, where the mEBG patch is located.

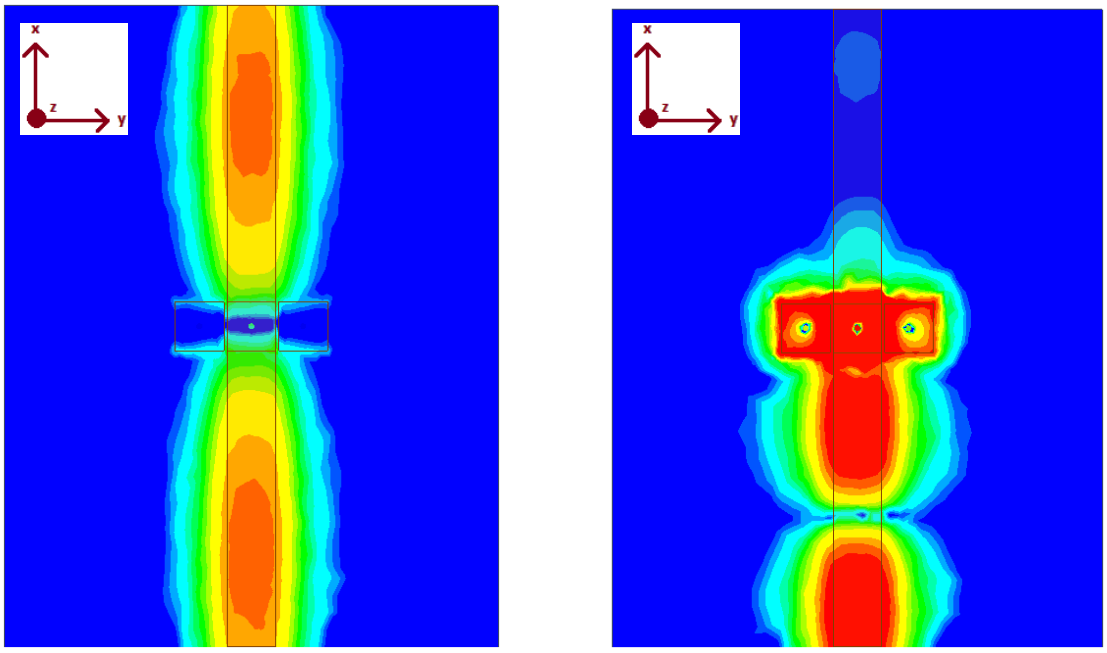

(a) 3 GHz (b) 6. 9 GHz

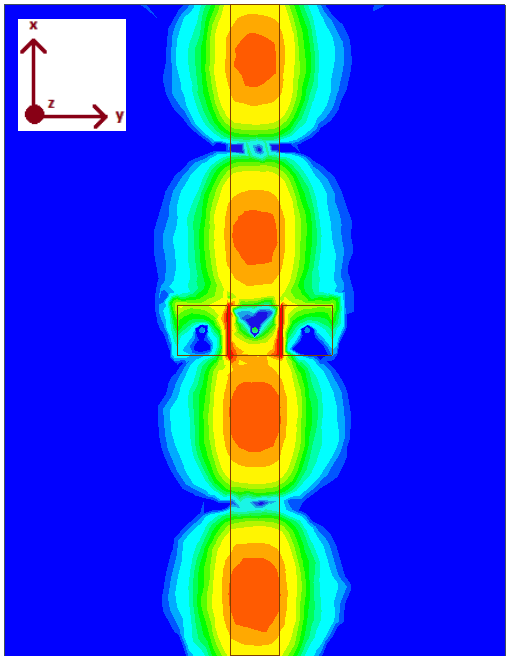

(c) 7.4 GHz

Figure 4.18.- Magnitude of the electric field E on the plane between dielectrics, where the mEBG patches are located.

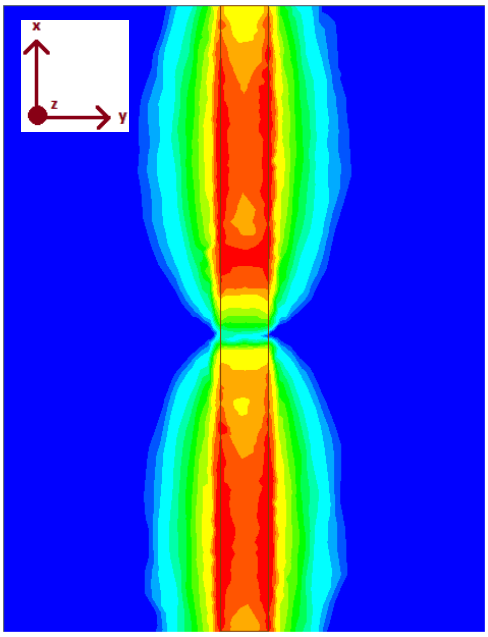

(a) 3 GHz

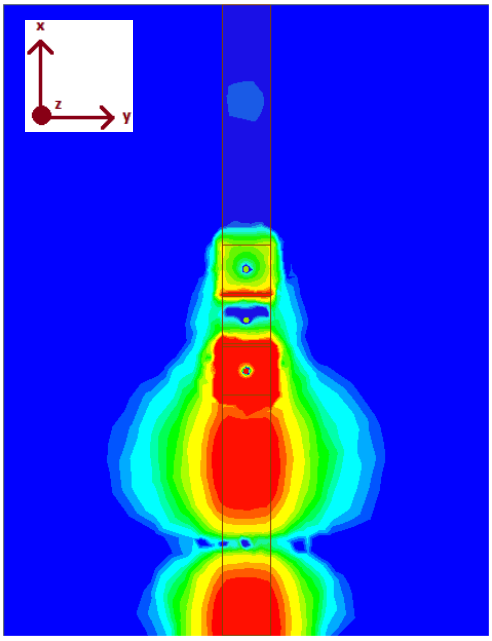

(b) 6.9 GHz and 7.4 GHz

Figure 4.19.-Magnitude of the electric field E on the plane between dielectrics, where the mEBG patches are located.

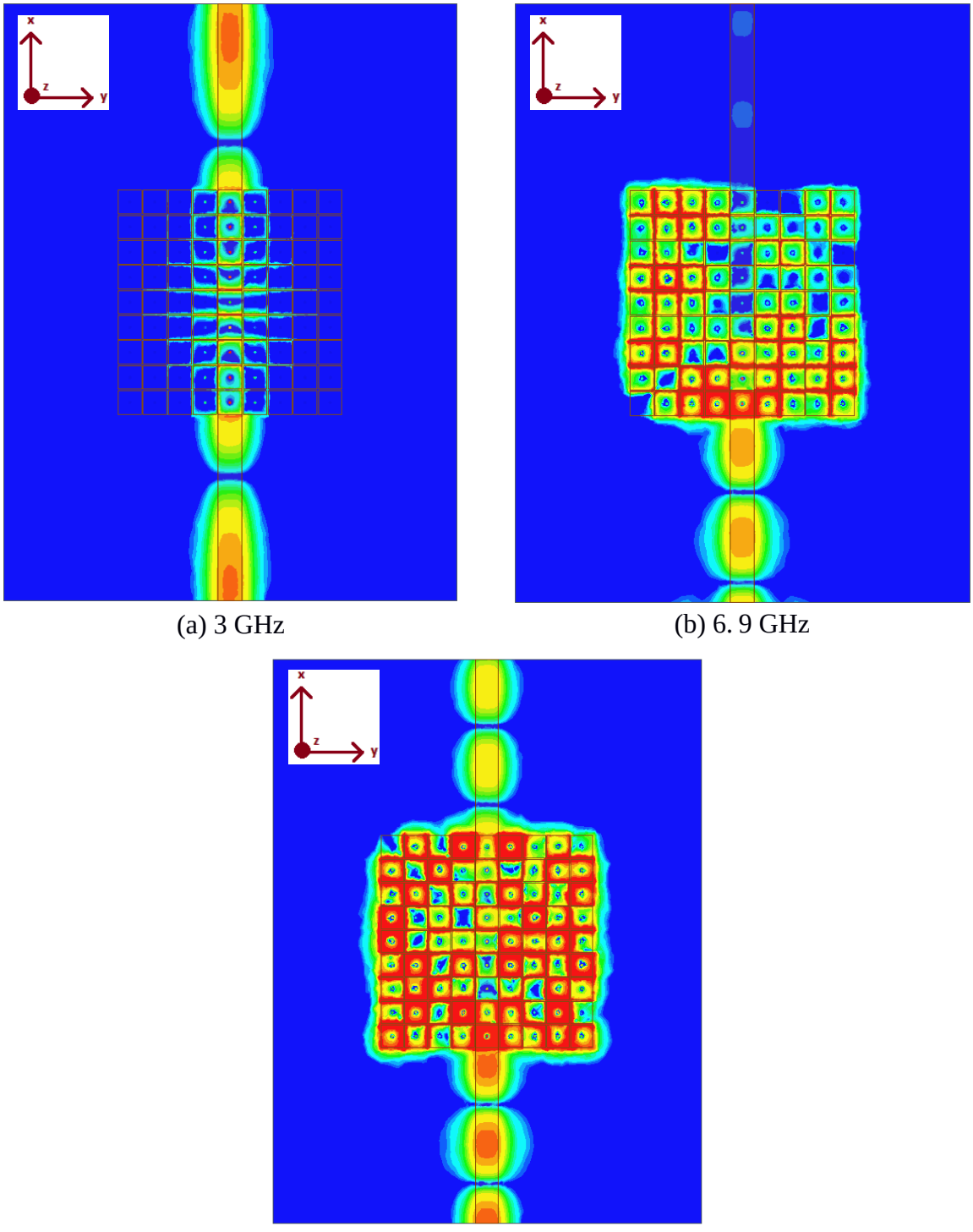

(a) 3 GHz

(b) 6. 9 GHz

(c) 7.4 GHz

Figure 4.20.- Magnitude of the electric field E on the plane between dielectrics, where the mEBG patches are located.

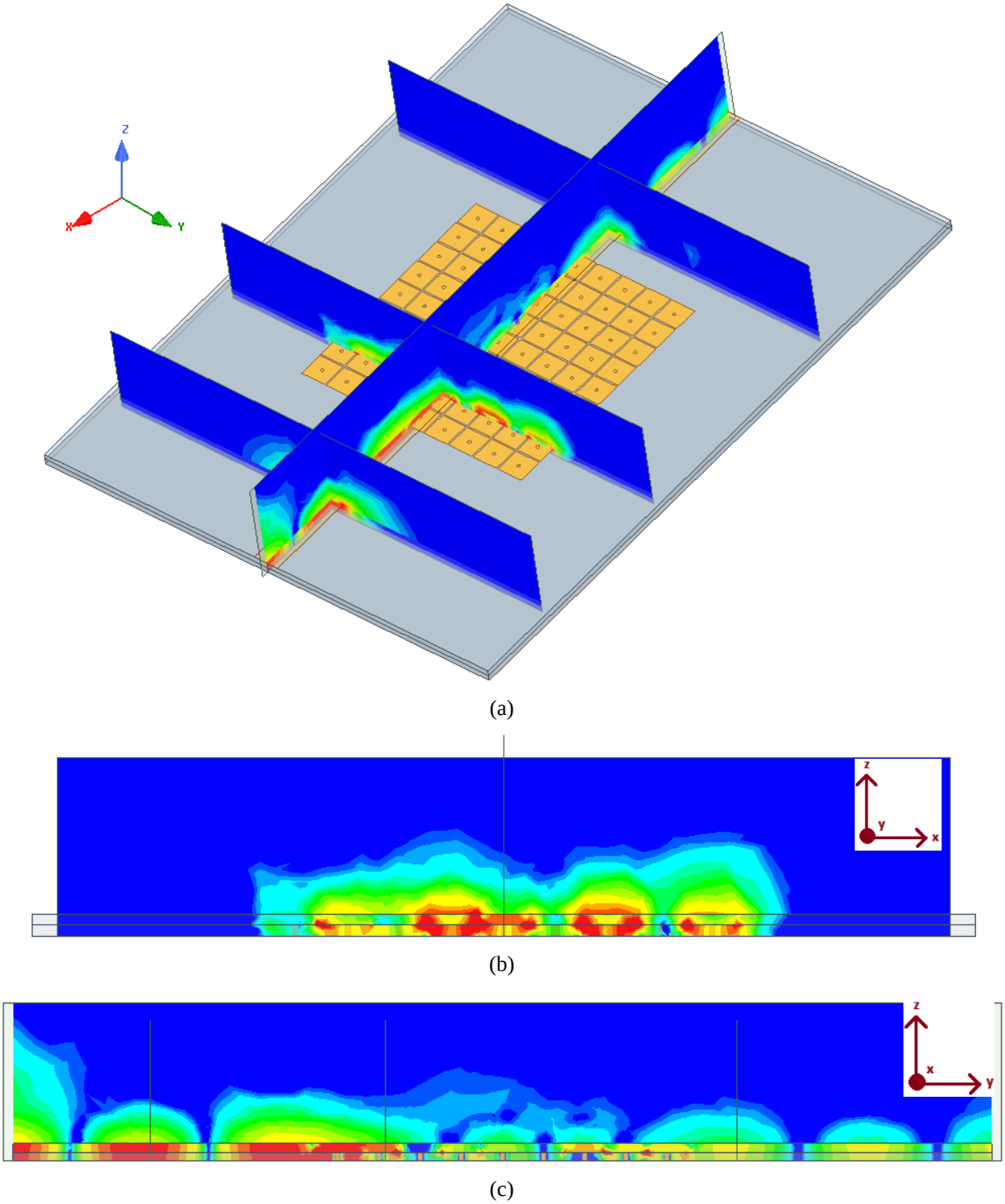

(a)

(b)

(c)

Figure 4.21.- Field cuts for 9x9 mEBG grid with microstrip line on top: (a) simulated structure, (b) middle cut perpendicular to microstrip line, (c) cut along microstrip line.

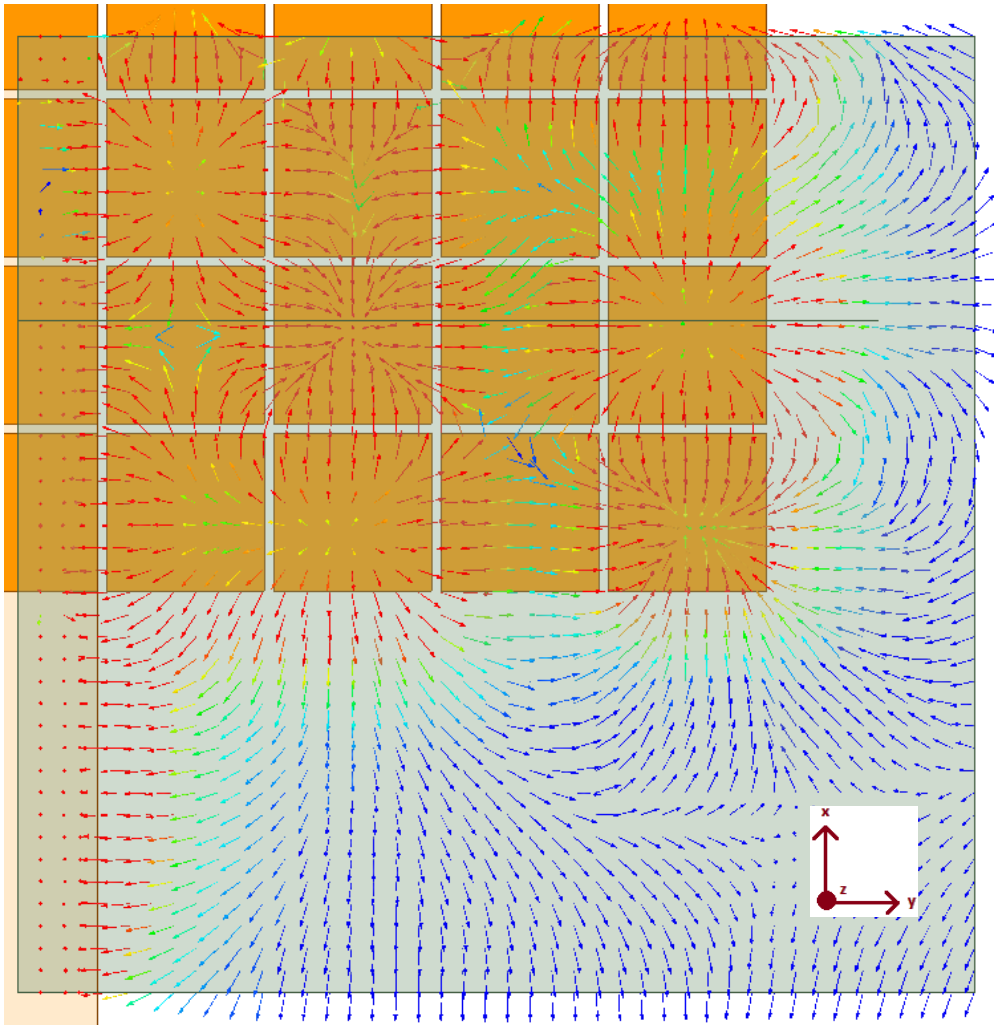

(a)

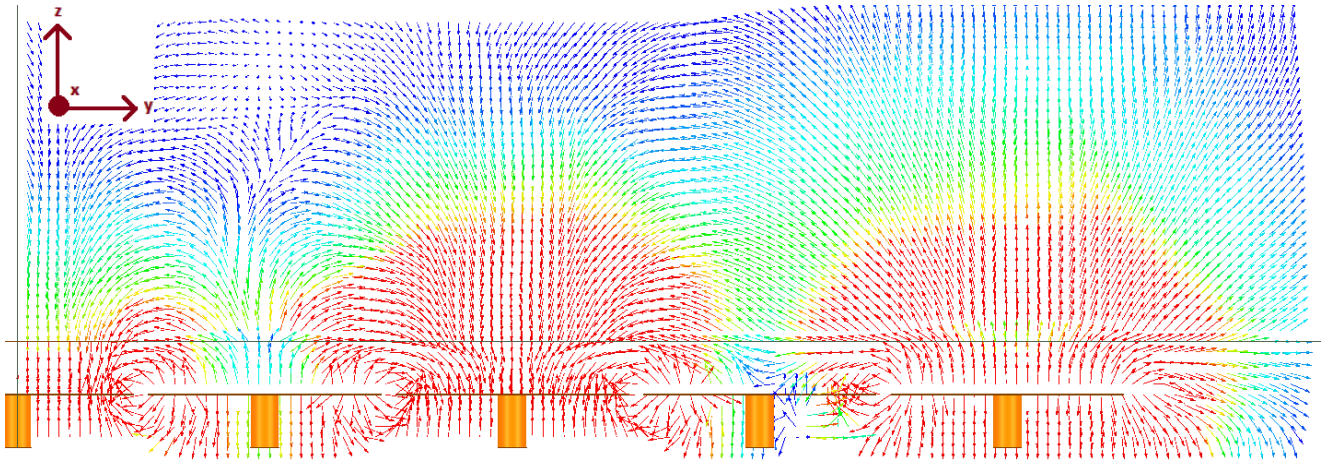

(b)

Figure 4.22.- Vector cuts: (a) horizontal on mEBG plane, (b) transversal and perpendicular to microstrip line.

Since the predicted band gap for the isolated mEBG goes from 6.5 GHz to 10.5 GHz approximately, the spikes in the S21 that allow for propagation at 7.4 GHz (within the bandgap) for the cases in Figure 4.18 and Figure 4.20 need to be explained, since it is "contradicting" the theory. The explanation for this phenomenon relies on the fringing fields of the microstrip line and their interaction with the mEBG. For the cases in figures Figure 4.17 and Figure 4.19, the fringing fields do not interact with the mEBG because these are entirely covered by the microstrip line. In Figure 4.18 there are not enough mEBG to effectively understand how the interaction behaves. Therefore, the case in Figure 4.20 is analyzed in more detail (Figure 4.21).

Paying close attention to Figure 4.22.b, it is observed that the direction of the electric field is opposite on the upper and lower sides of the mEBG patches, resembling the pattern of a fundamental microstrip mode. From Figure 4.21 and Figure 4.22.a it is also seen that such mode propagates from mEBG to mEBG both in the x and y directions. This mode, however, is not the fundamental microstrip mode, but it is excited on the mEBG by the fringing fields of the fundamental microstrip mode.

Once clarified why the row of mEBG underneath the line and parallel to it yields optimal results, several analysis are carried out with a different number of mEBG, as shown in Figure 4.23. It is thus demonstrated that increasing the number of mEBG improves the band-gap behavior. Again, simulated values of the S21 show how well each configuration works, but the yielded values are the result of solving an electromagnetic model and do not take into account limitations that imply that in reality values of -50 dB or -90 dB will most likely never be reached. Additionally, increasing the number of mEBG also increases the ripple of the response outside the band gap, and consumes more space, which can be a limiting factor in the feasibility of the design.

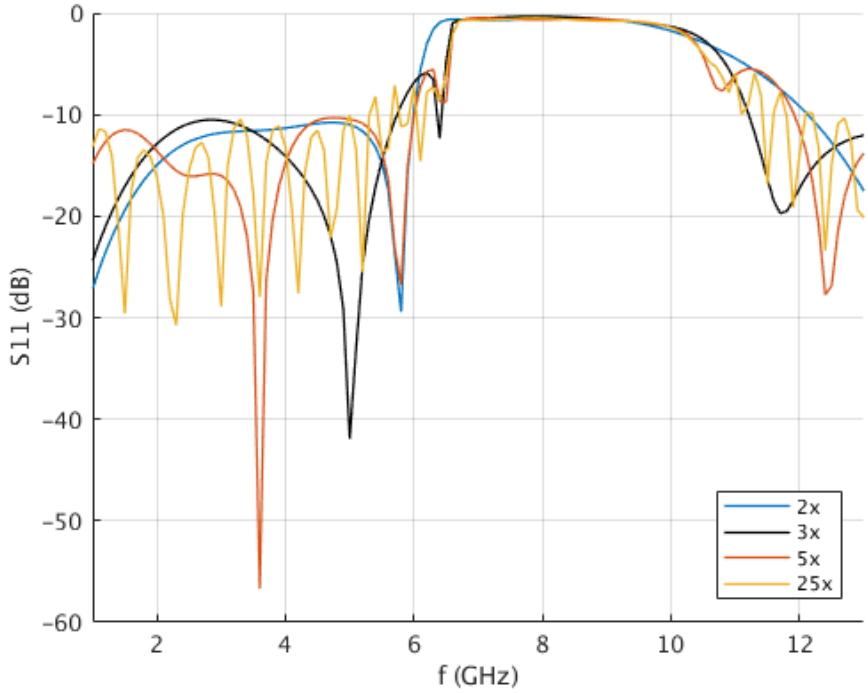

(a) S11

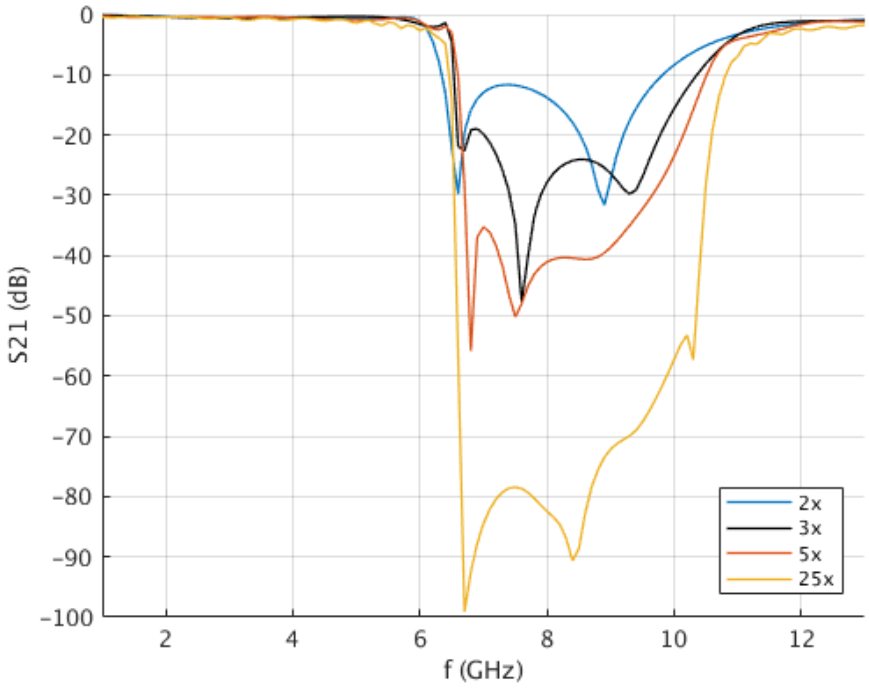

(b) S21

Figure 4.23.-Comparison of S-parameters of mEBG rows underneath the microstrip line for different numbers of mEBG.

4.2.3.- Matching optimization

The mEBG parallel structure shows a good stop band behavior (Figure 4.23.b) but has poor impedance matching at the operating frequency of 3 GHz, as can be seen by its S11 levels (Figure 4.23.a), close to -10 dB at 3 GHz. To improve this, two ideas are proposed:

- Place the mEBG row lower under the microstrip line, so that the mEBG patches are at the same level as the ground plane. With this action, the field traveling under the line will still resonate at band gap frequencies, but will be more easily allowed to propagate outside the band gap, because the "sandwich" effect seen in Figure 4.24 is eliminated.
- Use a number of mEBG that allow for its length to be an odd multiple of a quarter wavelength at 3 GHz. That way, reflections caused by the impedance change at the beginning and ending of the row of mEBG cancel each other out, yielding a better matching.

Taking these factors into account, a new design is made (Figure 4.25) that has the same band gap as in the previous section, but brings the S11 levels down significantly from -10 dB to -20 dB at 3 GHz (Figure 4.26). It also shows a faster roll-off. The main downside is a reduction in the bandwidth. The new mEBG patch length was calculated as follows:

$$\lambda_{3GHz} = \frac{3 \cdot 10^8}{3 \cdot 10^9 \sqrt{3.55}} \rightarrow \frac{\lambda_{3GHz}}{4} = 13.27\ mm \tag{4.1}$$

$$\frac{\lambda_{3GHz}}{4} - 4 * W_{gap} = 12.47\ mm \rightarrow \frac{12.47mm}{3} = 4.15\ mm/mushroom \tag{4.2}$$

The width was calculated by means of a parametric sweep from 1.5 mm to 3.5 mm and a 0.5mm step, where the 2mm width yielded optimal results.

Additionally, the microstrip line width needs to be adjusted to a 50 Ω impedance line, given that the new ground plane is placed closer to it than in the previous case. Applying equations (2.1), (2.2), the new width of the microstrip line is 1.5 mm.

It is interesting to note that the impedance of the mEBG filter (depicted in Figure 4.25) matches that of the standalone microstrip line, that is, the mEBG barely alters the line impedance, as shown in Figure 4.27.

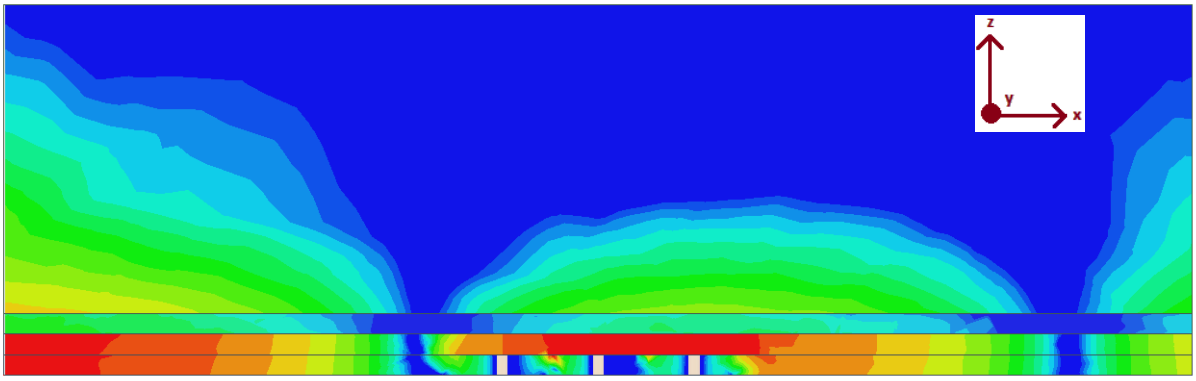

Figure 4.24.- E field module at 3 GHz. Side cut of the mEBG row. The mEBG patches act as a higher ground plane under the microstrip line, producing an impedance mismatch in the transitions and forcing the field to be "sandwiched" between the patches and the line.

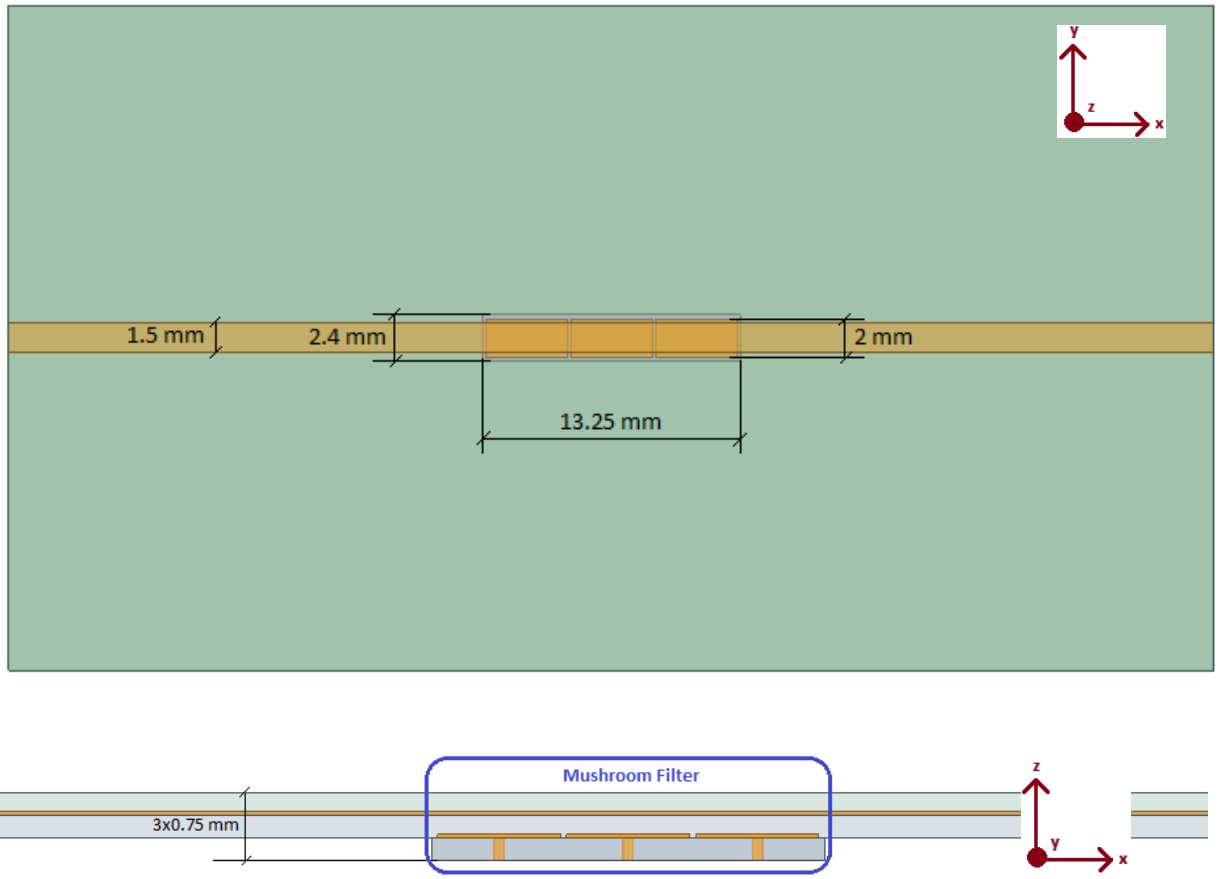

Figure 4.25.- Quarter wavelength arrangement of the mEBG.

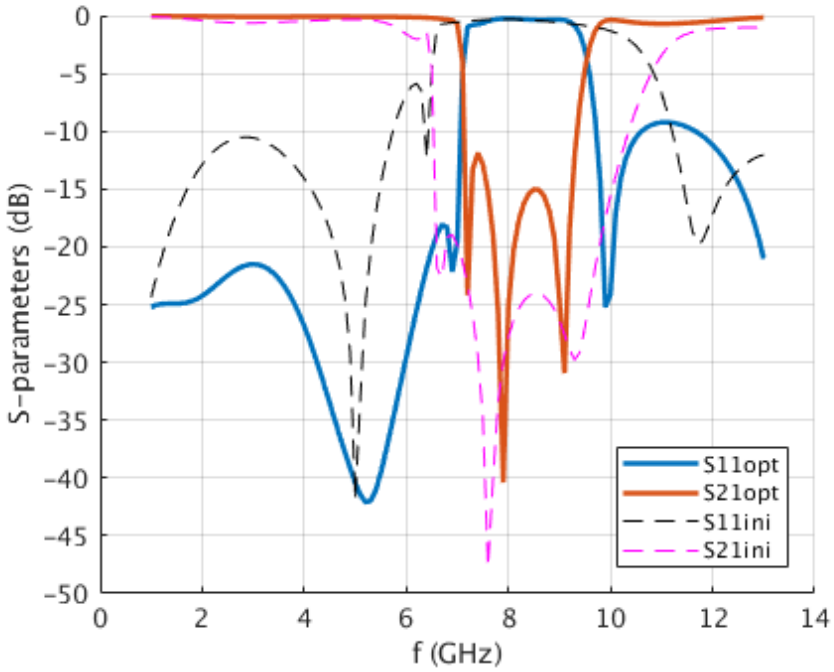

Figure 4.26.-S-parameters of row of mEBG in figure 4.14.e (ini) versus optimized design (opt).

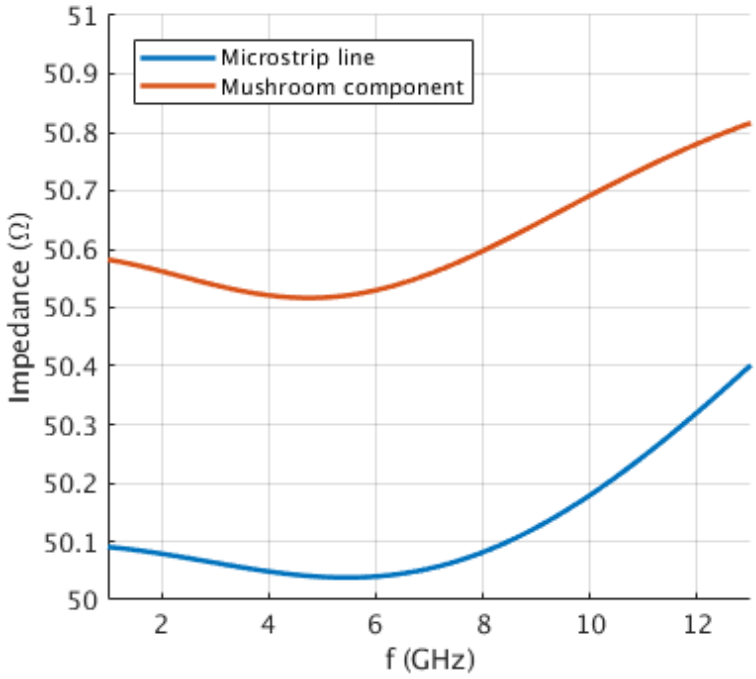

Figure 4.27.-Impedance of the microstrip line compared to the impedance of the mEBG filter component.

4.2.4.- Bandwidth enhancement

As seen in Figure 4.26, the necessary resizing for impedance matching of the mEBG has the downside of a reduced stopband width. This can be overcome by applying slight variations to parameters that affect the bandwidth, namely:

- Varying the diameter of the vias. This way slightly different inductances are incorporated into the filtering structure, adding some resonances at the bottom or top side of the stopband as such inductance is increased or decreased, respectively. This can also be interpreted in terms of band gap: varying via diameter creates different band gaps for each mEBG, The effect of such diameter variations can be increased by increasing mEBG height. Therefore, it is doubled with respect to the previous design (Figure 4.25) (from 0.75 mm to 1.5 mm). This, however, lowers the band gap frequency, which can be compensated by further reducing mEBG patch width, from 2 mm in the previous design (Figure 4.25) to 1.5 mm.
- Increasing the length of the structure. A quarter wavelength, three-mEBG filter (Figure 4.25) can offer a very limited bandwidth enhancement because only the center via or the side vias can be modified. Thus, bandwidth enhancement is carried out in a longer 9-mEBG filter, whose length equals 3 quarter wavelengths at 3 GHz in order to maintain impedance matching at the operating frequency.
- Reducing the permittivity of mEBG substrate. As it was seen in section 4.1.2, this action increases band gap frequency and width. Therefore, the RO4003 substrate of the bottom layer is replaced by air.

The designs resulting from applying the above mentioned variations are depicted in Figure 4.28 and Figure 4.29, differing only in the way that via diameter is tuned (symmetrically versus progressively, respectively). Specific diameter figures are not disclosed due to Thales confidentiality policy. Figure 4.30 and Figure 4.31 show the results of the symmetric design (Figure 4.28) compared to previous results (initial and quarter wavelength, obtained in Figure 4.15.c and Figure 4.26, respectively). The same comparison is carried out for the progressive design in Figure 4.32 and Figure 4.33.

The design that yields better results in terms of band stop rejection levels and band stop width is the design with progressive vias and air as mEBG substrate (Figure 4.29). It shows a band stop width at -10 dB of 4.9 GHz (6.9 GHz to 11.8 GHz) while maintaining a good matching at 3 GHz (S11 at -23.45 dB, below -20 dB). Because of these reasons, this design is potentially the best option for the final design among the studied ones.

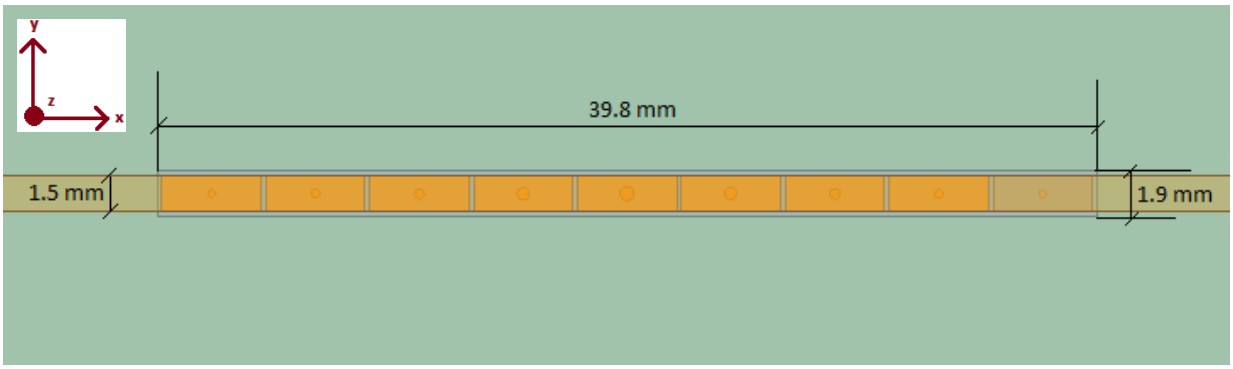

(a)

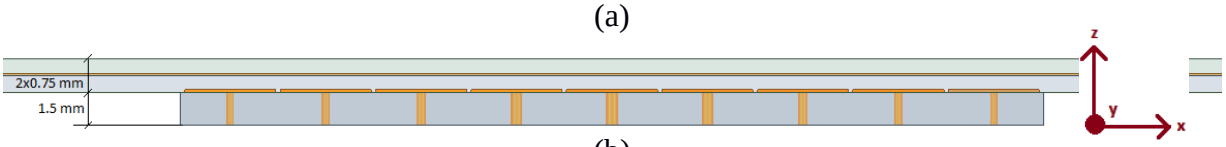

(b)

Figure 4.28.-Three quarter wavelength filter with symmetrically thick vias.

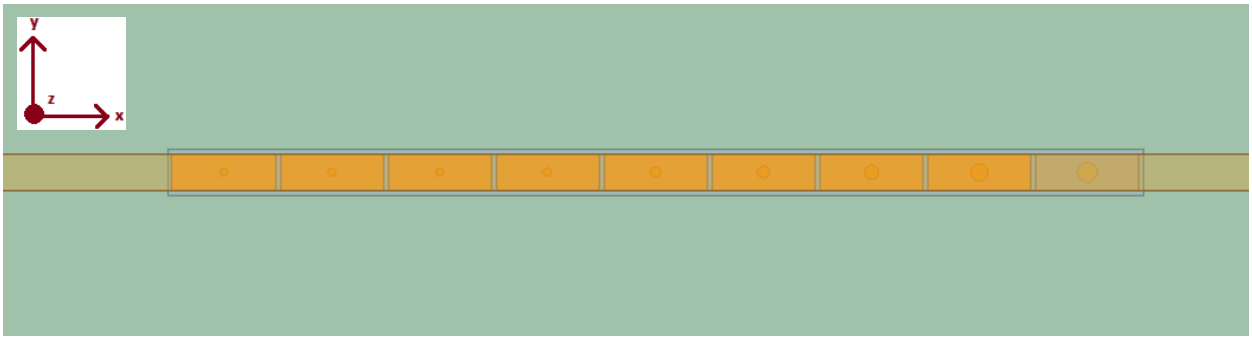

(a)

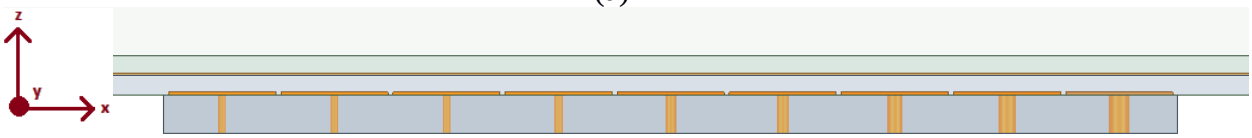

(b)

Figure 4.29.-Three quarter wavelength filter with progressively thicker vias. Only via diameter differs from dimensions in Figure 4.28.

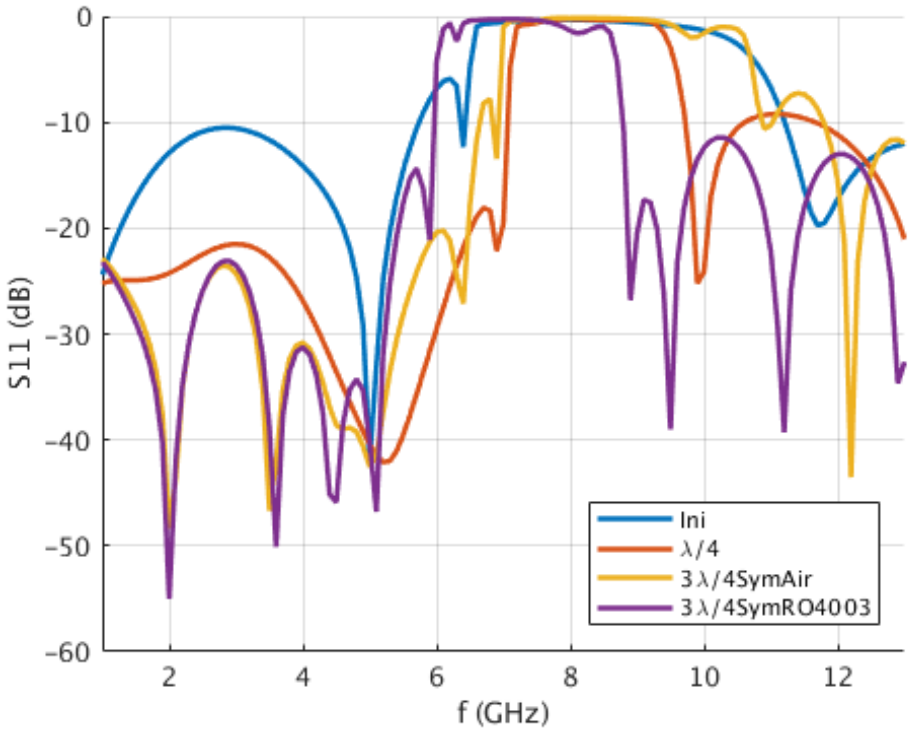

(a)

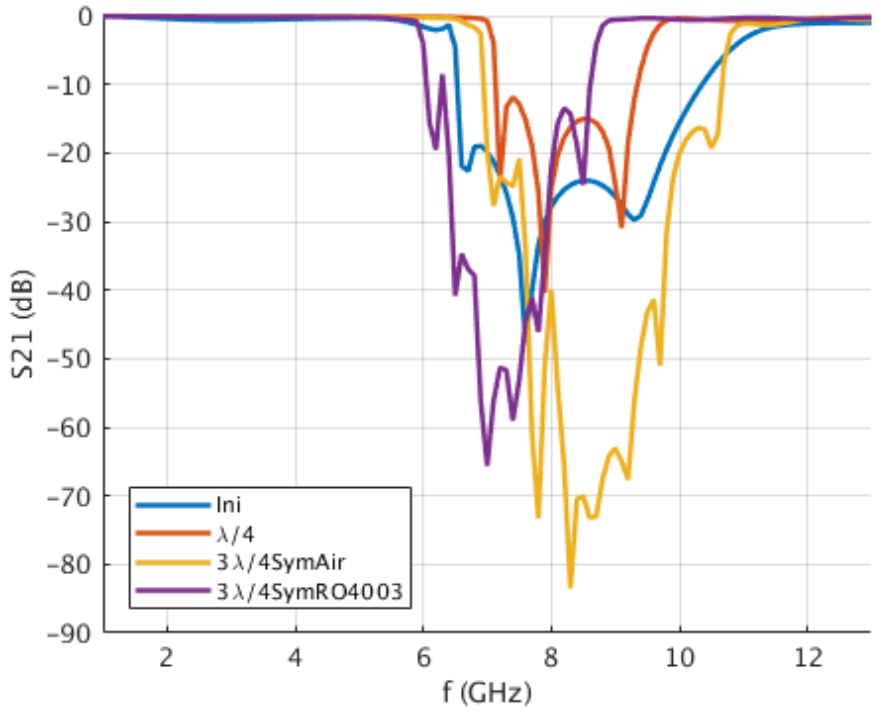

(b)

Figure 4.30.- S-parameters of three quarter wavelength filter with symmetrical vias configurations versus previous designs.

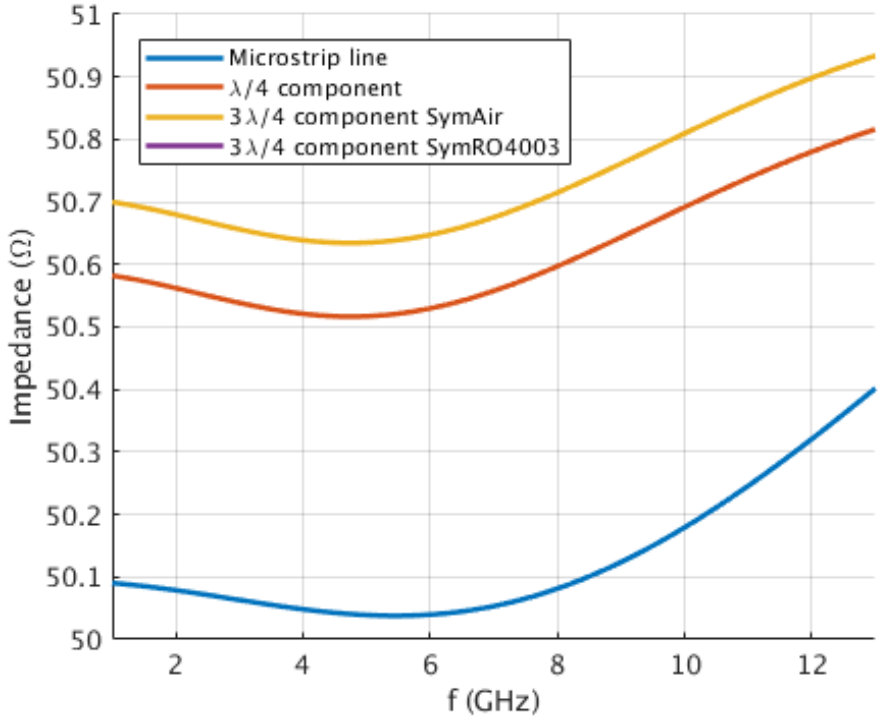

Figure 4.31.- Impedance comparison of three quarter wavelength filter with symmetrical vias configurations versus previous designs.

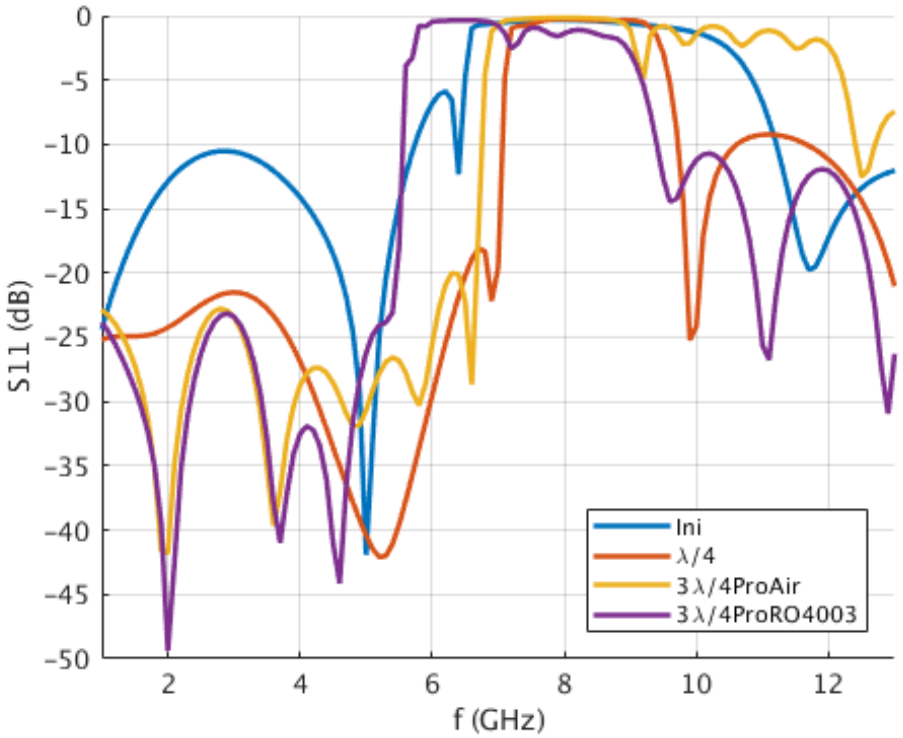

(a)

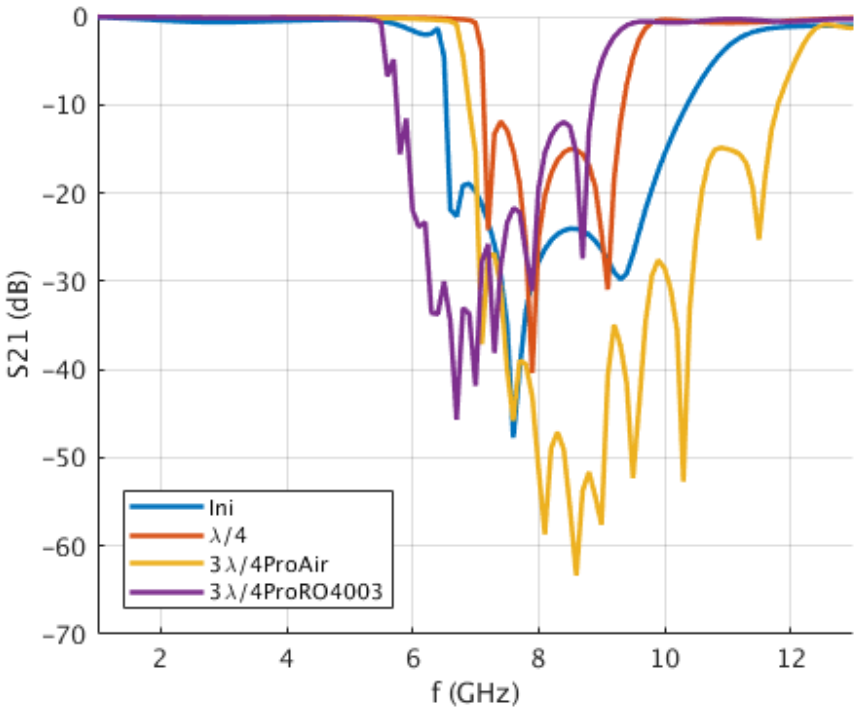

(b)

Figure 4.32.- S-parameters of three quarter wavelength filter with progressive vias configurations versus previous designs.

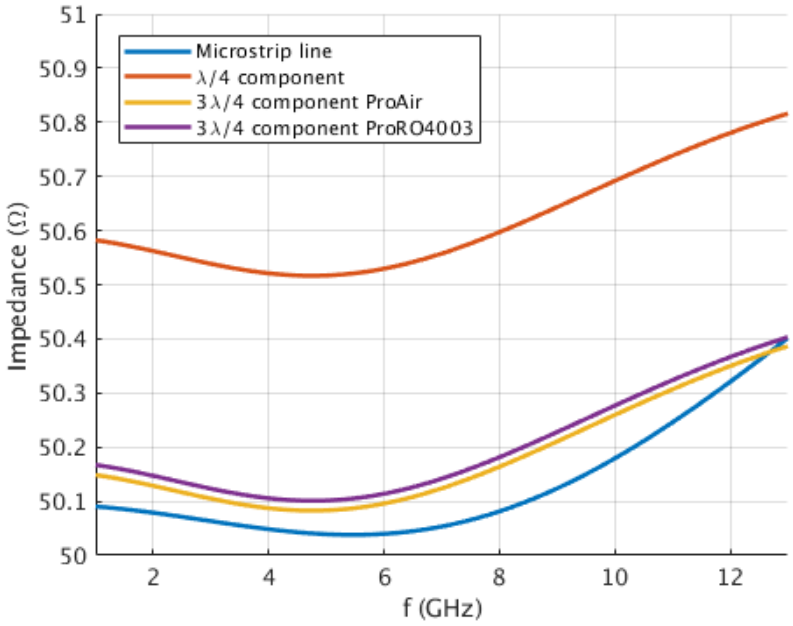

Figure 4.33.- Impedance comparison of three quarter wavelength filter with progressive vias configurations versus previous designs.

4.3.- Microstrip patch – Mushroom EBG

After the study carried out in section 4.2, where the mEBG is integrated with a microstrip line in different arrangements, this section extends such analysis to the mEBG in combination with a microstrip patch. For that, both an eigenmode analysis (section 4.3.1) and driven mode simulations (section 4.3.2) are carried out.

4.3.1.- Determining band gap and modes with HFS

The setup for the dispersive analysis of a mEBG covered by a patch antenna is shown in Figure 4.2, the dimensions are those of MushTuned, and the top layer of substrate 2 is covered by a PEC. Results of the simulation are shown in Figure 4.34, where it can be seen that the band gap property disappears, since the upper limit of the TM mode is higher than the point where the TE mode crosses the light line. The following subsection confirms these results through two driven mode simulations.

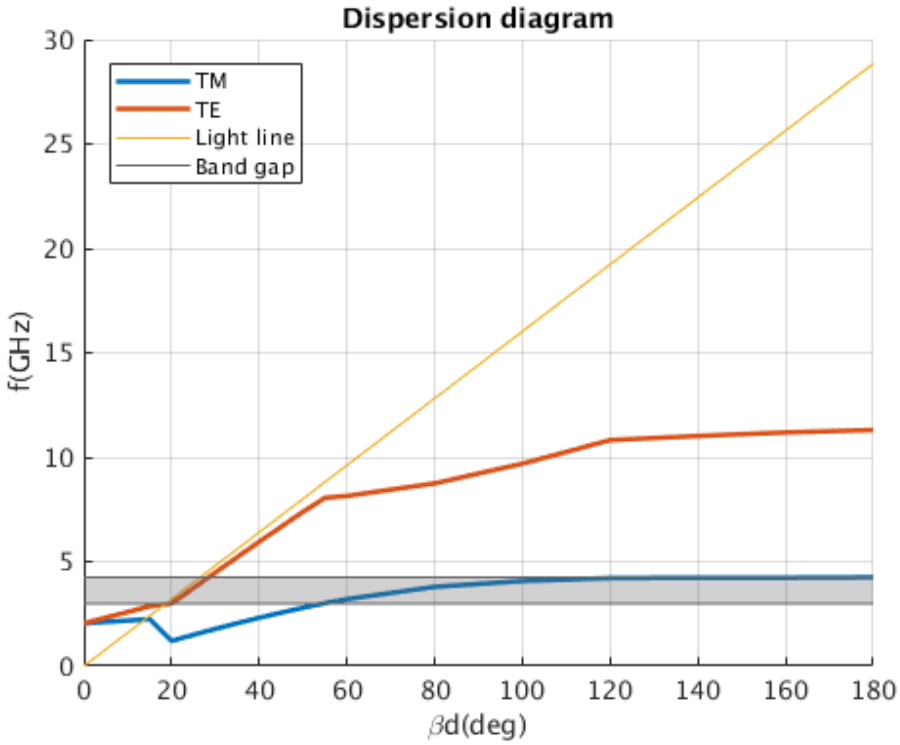

Figure 4.34.-Dispersion diagram of mEBG with PEC resembling patch on top.

4.3.2.- Application to microstrip patch antenna

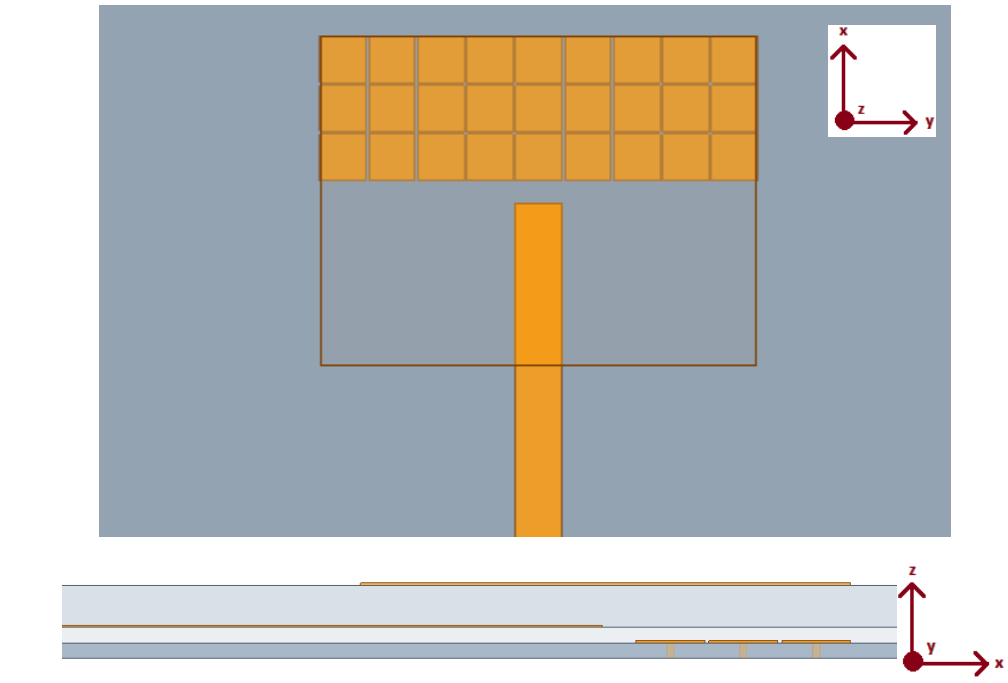

(a)

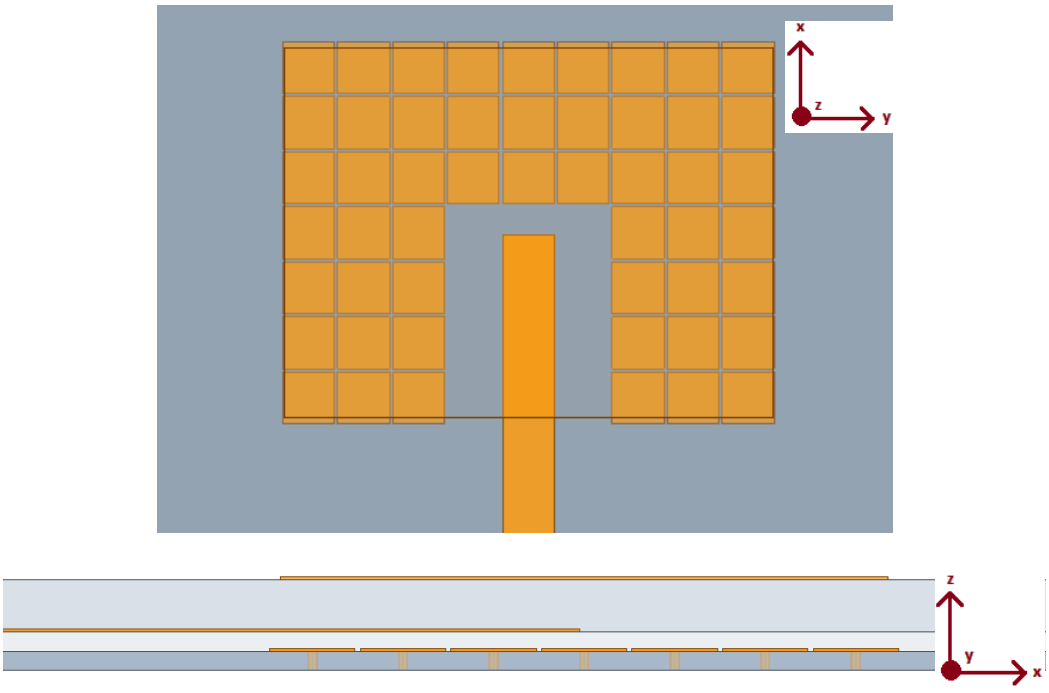

(b)

Figure 4.35.- mEBG structure under patch.

A grid of mEBG are placed underneath the patch antenna as shown in Figure 4.35. Both configurations try to avoid the fringing fields of the microstrip feeding line to minimize the effects described in section 4.2.2. Results are depicted in Figure 4.36, and confirm the lack of bandgap predicted in section 4.3.1. Therefore, this configuration is discarded for filtering purposes, and it can be concluded that the best option to achieve an effective filtenna design is the mEBG parallel to the microstrip line, as was predicted in section 4.2.

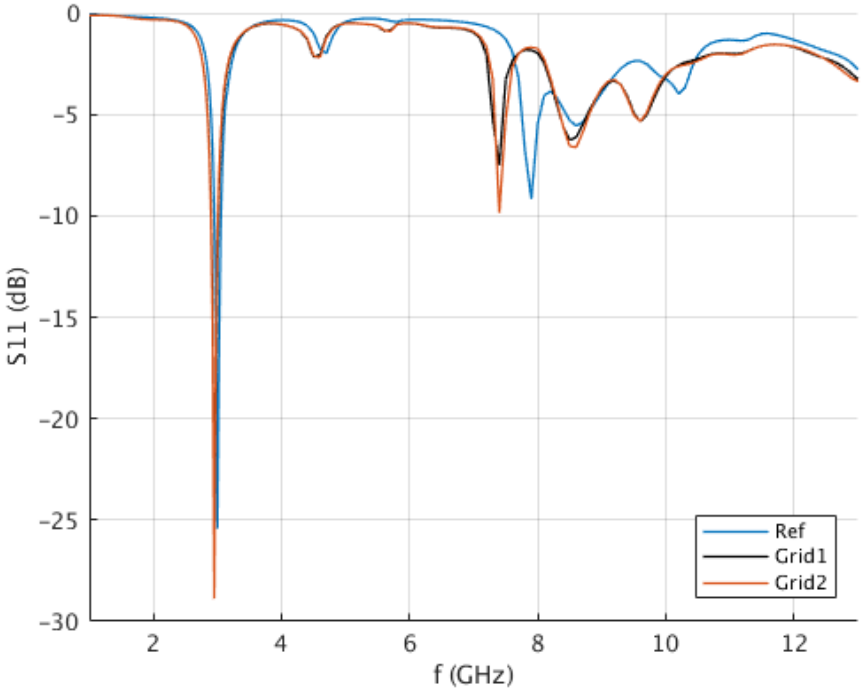

Figure 4.36.-S11 of mushroom structures under patch.

5.- APPLICATION TO PATCH ANTENNA

After the studies carried out in chapters 3 and 4, the mEBG that shows best results for the purpose of this work is the three quarter wavelength mEBG parallel row with progressively thick vias (Figure 4.29). Its combination with the 2nd harmonic suppression technique proposed in section 3.1 for the proximity coupled fed patch generates unsatisfactory results as explained in section 5.1. As a result, a new approach based on direct microstrip feeding is proposed in section 5.2, and yields the final solution of this work.

5.1.- Results based on proximity coupled fed patch

The design in Figure 4.29.b is placed underneath the proximity coupled fed patch in order to cancel out the frequency band around the 3rd harmonic from the patch response, as depicted in Figure 5.2. Figure 5.2 combines S21 filter response with the S11 antenna response to illustrate how the filtering mechanism should avoid propagation in the band from 7 GHz to 11 GHz, thus ideally increasing the S11 level of the patch response in that band. Nevertheless, the responses shown in Figure 5.2 are those of the isolated components: the filter, on one side (section 4.2.4), and the proximity coupled patch, on the other side (section 3.1).

The S11 of the model in Figure 5.2 was obtained for different values of D, from the inset length of the feed under the patch (Lin = 11.6mm or, alternatively, D = -11.6mm) up to D=23mm, in order to achieve close to half a wavelength ($\lambda_{3GHz} = 53.08\, mm$) of separation of the filter from the patch at 3 GHz (at such distance, the effects of the patch fringing fields on the mEBG are negligible, and are therefore not responsible for any unwanted results). To determine the best position D of the filter, the mean and variance of the S11 level outside the operating band (that is, all frequencies except those from 2.5 GHz to 3.5 GHz) are obtained and shown in Figure 5.3. The best filter location should be where the absolute value of the S11 mean is minimum (low spurious components) and the S11 variance is also minimum (smaller peaks). That location corresponds to D=0 mm, and the actual S11 values for it are shown in Figure 5.4. Other possible solutions include D=4 mm and D=8 mm, and are depicted in Figure 5.5, together with D=23 mm for completion.

The previous results pose a new problem. As it can be seen in Figure 5.4 and Figure 5.5, the predicted stop band is not effectively working. Instead, mismatches are spread throughout the entire band of swept frequencies, contradicting the ideal desired behavior described in the first paragraph of this section. The cause of this malfunctioning can be found by looking at the differences between the mEBG theory and the actual EBG implementation, and how they affect the integration of components.

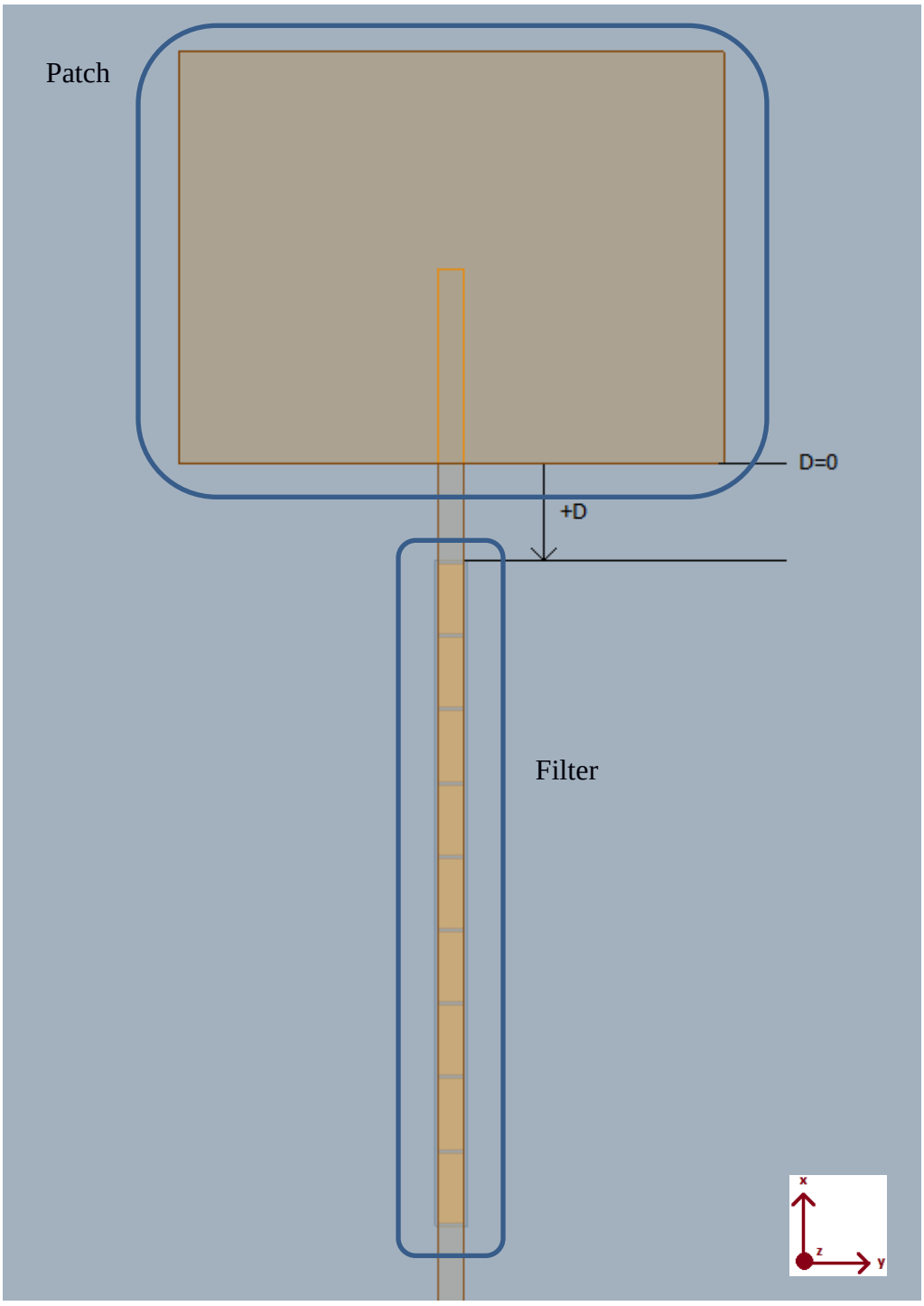

Figure 5.1.- Position of mEBG filter underneath feed line.

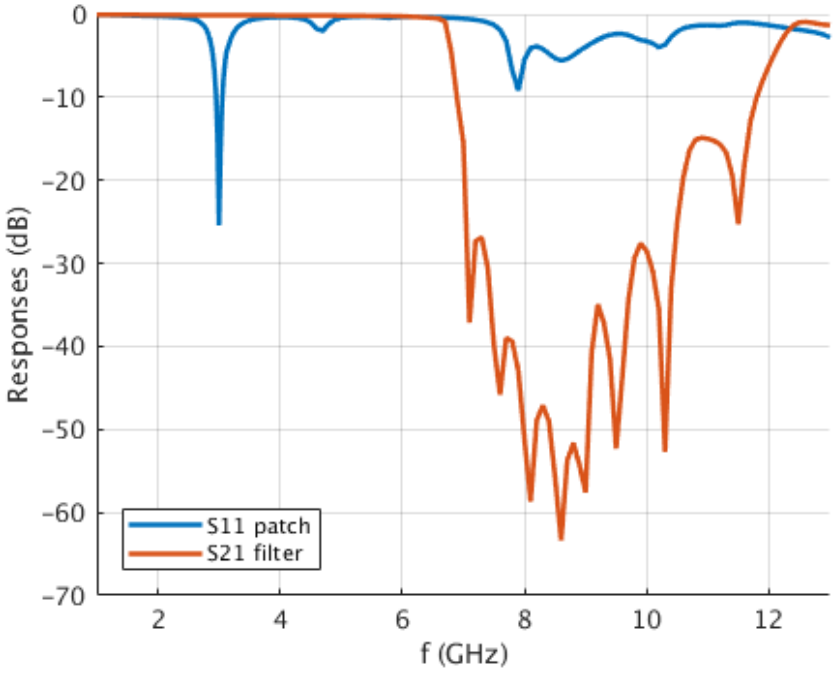

Figure 5.2.- S11 of reference proximity coupled fed patch and S21 of the filter applied to its feeding line. Individual responses.

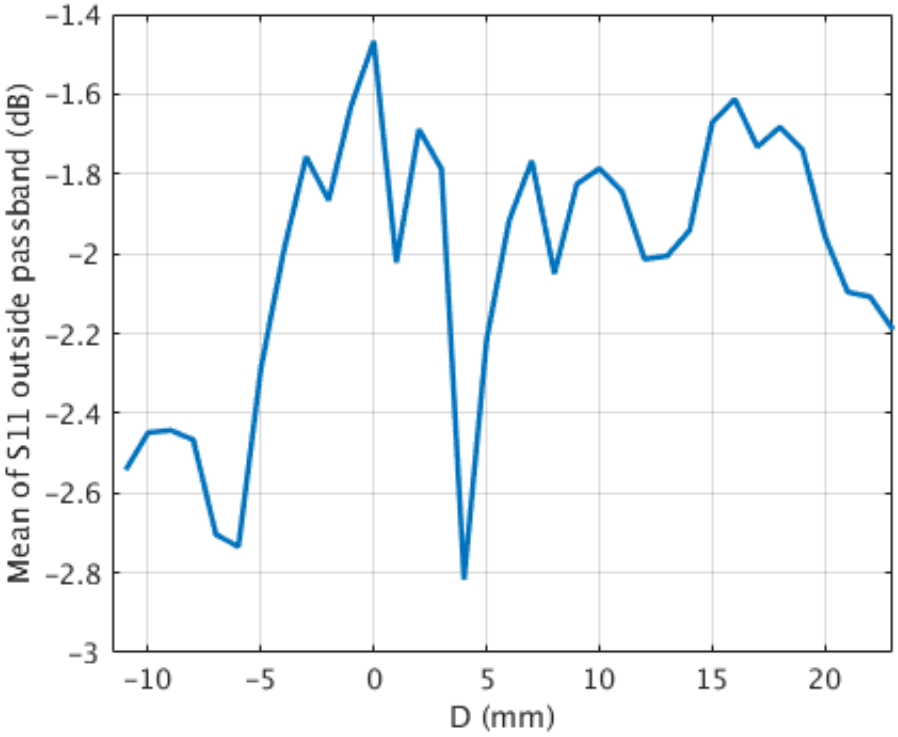

(a)

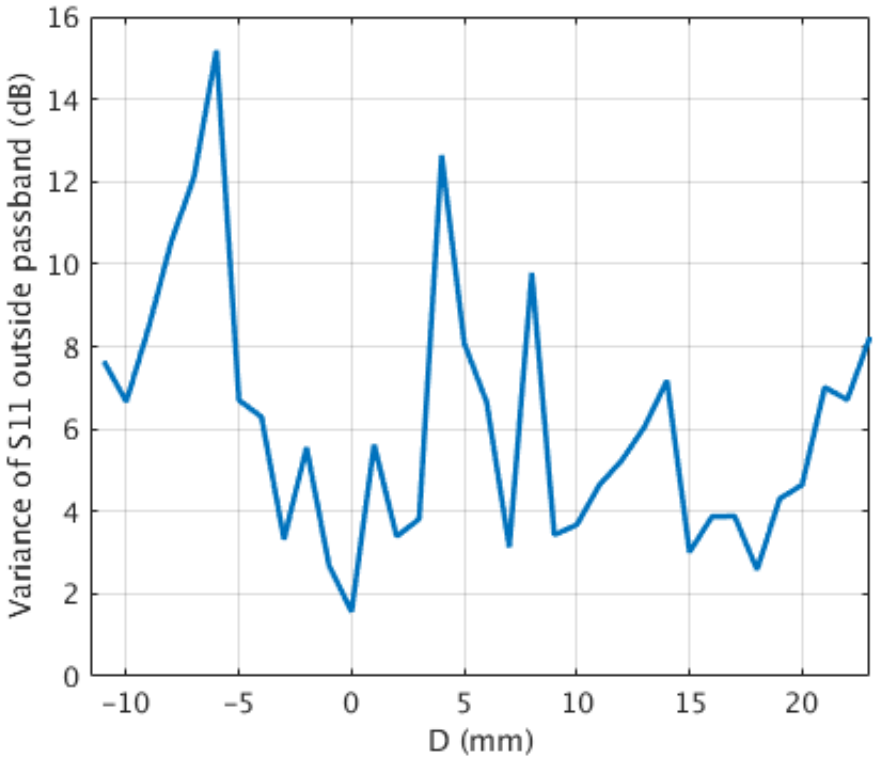

(b)

Figure 5.3.- Statistic results of the S11 of the structure under study for different positions D of the filter.

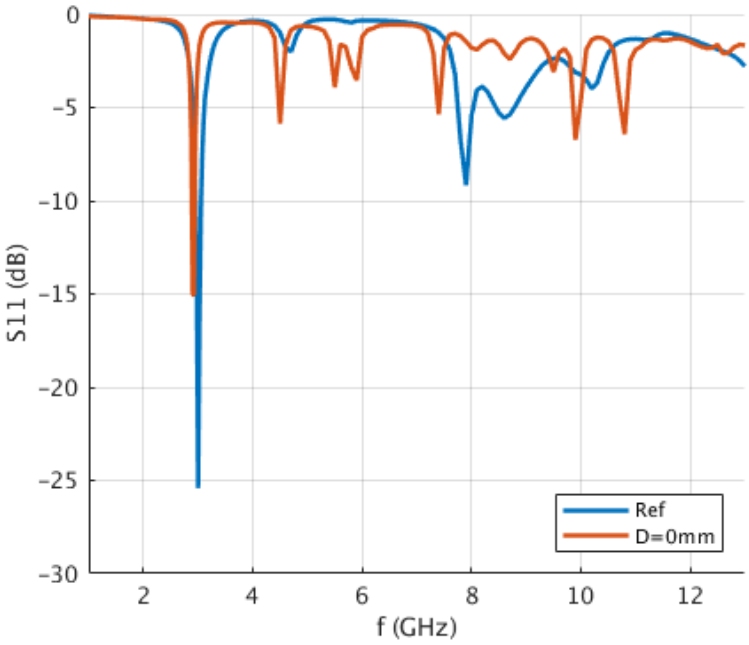

Figure 5.4.- S11 of reference proximity coupled fed patch versus same patch with mEBG filter at D=0 mm.

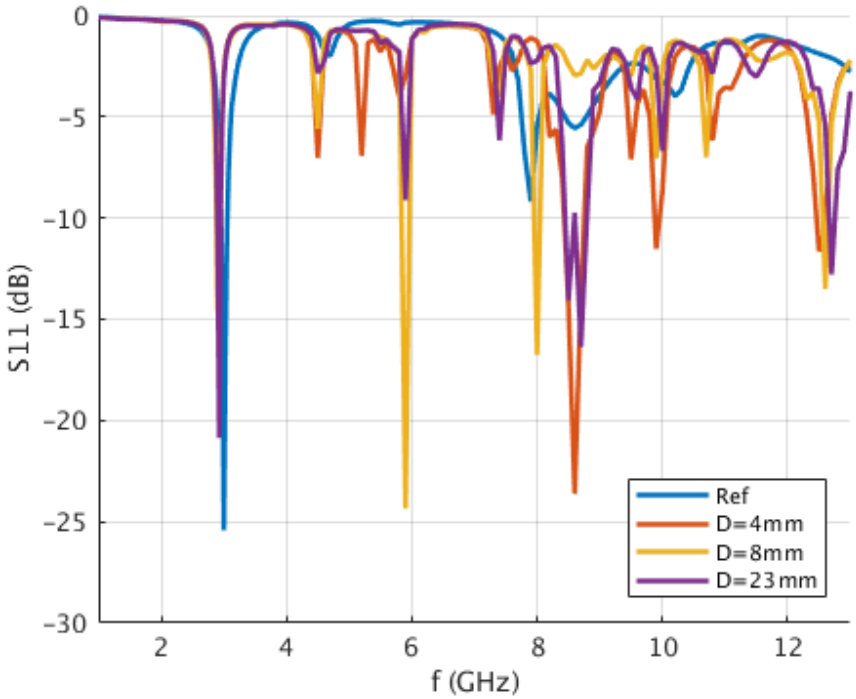

Figure 5.5.- S11 of reference proximity coupled fed patch versus same patch with mEBG filters at D=4mm, D=8mm and D=23mm.

The theory (section 2.2) predicts a band gap for infinitely periodic EBG structures, and the mEBG in particular. Such infinite periodicity, combined with an analysis that assumes excitation in only one direction, means that the EBG model does not take possible reflections into account. This omission can be worked around in practice by matching the ports of our finite EBG structure, thus getting rid of unwanted reflections and securing that the theoretical model applies to our finitely periodic structure. As a result, the mEBG structure alone shows a good filtering response (section 4.2), as both ends of the filter were matched to its own 50 Ω impedance.

The proximity coupled feeding line in the present section, however, is terminated in an open circuit (infinite impedance), which causes a severe mismatch and therefore reflections appear in all the frequency band, including the band gap. As a consequence, the theoretical mEBG model is no longer applicable and results do no longer provide the desired filtering functionality (Figure 5.4 and Figure 5.5).

It is drawn from this study that, although the mEBG filter works very well when its ports are matched, it cannot be integrated in a design where a mismatch is produced. It cannot be applied to an open microstrip line, thus invalidating the possibility of using a proximity coupled fed patch. The next section attempts to solve the mismatch problem by using a microstrip fed patch, thus making sure that both ends of the mEBG filter see a 50 Ω impedance instead of an open circuit.

5.2.- Results based on microstrip fed patch

To verify that the unwanted results of section 5.1 are caused by the mismatch as explained in that section, and also to achieve a functioning design, the mEBG filter is applied in this section to a microstrip fed patch. This feeding technique guarantees that both ports of the mEBG filter are matched to 50 Ω when both the microstrip line and the patch antenna are designed to have that impedance. With this in mind, two designs are created, the second one being the final filtenna design.

The first one, depicted in Figure 5.7, integrates the patch with the mEBG filter (mEBG-only design), effectively filtering out the spurious frequencies around the 3rd order harmonic, from 7 GHz to 11 GHz, where the mEBG filter band gap is located. This result can be seen in Figure 5.6, and corresponds to a value of $D = Lp = 26.4$ mm.. The dimensions of the filter and microstrip line (Figure 5.7.b) are those specified in Figure 4.29. As for the patch (Figure 5.7.a), its dimensions are specified in Table 5.1, according to the convention established in Figure 3.1., and detailed again in Figure 5.7.a.

Wp (mm)	Lp (mm)	Ls (mm)	Ws (mm)
33.13	26.40	8.3	1.85

Table 5.1.- Final patch dimensions.

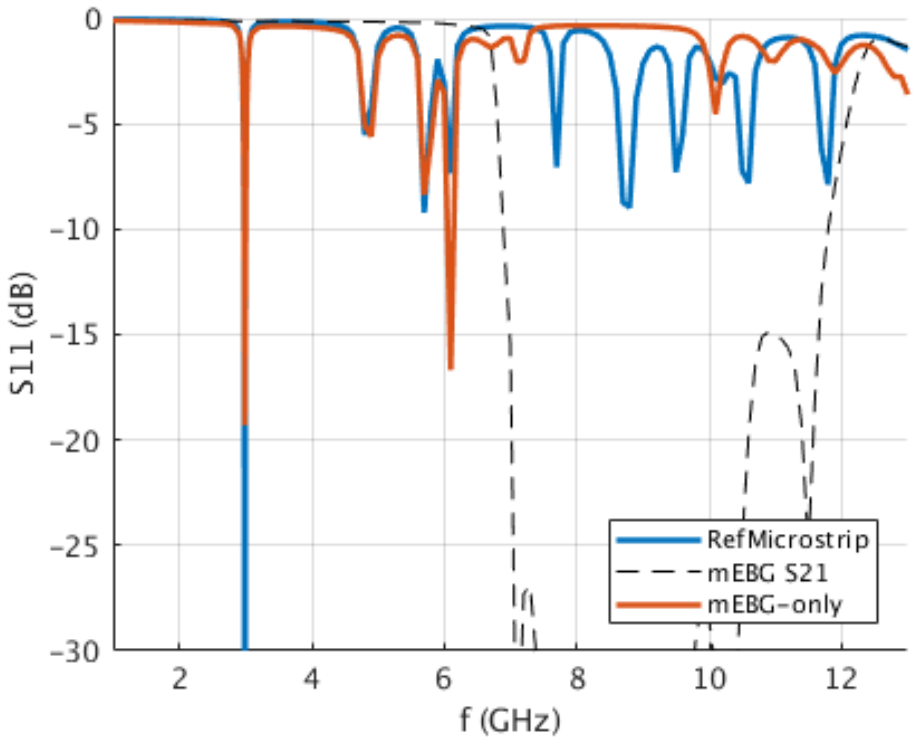

Figure 5.6.- S11 of final design versus reference designs and S21 of mEBG filter.

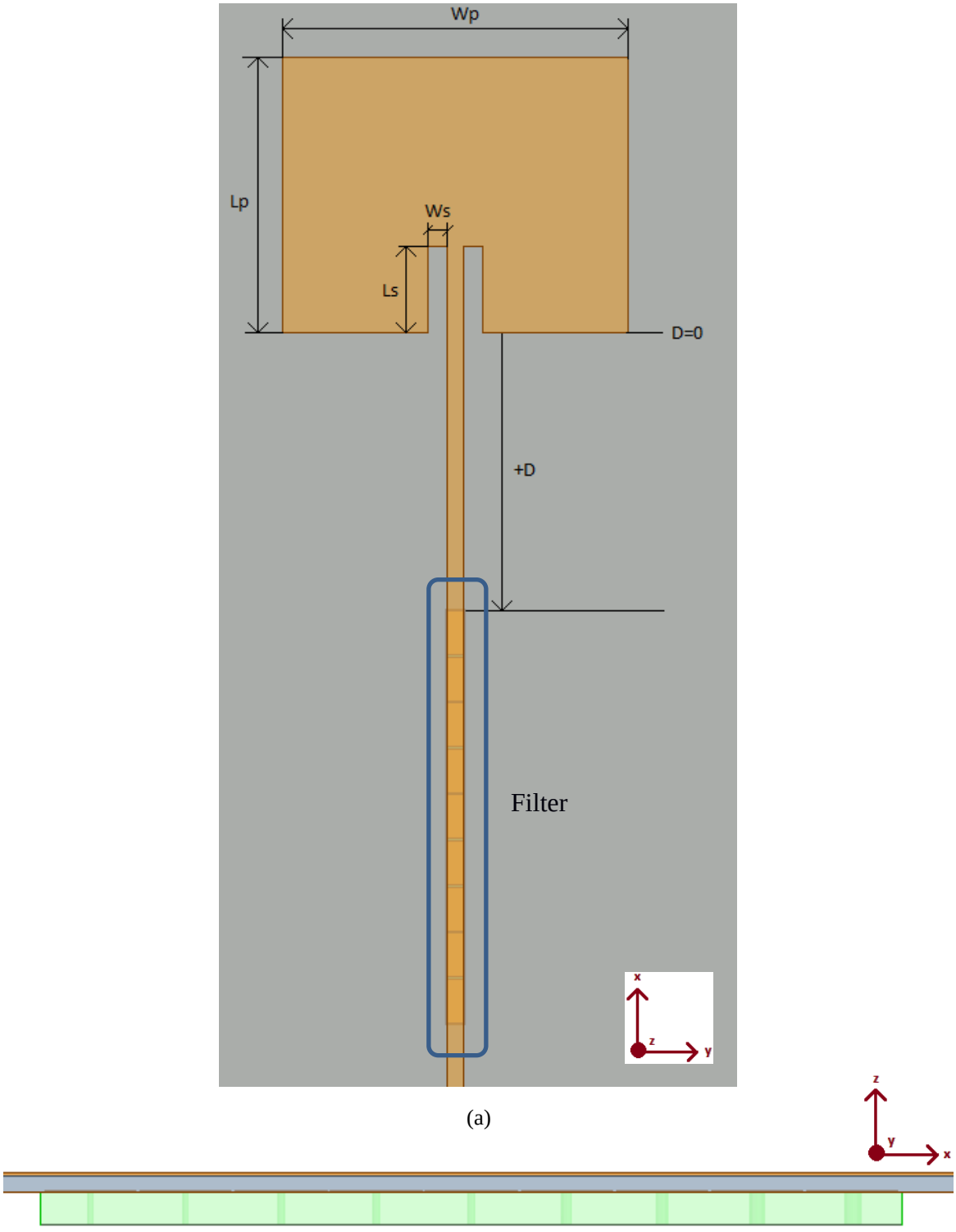

(a)

(b)

Figure 5.7.- Dimensioning and arrangement of final mEBG-only filtenna design.

Then, to reduce the level of the 2nd order harmonic located around 6 GHz, CMA techniques consisting of placing vias and slots are applied to a second and final design, depicted in Figure 5.8. The vias are placed in the middle of the patch, where the electrical field for the 2nd harmonic has a maximum, so that it gets grounded and its level is significantly reduced. In that location the value of the electrical field of the main 3 GHz harmonic is zero, and is therefore unaffected by the vias. A similar reasoning is applied to carve the additional slots that reduce the level of other spurious components. A more detailed explanation of CMA techniques is not given because they are outside the scope of this thesis.

The use of CMA techniques was not initially planned, but is necessary because the initially planned 2nd order harmonic technique was based on a proximity coupled feeding technique, that was proven ineffective due to impedance mismatching when integrated with the mEBG filter. As a consequence, the feeding technique was switched to microstrip, so a new method was required to mitigate 2nd order harmonics. CMA techniques (in-patch vias and slots) are thus used due to their fast applicability, but alternatives should be considered and are suggested in 6.2.

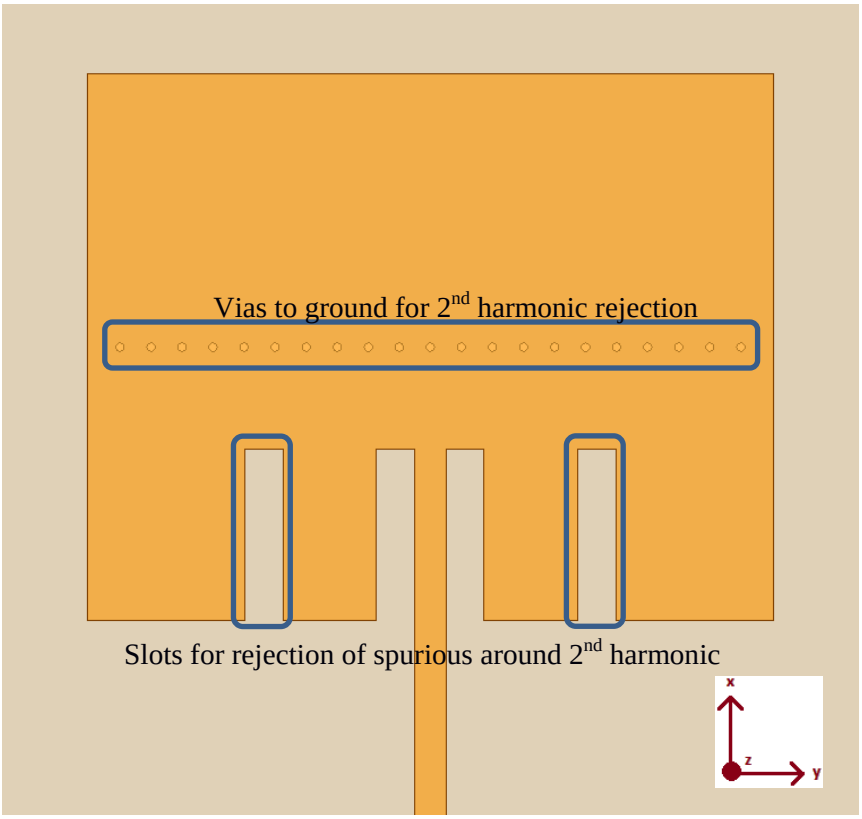

Figure 5.8.- CMA application to patch of mEBG-only design, yielding the final filtenna design. The distance separating the new slots from the previous ones is 7.13 mm. The vias to ground hava a diameter of 0.4 mm, with a separation of 1.5 mm, located in the middle of the patch.

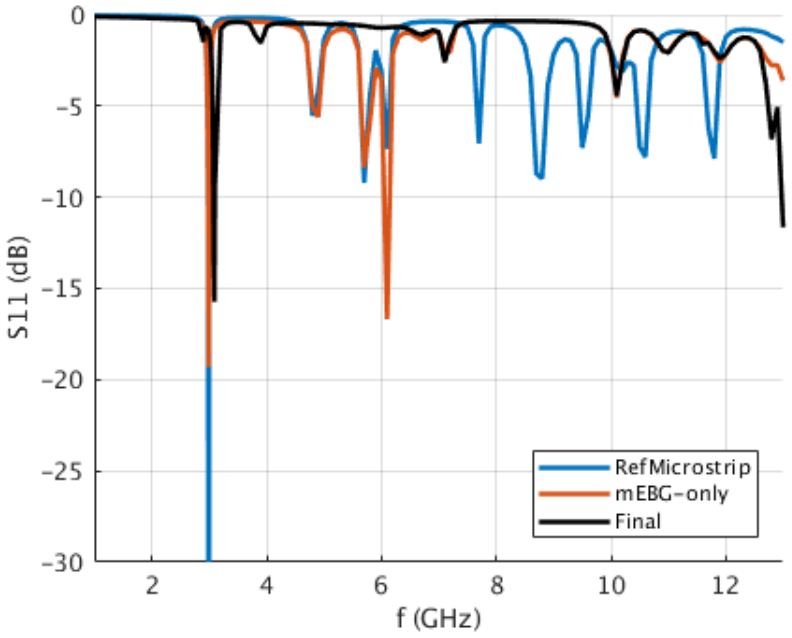

Figure 5.9.- Final CMA+mEBG filtenna design compared to mEBG-only design and reference patch.

The results for the final filtenna design are shown in Figure 5.9 compared to the reference design and the mEBG-only design. The final filtenna design achieves significant reduction of spurious levels for all the frequencies outside the operating bandwidth, up to 12 GHz. With the application of the mEBG filter, first, and the CMA techniques, second, the level of the main 3 GHz component is also reduced. This is because each new element introduces slight variations in the impedance of either the microstrip line (mEBG filter) or the patch (the vias behave as inductances and the slots reduce patch capacitance), shifting the matching of the main component. This shift can be easily corrected by tuning patch dimensions, but this fine tuning process is outside the scope of the thesis and is left for future work, also because 3 GHz is a reference frequency and a real prototype would have to be designed for operation in a different frequency, thus slightly altering all building parameters.

6.- CONCLUSIONS AND RECOMMENDATIONS

6.1.- Conclusions

A new approach based on metamaterials, the mEBG in particular, was investigated in this master thesis with the objective of achieving a filtenna operating at 3 GHz that meets certain criteria in terms of spurious rejection and roll-off factor, as described in section 1.2. The conclusions drawn from this work can be grouped in three groups: conclusions regarding the mEBG, conclusions regarding the integration of the mEBG with microstrip components, and conclusions regarding the final design.

Firstly, a comparison of the mEBG and other EBG structures was carried out, and the mEBG was preferred because it has been widely studied in literature and shows better band gap properties than other considered structures. Its theoretical model allowed to fully characterize the mEBG cell in terms of band gap by means of its dispersion diagram. The potential of the mEBG comes from its flexibility, since slight changes in physical building parameters and geometry can significantly change dispersion properties, and more importantly, such changes are predicted by the theoretical models, thus allowing to create accurate initial designs for a desired behavior.

Secondly, the mEBG was integrated with a microstrip line. After trying several configurations, it was concluded that placing a row of mushrooms underneath the microstrip line yields optimal results, showing a stopband with good rejection levels (reaching the goal of 20 dB rejection) in the band gap frequency region, thus validating the use of the mEBG as a filtering structure. However, this is restricted to matched networks. This is because the theory is valid for infinitely periodic mEBG grids (which are therefore perfectly matched), but in practice only a finite mEBG structure can be implemented. Thus, the impedance of the mEBG structure has to be matched in order for it to work as predicted by the theory. This reasoning was checked when the mEBG filter was integrated with a proximity coupled fed patch: its band gap feature no longer worked, with an S11 response full of reflections within the predicted band gap, both with the filter close and far away from the patch. This happened because the proximity coupled feeding technique required the microstrip line to be open circuited at its end, thus showing an infinite impedance that generated a severe mismatch with respect to the 50 Ω mEBG filter. It was also concluded that the mEBG structure has little impact on microstrip line impedance, which facilitates the integration process.

Finally, a mEBG filter was designed and implemented on a microstrip fed patch, solving the matching issue. The final mEBG filter was adapted to be three quarters of wavelength at

the operating frequency of 3 GHz, in order to minimize return loss at such frequency. Its band gap width could be enhanced by reducing the permittivity of the mEBG substrate and varying via diameters. As a result, a band stop filter in the range of 7 GHz to 11 GHz was obtained, with rejection levels in the environment of 40 dB throughout the stop band. This design was integrated with the microstrip fed patch antenna. Additionally, CMA techniques were applied in order to reduce 2nd harmonic levels, achieving a final compact filtenna design.

However, the proposed design does not show full filtenna functionality (as defined by the goals in section 1.2) because the structures employed (mEBG and CMA techniques) do not seem to affect the roll-off factor of the antenna, so this factor remains unchanged. Despite not meeting the roll-off factor goal, significant steps have been made in the direction of achieving a fully functional filtenna based on mEBG designs, as its potential application as a low-profile highly-tunable filtering structure has been proven, with a solid theory and results behind it. The possibility of using mEBG instead of CMA techniques to reduce the level of 2nd harmonic and other spurious components shows a good potential based on the obtained results, but is left for future work, given that, for now, the combination of mEBG and CMA techniques has yielded satisfactory results.

6.2.- Recommendations

As a result of the present work, and the conclusions that are drawn from it, future lines of work to achieve a fully functional filtenna are suggested, including:

- Combining present mEBG filter with additional mEBG designs to show band gap at 2nd harmonic frequencies, thus reducting the level of components from 4 GHz to 7 GHz, around the 2nd harmonic.
- Determining whether a mEBG-only design can show better characteristics than a mEBG+CMA design.
- Investigating feasibility of design regarding manufacturing process.

BIBLIOGRAPHY

[1] Skolnik, M. (1981). *Introduction to radar systems.* McGraw-Hill.

[2] Itoh, T. &. (2006). Electromagnetic metamaterials: transmission line theory and microwave applications.

[3] Yang, F. &.-S. (2009). Electromagnetic band gap structures in antenna engineering. 156-201.

[4] Scarborough, C. P. (2011). Low-loss Radio-frequency Electromagnetic Materials Applied to Antennas and Imaging.

[5] Zeng, J. (2013). *Compact electromagnetic band-gap structures (EBG) and its applications in antenna systems.* Master Thesis, University of Waterloo.

[6] Smyth, B. P. (2016). Dual-band microstrip patch antenna using integrated uniplanar metamaterial-based EBGs. *IEEE Transaction on Antennas and Propagation, 64(12),* 5046-5053.

[7] Bafadhal, F. H. (2017). Antenna microstrip using electromagnetic band gap (EBG) with circular patch for inter-satellite link (ISL) on low orbit satellite. *Wireless and Mobile (APWiMob) IEEE Asia Pacific Conference,* 118-121.

[8] Huang, C. J. (2018). Combining FSS and EBG surfaces for High-Efficiency Transmission and Low-Scattering Properties. *IEEE Transactions on Antennas and Propagation*.

[9] Ermutlu, M. S. (2005). Patch antennas with new artificial magnetic layers. *arXiv Preprint Physics/0504075*.

[10] Sahoo, A. K. (2017). A 2x2 integrated filter antenna array. *IEEE,* 2205-2208.

[11] Monni, S. N. (2004, March 9-11). A Fast Design Methodology for Steep Roll-Off Frequency Selective Structures. *27th ESA Antenna Workshop on Innovative Periodic Antennas: Electromagnetic Bandgap, Left-handed Material, Fractal and Frequency Selective Surfaces,* 192-197.

[12] Shang, P. W. (2017). A novel compact dual-mode filtering antenna for WiMax applications. *IEEE,* 1-3.

[13] Hadarig, R. C.-H. (2012). Microstrip patch antenna bandwidth enhancement using AMC/EBG structures. *International Journal of Antennas and Propagation*.

[14] Inclán-Sánchez, L. V.-R.-I. (2006). Microstrip patch antenna with compact feed to reduce harmonics. *IEEE*, 1-4.

[15] Inclán-Sánchez, L. V.-R.-I. (2009). Proximity coupled microstrip patch antenna with reduced harmonic radiation. *IEEE Transactions on antennas and propagation, 57(1)*, 27-32.

[16] Rahman, M. &. (2001). Wideband microstrip patch antenna with planar PBG structure. *Antennas and Propagation Society International Symposium, IEEE, 2*, 486-489.

[17] Pozar, D. M. (2009). *Microwave engineering.* John Wiley & Sons.

[18] Constantine, A. B. (2005). *Antenna theory: analysis and design.* Second edition, John Wiley & Sons.

[19] Ansoft Corporation, I. (2007). *Left-Handed Metamaterial Design Guide.*

[20] Raza, S. (2012). *Characterization of the Reflection And Dispersion Propoerties of Mushroom-Related Structures and Their Application to Antennas.* Doctoral dissertation, University of Toronto.

[21] Hurshkainen, A. A. (2016). Element decoupling of 7 T dipole body arrays by EBG metasurface structures: Experimental verification. *Journal of Magnetic Resonance*, 87-96.

[22] Sievenpiper, D. Z. (1999). High-impedance electromagnetic surfaces with a forbidden frequency band. *IEEE Transactions on Microwave Theory and Techniques, 47(11)*, 2059-2074.

[23] Rambabu, K. &. (2005). Design and application of grounded pin-pad resonators in LTCC components. *Microwave Optical Technology Letters, 47(4)*, 321-323.

[24] Rahman, M. &. (2001). Modeling and application of 2D photonic band gap structures. *IEEE Proceedings, 2*, 2-893.

[25] Luukkonen, O. Y. (2008). Comparative study of surface waves on high-impedance surfaces with and without vias. *IEEE*, 1-4.

[26] Luukkonen, O. S. (2008). Simple and accurate analytical model of planar grids and high-impedance surfaces comprising metal strips or patches. *IEEE Transactions on Antennas and Propagation, 56(6)*, 1624-1632.

[27] Tretyakov, S. (2003). Analytical modeling in applied electromagnetics. *Artech House*.

[28] De Louw, S. (2017). *Control Surface Waves by Modifying Surface Properties of a Microstrip Patch Antenna Array.* University of Twente.

[29]. (n.d.). *Ansys HFSS Capabilities*. Retrieved from https://www.ansys.com/products/electronics/ansys-hfss/hfss-capabilities

[30] Milligan, T. A. (2005). *Modern antenna design.* John Wiley & Sons.

[31]. (n.d.). *HFSS Online Help Guide*. Retrieved from http://anlage.umd.edu/hfss_onlinehelp.pdf

[32] Leung, K. W. (2012). Dielectric resonator antennas: From the basic to the aesthetic. *Proceedings of the IEEE, 100(7)*, 2181-2193.

[33] Gonzalo, R. D. (1999). Enhanced patch-antenna performance by suppressing surface waves using photonic-bandgap substrates. *IEEE Transactions on Microwave Theory and Techniques, 47(11)*, 2131-2138.

[34] Lai, A. (2009). *Left-handed metamaterials for microwave Engineering applications.* UCLA Department of Electrical Engineering.

[35] Mulenga, C. B. (2010). Planar electromagnetic bandgap structures based on polar curves and mapping functions. *IEEE Transactions on Antennas and Propagation, 58(3)*, 790-797.

[36] Rowe, W. S. (2006). Investigation into the performance of proximity coupled stacked patches. *IEEE Transactions on Antennas and Propagation, 54(6)*, 1693-1698.

[37] Arnedo, I. C. (2017). Synthesis of One Dimensional Electromagnetic Bandgap Structures with Fully Controlled Parameters. *IEEE Transactions on Microwave Theory and Techniques, 65(9)*, 3123-3134.

[38] Rahman, M. &. (2001). Transmission line–periodic circuit representation of planar microwave photonic bandgap structures. *Microwave and Optical Technology Letters, 30(1)*, 15-19.

[39] Yakovlev, A. B. (2009). Analytical modeling of surface waves on high impedance surfaces. In Metamaterials and Plasmonics: Fundamentals, Modelling, Applications. 239-254.

[40] Bist, S. S. (2014). Study The Various Feeding Techniques of Microstrip Antenna Using Design and Simulation Using CST Microwave Studio. *International Journal of Emerging Technology and Advanced Engineering, 4(9).*

[41] Kaur, G. S. (2017). Performance analysis of conductive patch materials for the design and fabrication of microstrip patch antennas. *IEEE,* 502-508.

[42] Barth, S. &. (2016). A miniaturized uniplanar metamaterial-based EBG for parallel-plate mode suppression. *IEEE Transactions on Microwave Theory and Techniques, 64(4),* 1176-1185.

[43] Ikonen, P. M. (2007). Modeling and analysis of composite antenna superstrates consisting on grids of loaded wires. *IEEE Transactions on Antennas and Propagation, 55(10),* 2692-2700.

[44] Costa, F. G. (2009). On the bandwidth of high-impedance frequency selective surfaces. *IEEE Antennas and Wireless Propagation Letters, 8,* 1341-1344.

[45] Garcia-Adeva, A. (2006). Band gap atlas for photonic crystals having the symmetry of the kagome and pyrochlore lattices. *New Journal of Physics, 8(6),* 86.

[46] Joannopoulos, J. D. (2011). Photonic crystals: molding the flow of light.

[47] Orta, R. &. (1997). Frequency Selective Surfaces-Analysis and Design.

[48] Civerolo, M. &. (2011). Aperture coupled patch antenna design methods. *IEEE,* 876-879.

[49] De Cos, M. E.-H. (2011). Troubleshooting RFID Tags Problems with Metallic Objects Using Metamaterials. *Current Trends and Challenges in RFID. InTech.*

[50] Singh, M. B. (2006). Design of aperture coupled fed micro-strip patch antenna for wireless communication. *IEEE,* 1-5.

[51] Chuang, C. T. (2009). New printed filtering antenna with selectivity enhancement. *IEEE,* 747-750.

[52] Osman, L. H. (n.d.). Proximity coupled microstrip patch antenna design with reduced out

of band harmonics device at 2.45 GHz. *IEEE*, 182-184.

[53] Amir, N. A. (2016). 2x1 microstrip patch array antenna with harmonic suppression capability. *IEEE*, 272-276.

[54] Biswas, S. G. (2016). Harmonics suppression of microstrip patch antenna using defected ground structure. *IEEE*, 1-4.

[55] Batista, F. F. (2017). Harmonic suppression in microstrip patch antenna using spur-line filter. *IEEE*, 1-5.

[56] Cohn, S. B. (1958). Parallel-coupled transmission-line-resonator filters. *IRE Transactions on Microwave Theory and Techniques, 6(2)*, 223-231.

[57] Coccioli, R. Y. (1999). Aperture-coupled patch antenna on UC-PBG substrate. *IEEE Transactions on microwave theory and techniques, 47(11)*, 2123-2130.

[58] Coccioli, R. M. (1999). UC-PBG substrate for planar antennas. *IEEE, 3*, 158-161.

[59] Yang, F. R. (1999). PBG-assisted gain enhancement of patch antennas on high-dielectric constant substrate. *IEEE, 3*, 1920-1923.

[60] Radisic, V. Q. (1998). Novel 2-D photonic bandgap structure for microstrip lines. *IEEE Microwave and guided wave letters, 8(2)*, 69-71.

[61] Coccioli, R. D. (1998). Radiation characteristics of a patch antenna on a thin PBG substrate. *IEEE, 2*, 656-659.

[62] Tarbouch, M. E. (2016). Contribution to the Miniaturization of Antennas: State of the Art. *Transactions on Networks and Communications, 4(5)*, 48.

[63] Wiesbeck, W. S. (2015). Radar 2020: The future of radar systems. *IEEE*, 188-191.

[64]. (n.d.). *Radar: Basics, Types and Applications*. Retrieved from https://www.elprocus.com/radar-basics-types-and-applications/

[65] Liu, H. L. (2005). Harmonic suppression with photonic bandgap and defected ground structure for a microstrip patch antenna. *IEEE microwave and wireless components letters, 15(2)*, 55-56.

APPENDIX A. HFSS SIMULATION SETUPS.

Correctly setting up HFSS simulations is key to achieving coherent results and helps make a good interpretation of them. Appendices A.1. HFSS Driven Mode Simulation and A.2 explain how to set up two different modes of HFSS simulations: driven and eigensolver, respectively. The setup configurations in this appendix apply to the designs in the current work and must be reviewed and adapted for different HFSS designs, but they can be used as a guideline to the way a simulation is set up. HFSS Release 2017b has been used in this work.

A.1. HFSS Driven Mode Simulation

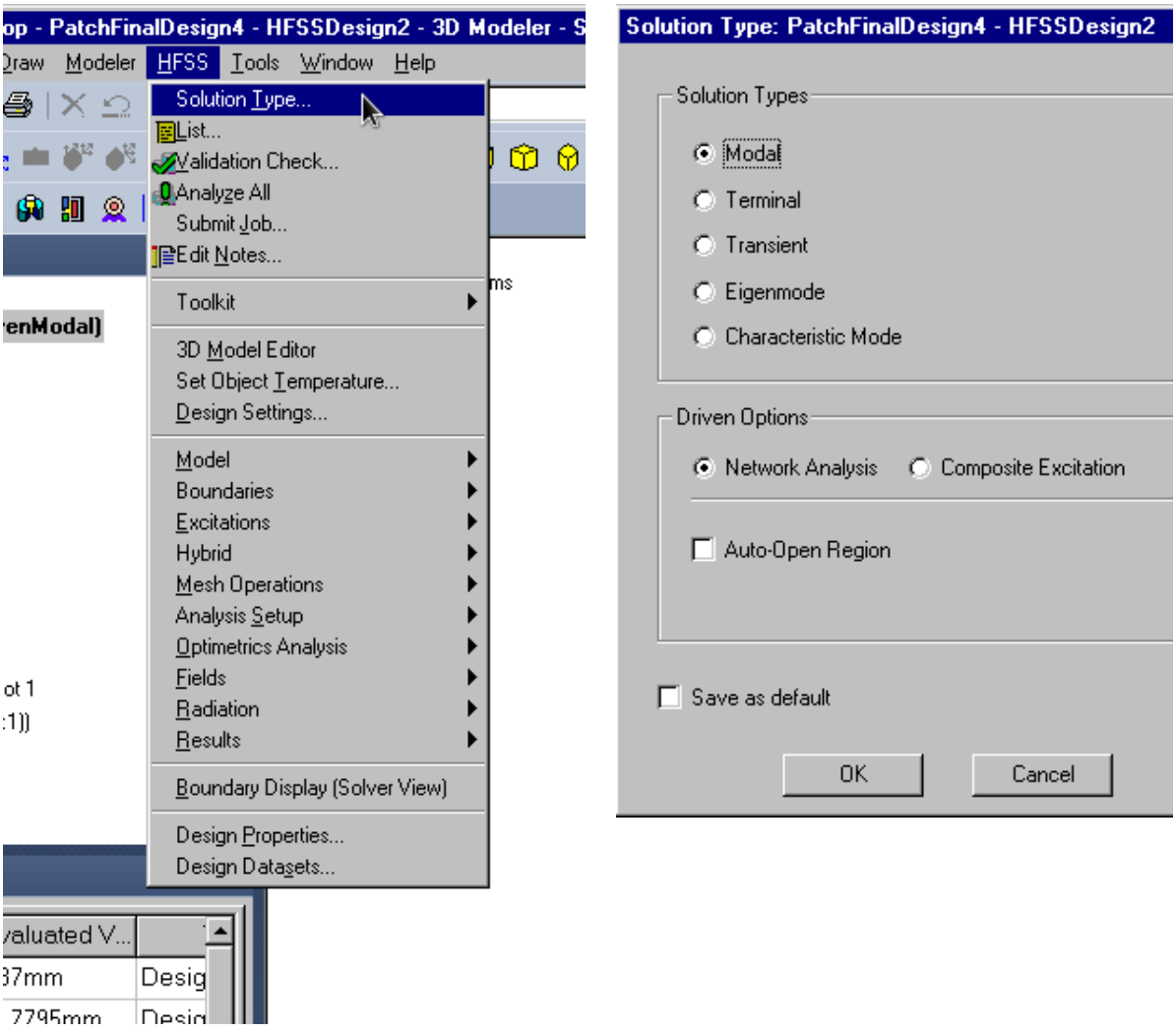

Figure A. 1.- Specifying simulation solution type.

Driven mode simulations are used to find how a given structure (N-port network) behaves when it is excited by one or several ports. In all our designs, wave ports are used (right click of port surface in model and assign wave port excitation) injecting a power of 1 W into the model. Once an HFSS model is drawn and ready to simulate, driven mode simulation is selected by (figure A.1):

HFSS > Solution Type > Modal

And

HFSS > Solution Type > Driven option > Network analysis

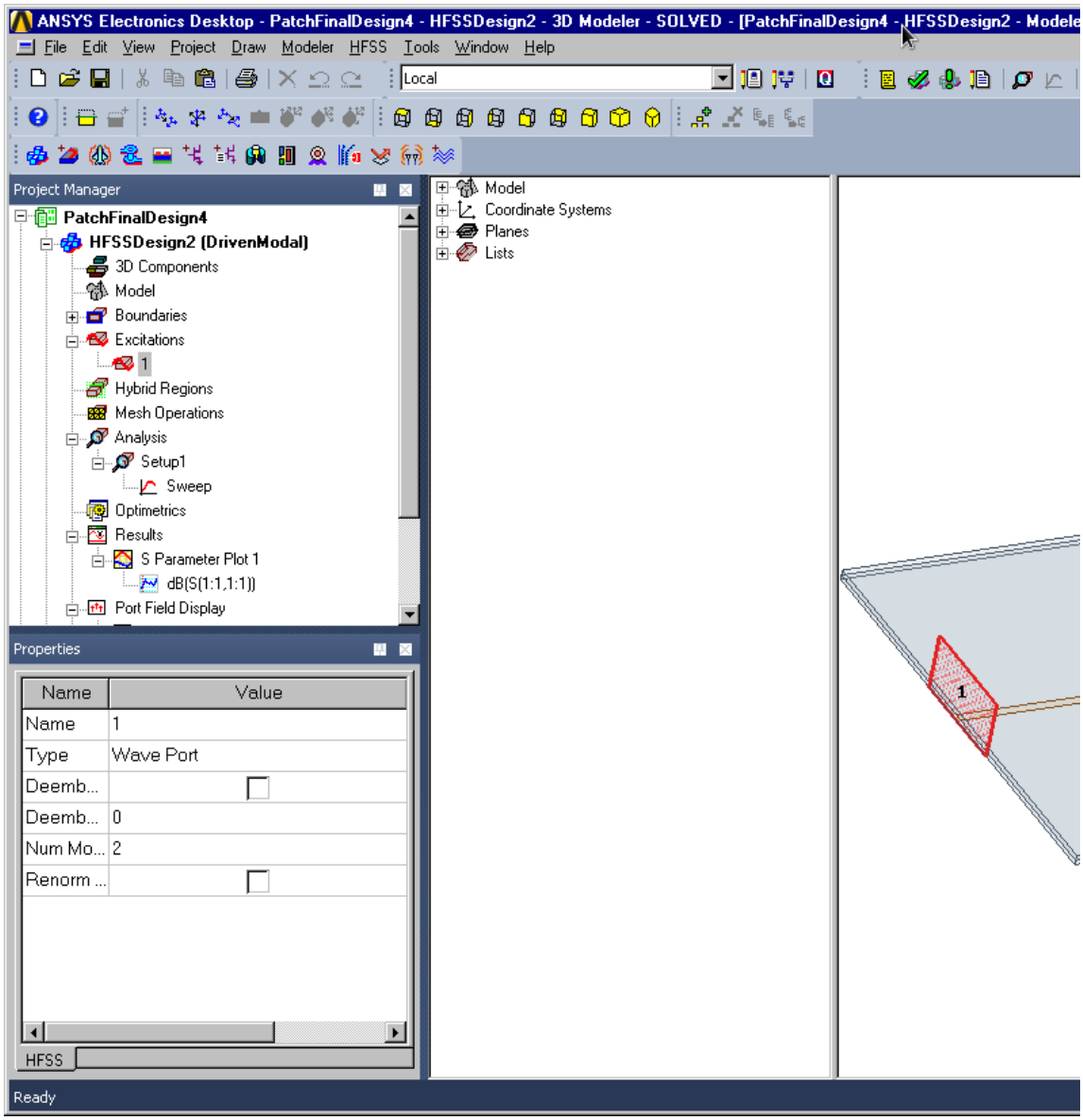

Figure A. 2.- Some features of the Project Manager window.

Then, in the Project Manager window (figure A.2), go to:

Analysis (right click) > Add solution setup

Then, parameters in the General and Options tabs are adjusted accordingly to our desired simulation results (figure A.3). Some important parameters are:

- Solution frequency: frequency for which the meshing operation is assigned. Setting it to the maximum frequency of the simulated frequency range guarantees that the mesh will be small enough for the whole range, but slows down the simulation. The center frequency can also be chosen for this field, depending on the model to be simulated.
- Maximum number of passes: maximum number of iterations that the software performs. It is necessary to ensure that the simulation will end if convergence is not reached.

Maximum Delta S: tolerance value of the S parameters. Convergence is reached when Delta S is lower than the maximum.

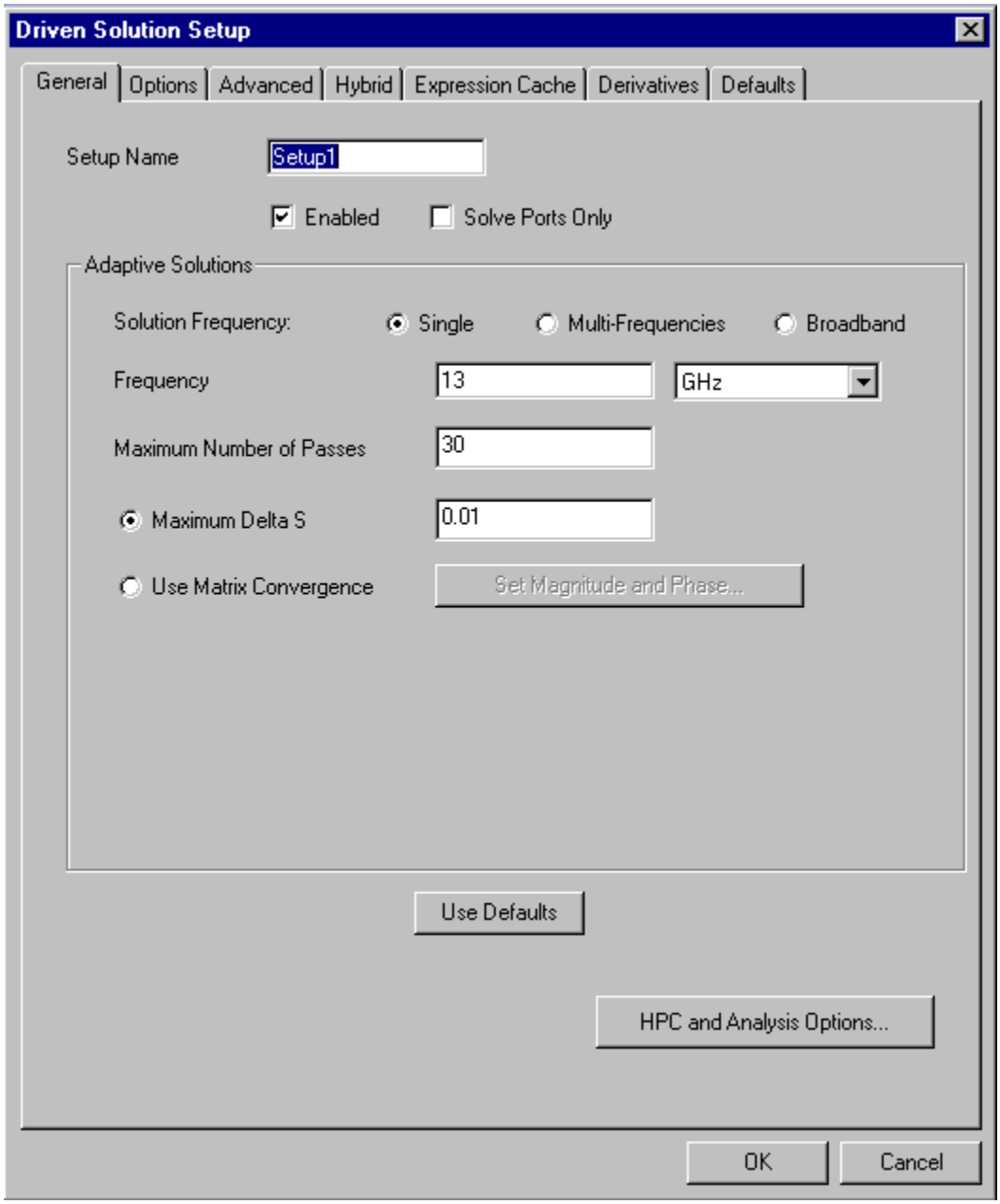
Driven Solution Setup
General
Options
Advanced
Hybrid
Expression Cache
Derivatives
Defaults
Setup Name
Setup1
Enabled
Solve Ports Only
Adaptive Solutions
Solution Frequency:
Single
Multi-Frequencies
Broadband
Frequency
13
GHz
Maximum Number of Passes
30
Maximum Delta S
0.01
Use Matrix Convergence
Set Magnitude and Phase...
Use Defaults
HPC and Analysis Options...
OK
Cancel

(a)

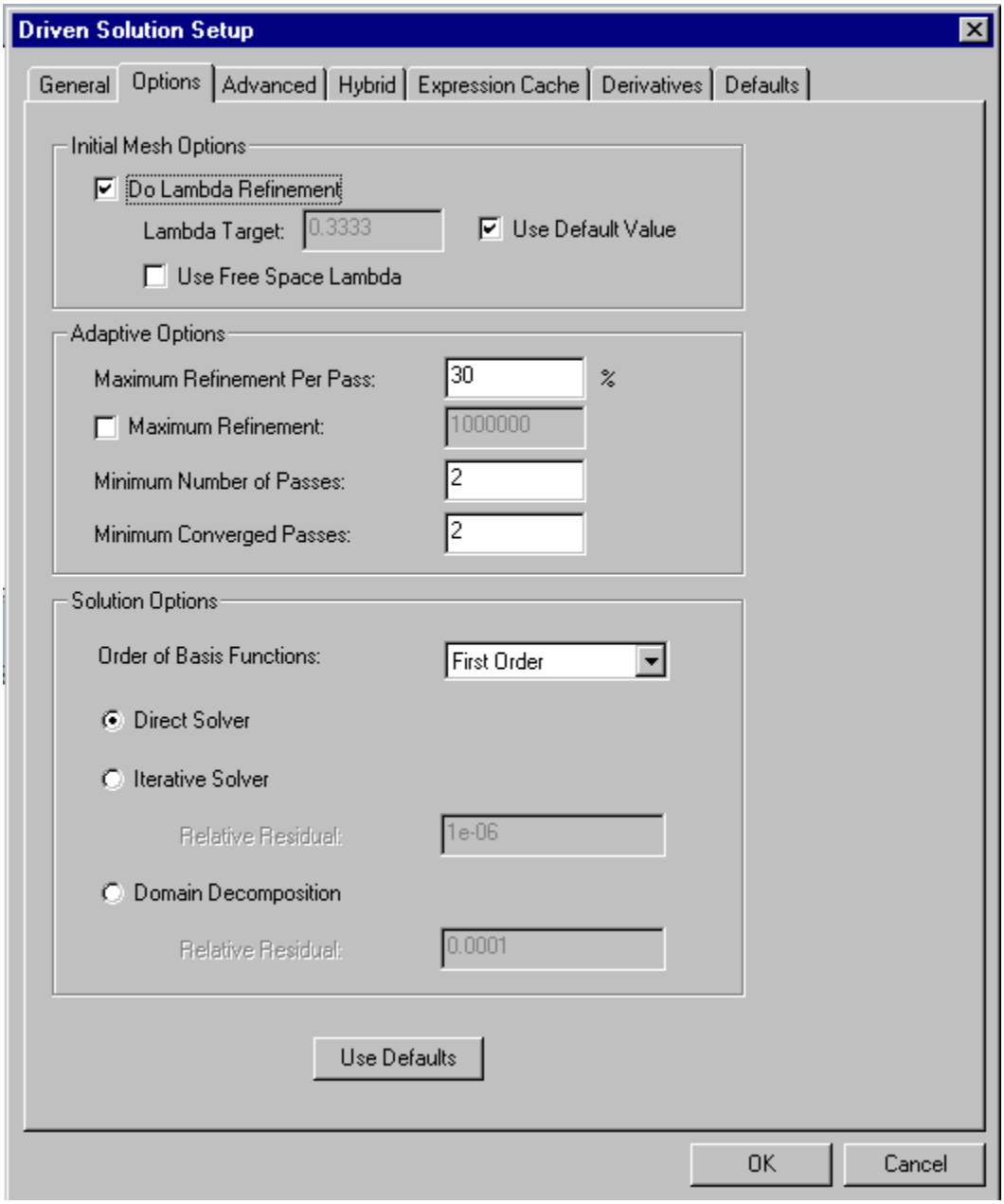

(b)

Figure A. 3.- Setup configuration: (a) General tab, (b) Options tab.

A frequency sweep is added next (figure A.4):

Analysis > SetupName (right click) > Add frequency sweep

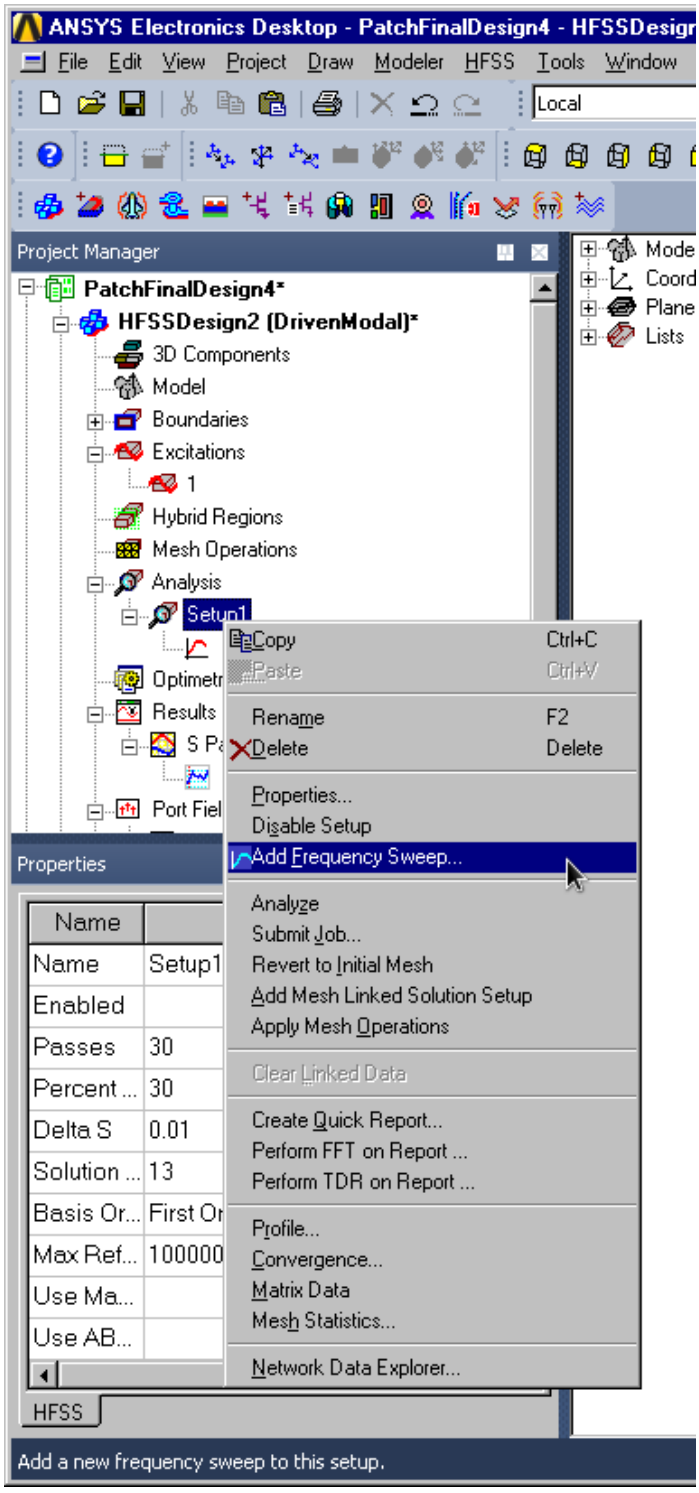

Figure A. 4.- Adding a frequency sweep.

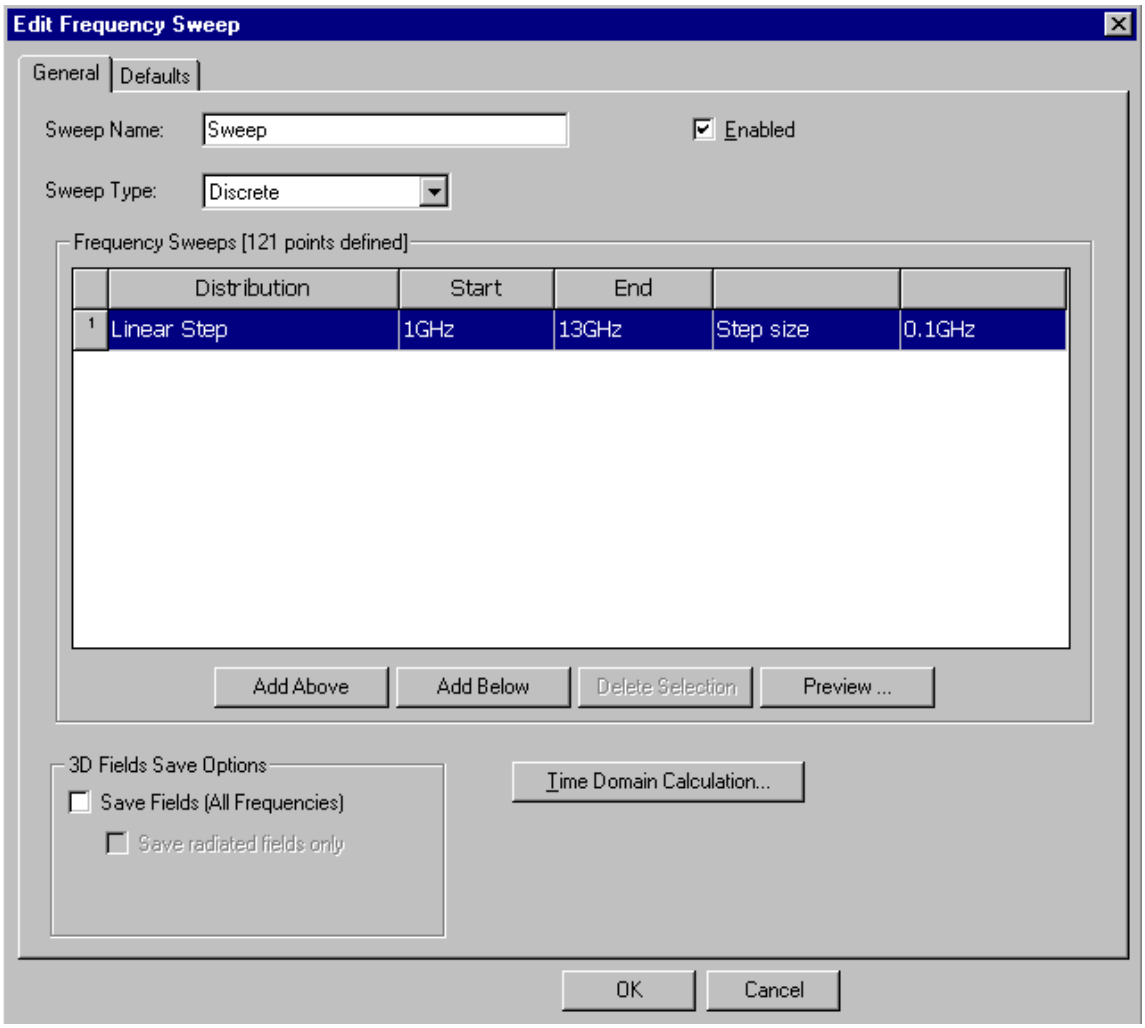

Figure A. 5.- Frequency sweep properties.

A discrete sweep type is chosen for our simulations (figure A.5). Small frequency steps yield high resolution results. Using an appropriate resolution is important to optimize simulation time and accuracy of the results. Therefore, small steps are used for the frequency bands where results are critical, such as around the working frequency, to obtain an accurate response, and bigger steps are used in less important frequency bands in order to speed up simulation time.

Besides a frequency sweep for the model, parametric sweeps can be performed to obtain results as one or several building parameters of the model are varied. This is used in our work to optimize matching parameters such as patch size, dielectric height and microstrip feed position relative to the patch. It is also used to determine the best position of the mushroom EBG filter relative to the patch and other fine adjustments. They way to specify this in HFSS is in the Project Manager window (figure A.6):

Optimetrics (right click) > Add > Parametric

Where the variable to be swept can be chosen and the number and magnitude of steps can be specified (figure A.7).

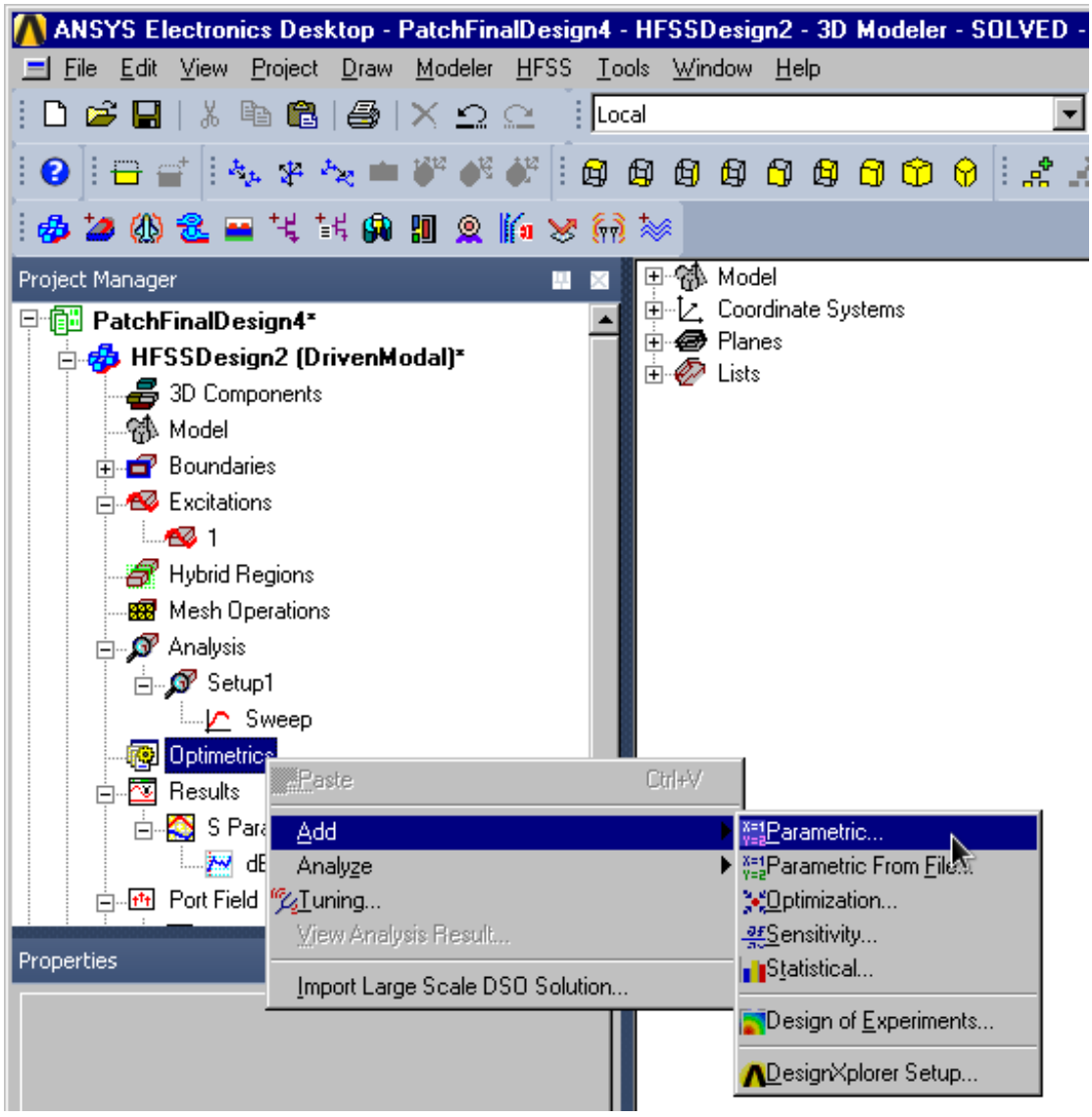

Figure A. 6.- Adding a parametric analysis.

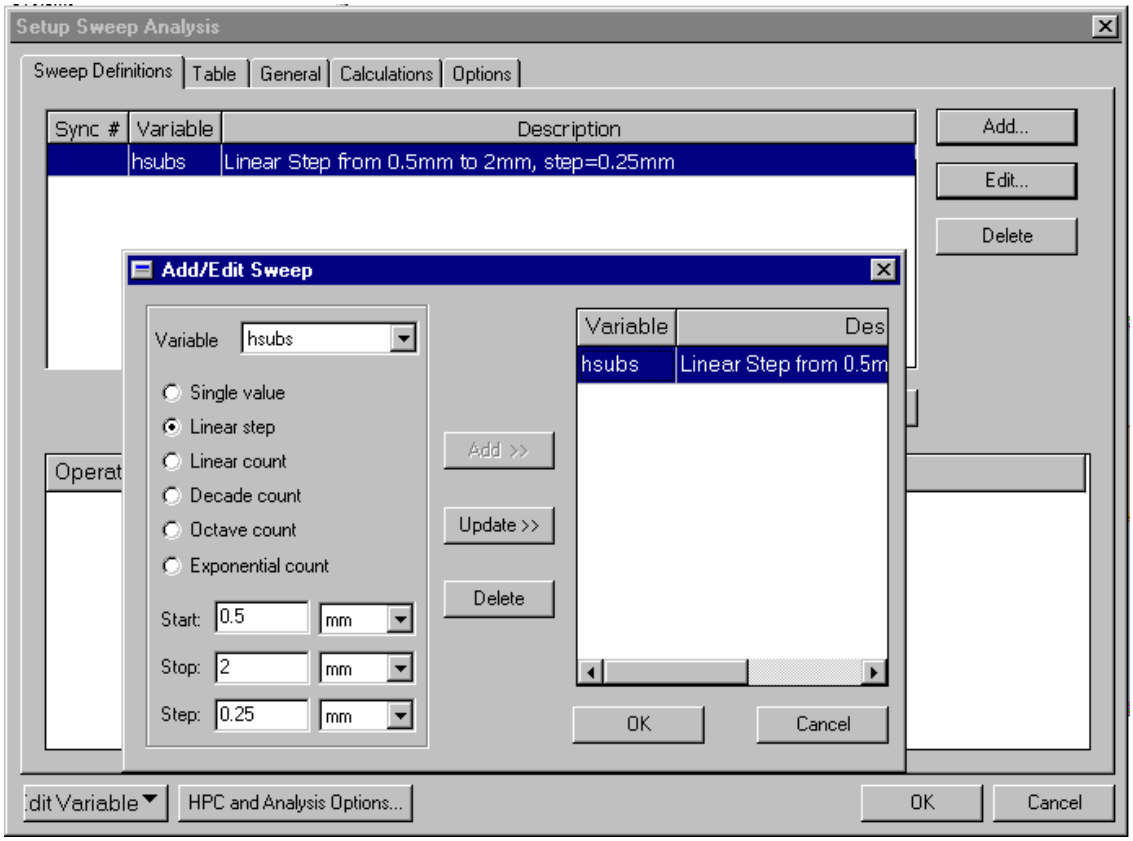

Figure A. 7.- Parametric sweep properties.

Once this process is concluded, the ***Validate*** button should be hit to make sure that there are not design errors and the simulation can be run (figure A.8)

Figure A. 8.- Validate design (green check).

.

When the simulation finishes, results are obtained by right clicking ***Results*** > ***Create Modal Solution Data Report*** and selecting the desired variable to plot. Field plots are also depicted by right clicking the target volume or surface and going to ***Plot Fields***. Of the several options available, the ***MagE*** and ***VecE*** (magnitude and vector plots for the electrical field) are the ones used in this work.

As for convergence parameters (figure A.9), the driven mode results shown in this work correspond with simulations that converged, with at least one converged pass and a maximum tolerance of the magnitude of the S-parameters (Max. Mag. DeltaS) equal to 0.01 (figure A.10). This means that all results are accurate in a range of ± 0.01 the value of the S-parameters at each frequency point.

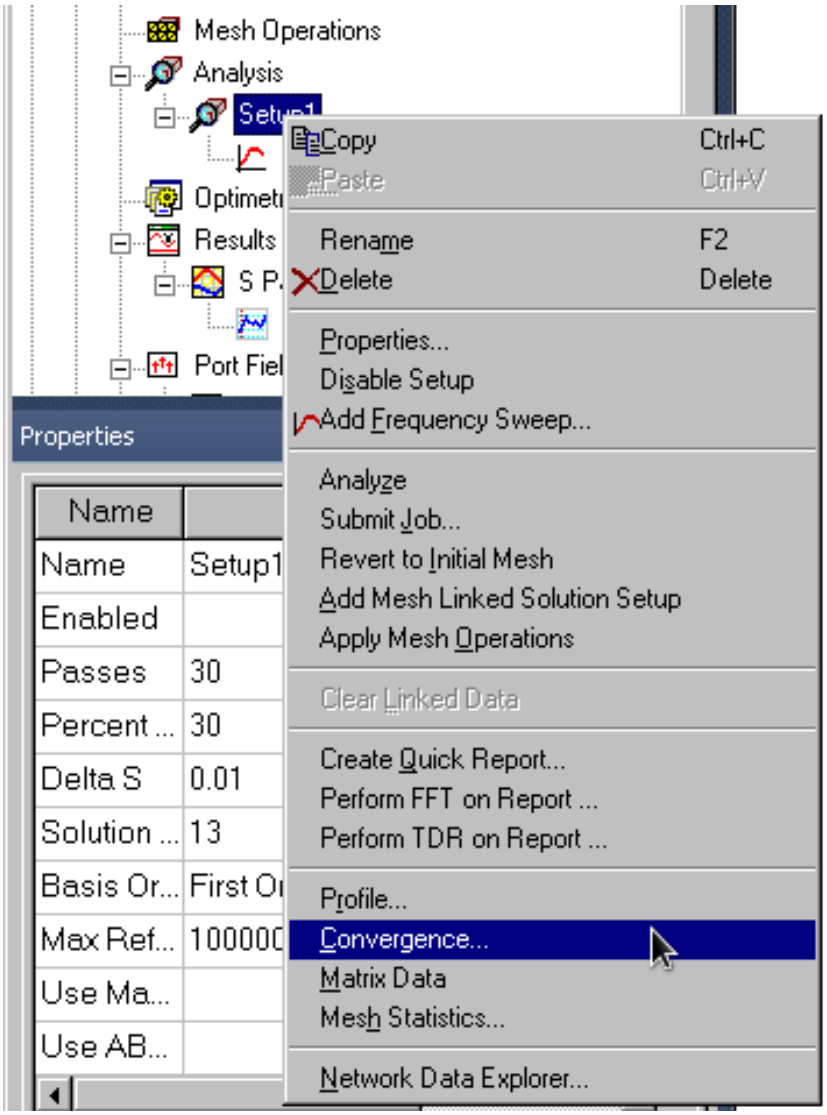

Figure A. 9.- Checking for convergence.

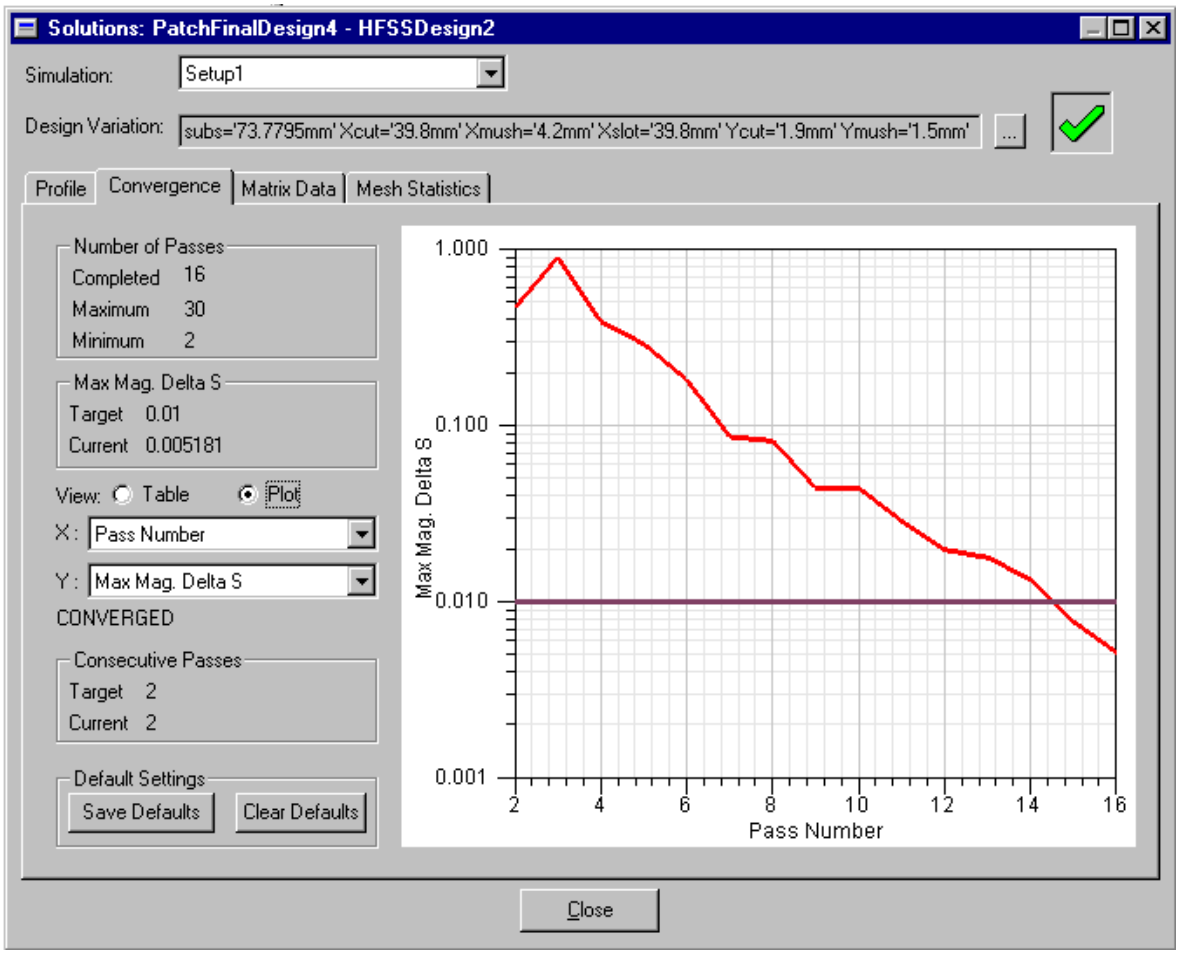

Figure A. 10.- Convergence results.

A.2. HFSS Eigen Mode Simulation

Eigen mode simulations are used to find the dispersion properties of a structure, that is, the value of the propagation constant of different modes as function of frequency. In this work, the eigensolver mode is used to simulate different configurations of mushroom EBGs by modeling a unit cell and applying periodic Master-Slave (M-S) boundary conditions to it. First, the eigenmode solver must be selected (figure A.1):

HFSS > Solution Type > Eigenmode

Then

Analysis (right click) > Add solution setup

And under the ***General*** and ***Options*** tabs, set up the solver configuration. The values used in this work are detailed in Figure A.11. In this mode no frequency sweep configuration is needed.

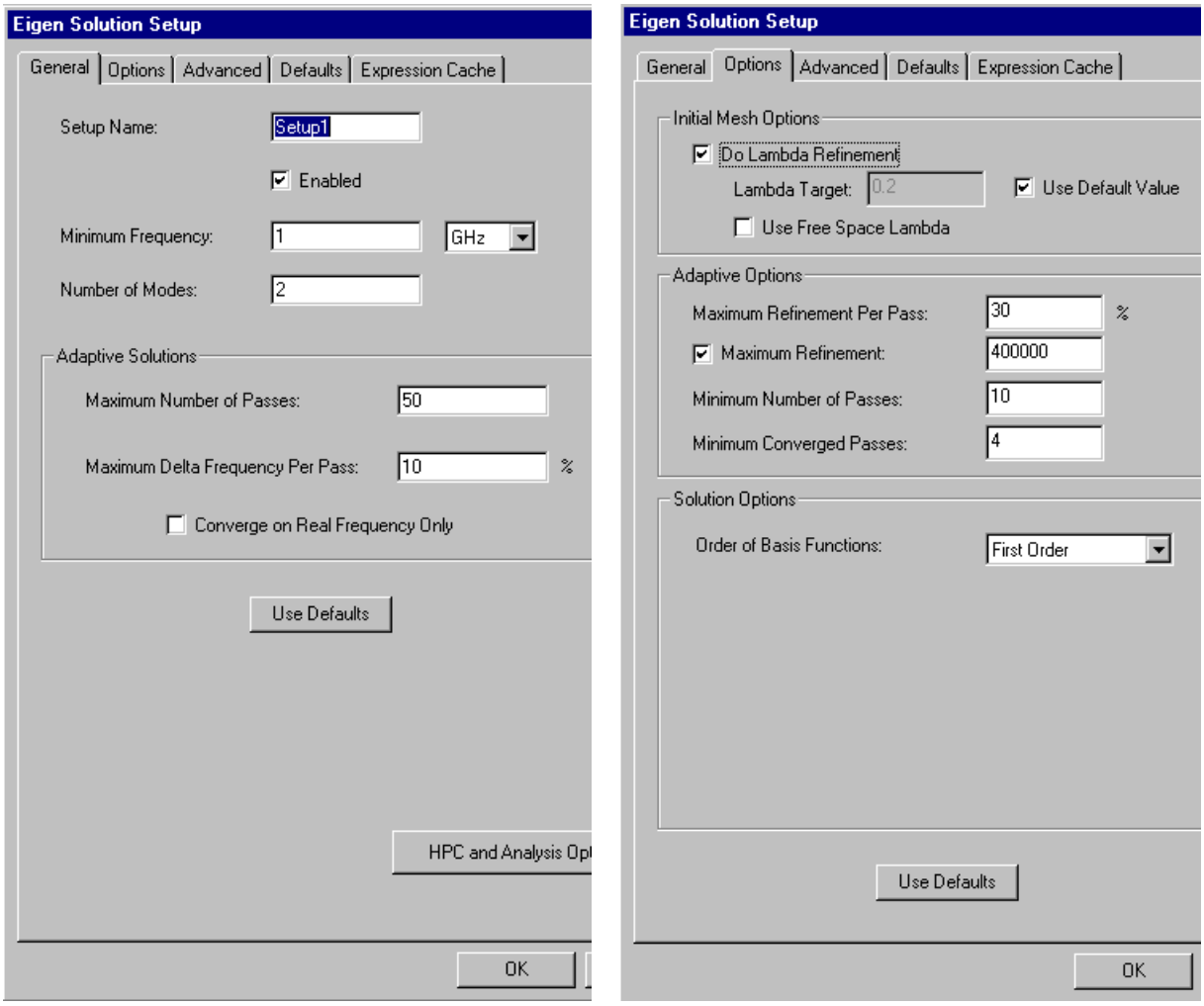

Figure A. 11.- Eigensolver setup configuration.

Some aspects of the eigensolver mode need to be pointed out. First, no radiation boundaries are allowed, so to simulate free space a PML (*Perfectly Matched Layer*) needs to be included in the design.

This is shown in figure A.12 together with the mushroom EBG unit cell model used in this work. Note the PML layer on top. The orange parts represent conducting material: a PEC (*Perfect Electric Conductor*) boundary is used in the case of the mushroom patch, and a copper cylinder for the via (although it is also possible to make a via hole and assign a PEC boundary inside it).

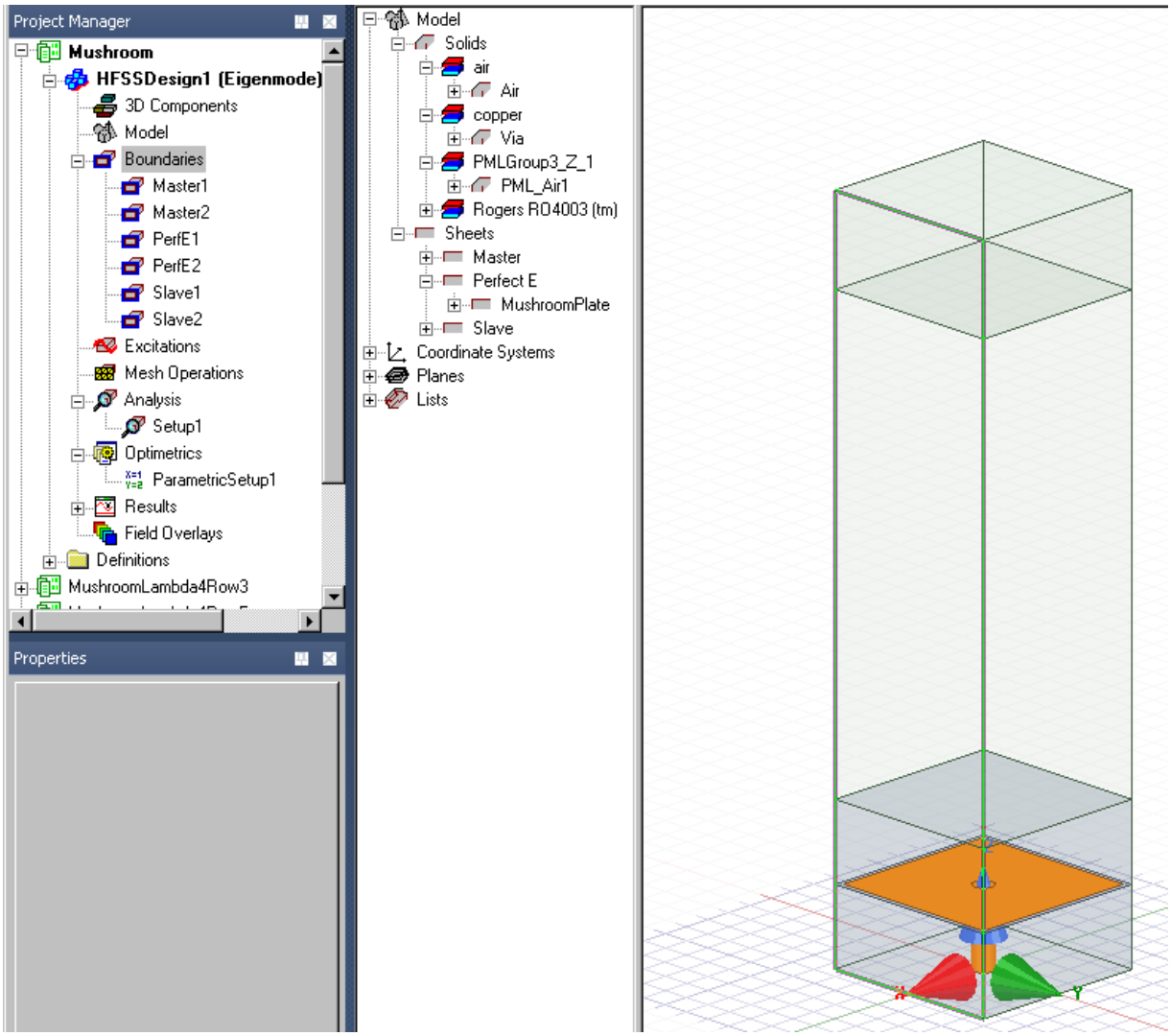

Figure A. 12.- Mushroom EBG model for the eigenmode solver.

The Master-Slave boundaries, necessary for simulating an "infinitely" periodic repetition of the structure in the x and y directions, are added on the side faces as shown in figure A.13. Only the x boundaries are depicted since the process for the y boundaries is identical. When setting up the M-S boundaries, a phase difference between the fields in them must be provided to the solver, as specified in figure A.14.

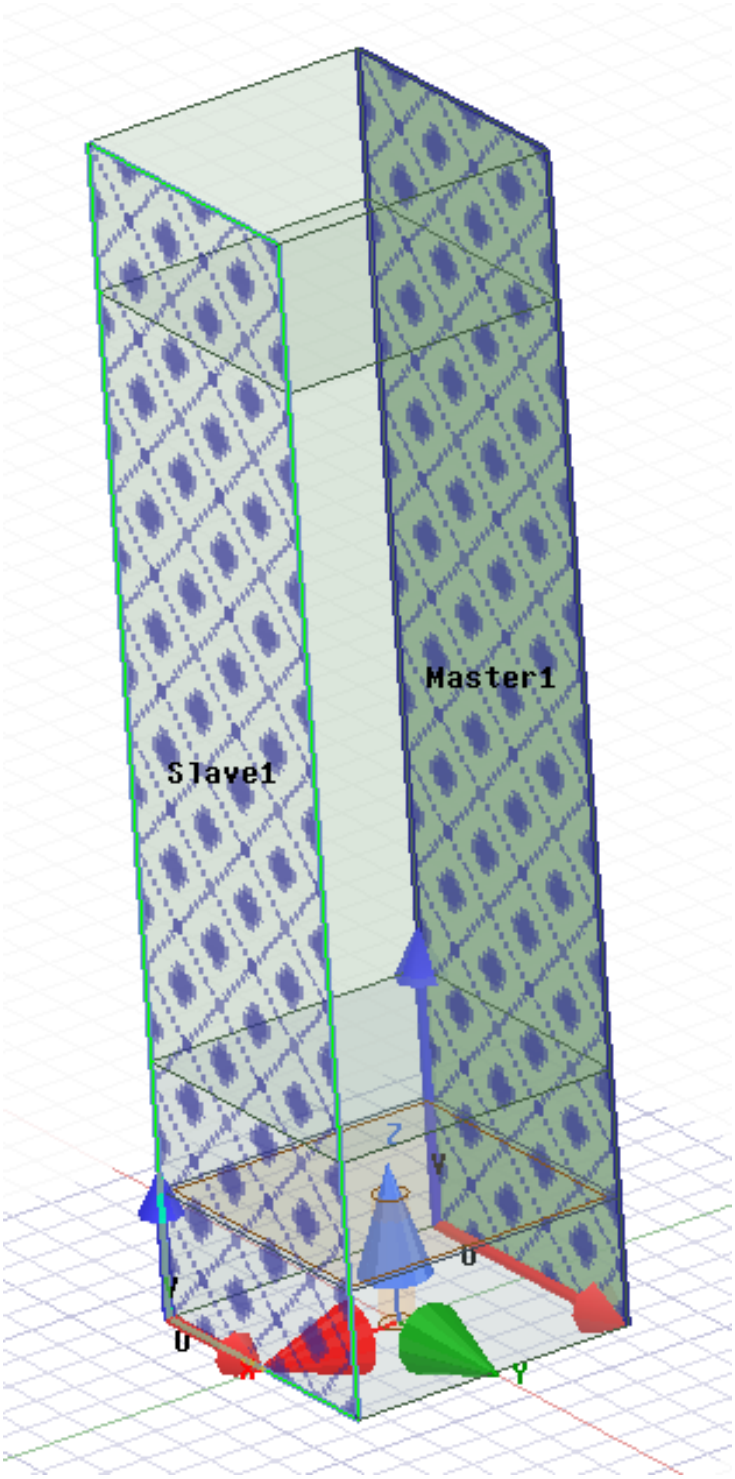

Figure A. 13.- Master-Slave boundary configuration in the x direction. The y M-S boundaries are similarly configured.

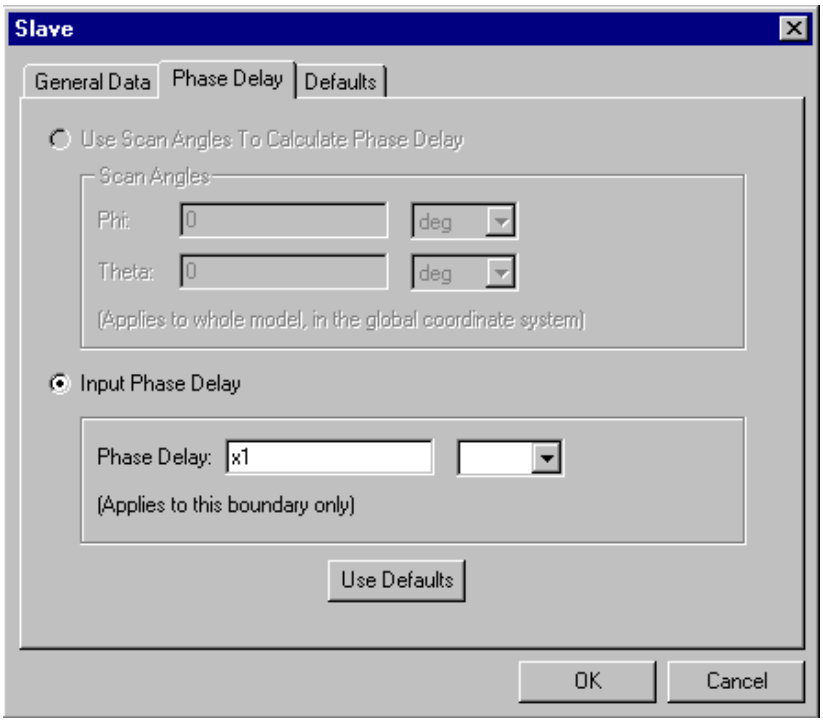

Figure A. 14.- Phase delay introduction on Slave boundary with respect to Master boundary.

Next, in ***Optimetrics***, make a sweep of the phase difference between Master and Slave layers (x1 and y1 in this example, y1 is not shown because it is configured in the same way as x1). The eigensolver will solve each mode to match its amplitude at the Master and Slave faces, with a phase difference as selected in the parametric sweep (figure A.15).

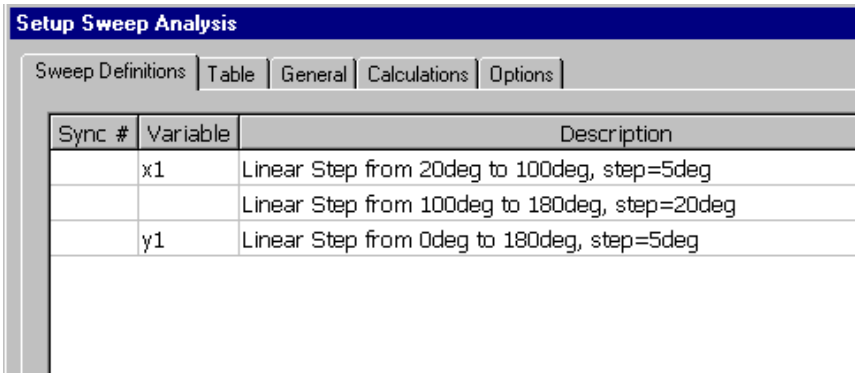

Figure A. 15.- Phase parametric sweep.

Validate and run the simulation. Results and fields can be obtained as in the driven mode setup.

APPENDIX B. GANTT DIAGRAM.